Assessing the Long Term Performance of a Shallow Water Cover to Limit Oxidation of Reactive Tailings at Louvicourt Mine

MEND Report 2.12.2

Assessing the long term performance of a shallow water cover to limit oxidation of reactive tailings at Louvicourt Mine.

by
B. Vigneault[+], Y.T.J. Kwong[+] and L. Warren[‡]

Work performed for:
MEND Program

[+] **Natural Resources Canada, CANMET-Mining and Mineral Sciences Laboratories (MMSL)**
[‡] **McMaster University, School of Geography and Earth Sciences.**

DISCLAIMER

Any determination and/or reference made in this report with respect to any specific commercial product, process or service by trade name, trademark, manufacturer or otherwise shall be considered to be opinion; CANMET-MMSL makes no, and does not intend to make any, representations or implied warranties of merchantability or fitness for a particular purpose nor is it intended to endorse, recommend or favour any specific commercial product, process or service. The views and opinions of authors expressed herein do not necessarily state or reflect those of CANMET-MMSL and may not be used for advertising or product endorsement purposes.

EXECUTIVE SUMMARY

The impact of periphyton layers on the performance of shallow-water covers to prevent oxidation of reactive tailings was studied at Louvicourt Mine (Aur Resources). A previous study reported the growth of a periphyton layer (biofilm) at the surface of the tailings, submerged under a 30 cm water cover in field experimental cells. The present study was initiated nine years after the tailings were submerged and integrated geochemical, mineralogical and biological data to provide an overall assessment of the long-term performance of the shallow water cover. Geochemical changes were monitored by *in situ* measurements of porewater chemistry. Samples of the biofilm, the oxic surface layer of tailings and the deeper tailings were also analyzed for total metals content, solid-phase speciation using sequential chemical extractions and detailed mineralogical analysis by SEM-based image analysis. Finally, molecular biological techniques (16S rRNA) were also used to characterize the microbial community associated with the biofilm. The mineralogical and chemical data confirmed that mobilisation of trace metals occurred in surface tailings but also indicated that the overlying biofilm effectively trapped the released metals. Results also indicate metal specificity in the nature of the processes involved and resulting fluxes. The sequential extractions suggested that Cd and Zn were captured by sorptive processes within the biofilm, while Cu was scavenged by the organic matter present in the biofilm. There was a 10 fold decrease in Cd and Zn fluxes to the overlying water over the last seven years whereas tailings switched from a sink to a source of Cu for the water cover. The Cu, Cd and Zn net releases to the overlying water calculated in this study were several orders of magnitude lower than the fluxes reported at other sites. Furthermore, the estimated water cover concentrations resulting from these fluxes would be well below discharge limits and equal to or below water quality guidelines. The results also highlighted that the disposal system had not reached equilibrium after nine years of operation. The tailings were still acting as a net source of dissolved solids to the overlying water and chemical changes were still observed in the deeper part of the porewater profiles. Finally, the pH and oxygen microprofiles and the molecular biological analyses of the biofilm community structure indicated that the biofilm included a variety of different metabolic pathways, and acted both as a source and a sink of H^+ and oxygen depending on diurnal light conditions. This study concludes that biofilm development was beneficial since it likely protected tailings from resuspension and contributed to the maintenance of anoxic conditions in the underlying sediments. In addition, the biofilm trapped mobilized dissolved metals and decreased fluxes out of the tailings into the overlying water column.

SOMMAIRE EXÉCUTIF

Les répercussions de l'établissement d'une couche de périphytons sur la capacité des couvertures aqueuses peu profondes de limiter l'oxydation des résidus réactifs ont été étudiées à la mine Louvicourt (Aur Ressources). Les auteurs d'une étude précédente avaient noté la croissance d'une couche de périphytons (biofilm) à la surface des résidus, submergés sous une couverture aqueuse de 30 cm, dans des cellules expérimentales. La présente étude a été entamée neuf ans après la déposition des résidus directement sous l'eau et les données géochimiques, minéralogiques et biologiques ont été intégrées aux fins d'une évaluation globale de l'efficacité à long terme de la couverture aqueuse peu profonde. Les variations géochimiques ont été étudiées au moyen de mesures *in situ* de la chimie de l'eau interstitielle. Des échantillons du biofilm, de la couche superficielle oxique des résidus et des couches profondes des résidus ont été analysés pour en déterminer les teneurs en métaux totaux; la spéciation de la phase solide, au moyen d'extractions chimiques séquentielles; et la composition minéralogique détaillée, au moyen de l'analyse d'image par MEB. Des techniques de biologie moléculaire (16S rRNA) ont été utilisées pour caractériser la communauté microbienne associée au biofilm. Les données chimiques ont confirmé une mobilisation de métaux-traces dans les résidus superficiels mais elles ont aussi indiqué que le biofilm retenait les métaux libérés. Les résultats montrent également que la spécificité du métal joue un rôle dans la nature des processus, et des flux qui en résultent. D'après les extractions séquentielles, le Cd et le Zn ont été capturés par des processus de sorption à l'intérieur du biofilm, alors que le cuivre a été piégé par la matière organique présente dans le biofilm. Les flux de Cd et de Zn vers la couverture aqueuse étaient 10 fois plus faibles qu'il y a sept ans, alors que les résidus ont cessé d'être un piège pour le cuivre pour en devenir une source de cuivre pour la couverture aqueuse. Les flux nets de cuivre, de Cd et de Zn vers la couverture aqueuse qui ont été calculés dans cette étude sont inférieurs de plusieurs ordres de grandeur aux flux signalés à d'autres sites. En outre, les concentrations en métaux estimées pour la couverture aqueuse résultants de ces flux seraient bien en deçà des limites établies pour les effluents miniers et seraient inférieures ou égales aux recommandations sur la qualité de l'eau. Les résultats ont aussi révélé que le système de déposition n'avait pas atteint son équilibre après neuf ans d'exploitation. Les résidus étaient encore une source nette de solides dissouts pour la couverture aqueuse et des variations chimiques pouvaient toujours être observées dans la partie profonde des profils de l'eau interstitielle. Enfin, les microprofiles du pH et de l'oxygène et les analyses biologiques moléculaires de la structure de la communauté biologique du biofilm ont indiqué que le biofilm contenait différentes voies métaboliques et que, selon les conditions de luminosité, il était un puits ou une source de H^+ et d'oxygène. Cette étude conclut que le biofilm est bénéfique parce qu'il empêche la remise en suspension des résidus et qu'il contribue au maintien des conditions anoxiques dans les sédiments sous-jacents. Enfin, le biofilm piège les métaux dissous entraînés et il diminue les flux de métaux vers la couverture aqueuse.

TABLE OF CONTENTS

TABLES

FIGURES

APPENDICES

INTRODUCTION

Acid mine drainage is a major environmental concern of the mining industry world-wide. Accordingly, considerable effort has been expended to develop techniques for the prevention of acid mine drainage (e.g., the Mine Environment Neutral Drainage (MEND) Program, Natural Resources Canada). The utilization of water covers is often considered to minimize oxidation of reactive tailings. In the case of a man-made tailings impoundment, the use of a water cover with a minimal depth is preferable for geotechnical considerations.

The efficiency of such shallow water covers to reduce the oxidation of sulphidic mine tailings has been demonstrated at several sites. However, few studies on submerged tailings have specifically measured *in situ* metal fluxes from submerged tailings to the water cover. It is essential to consider these fluxes for waste water management, especially in the context of closure with no planned additional treatment. In addition, for water covers with depths of a few meters or less there is generally intense penetration of light, which will eventually allow the growth of photosynthetic periphyton at the surface of submerged tailings. The impact of a fully established periphyton layer on the performance of shallow-water disposal has not been studied extensively to date, despite the widespread occurrence of such layers in these systems. Field experimental cells were constructed in 1996 at Louvicourt Mine (Aur Resources) to study the efficiency of a minimal water cover (about 30 cm) to minimize the oxidation of submerged fresh tailings under the MEND program (Project 2.12.1). The results of the various investigations related to the site were summarized in a Synthesis Report (MEND 2002). It was recommended that further research into the role of aquatic vegetation on the performance of the water covers and further monitoring of the test cells to assess their longer-term performance be completed. The experimental cells were to be decommissioned as part of the Louvicourt Mine closure in August 2005. For the current MEND project, field work was conducted in June and July 2005 in order to complete the recommended investigations prior to the destruction of the experimental cells.

Among the previous studies conducted at the Louvicourt Mine, the evolution of tailings geochemistry in the field test cells was followed *in situ* from 1996 to 1998 by INRS-Eau (MEND 2001;Vigneault *et al.* 2001). This study included *in situ* measurements of micro-variations of pH and dissolved oxygen at the tailings-water interface, quantification of metal fluxes to the water cover and sequential chemical extractions on the surface tailings. The collected data indicated that two years after tailings deposition, oxidation was limited to the first mm beneath the tailings-water interface and the shallow water cover was effective in reducing sulphide oxidation and metal fluxes to the water cover.

The sequential chemical extractions scheme developed by Tessier *et al.* (1979) has been mostly applied to natural sediments. Their interpretation for mine tailings is not straightforward. Sequential extractions have been rarely used to assess the relative metal mobility in submerged tailings (e.g. MEND 1990 and 1991). No particular care for the sampling and storage was taken in these studies to prevent the oxidation of the samples. Wallman *et al.* (1993) have also demonstrated using thermodynamic calculations that for anoxic sediments, some metal sulphides (including Cd and Zn sulphides) are soluble in the exchangeable and reducible fractions. This would likely be the case also for unoxidized tailings. Dold (2003) has since provided new data

on the selective solubility of mineral fractions from sulphide mine waste, and concluded that geochemical study of mine waste should always include mineralogical analysis in order to validate the interpretation of chemical observations.

The establishment of an oxygen-producing periphyton layer at the surface of the tailings, as well as a progression in the tailings surface oxidation were also observed in 1998 in the Louvicourt field cells (MEND 2001;Vigneault *et al.* 2001). The biofilm has continued to develop at the surface of the submerged tailings over the years and has remained dormant and viable in winter under the ice and snow cover. Such biofilm formation can dynamically influence metal behaviour across the interface through the associated metabolic activity. Key geochemical parameters, such as concentrations and types of reactive biominerals, can be altered in addition to pH and oxygen profiles. Garcia-Meza *et al.* (2005) suggested that extracellular immobilization of metals in the biofilm mucilaginous structure was a survival mechanism for algae growing at the surface of mine tailings. It can therefore be postulated that the biofilm itself could constitute an important sink for trace metals. It can also be hypothesized that the formation of a thick biologically derived mat over the tailings could prevent tailings resuspension during the ice-free period. Often the controls on these biofilm-associated processes are biological in nature, reflecting the need for information regarding the particular metabolic array present within the biofilm (Warren 2005). However, very little information is currently available on the biological composition of biofilms growing on submerged tailings. Garcia-Meza *et al.* (2005) reported that phototrophic biofilm growing in a Mexican mine tailings reservoir was composed mostly of a cyanobacterium (*Phormidium sp.*) and a chlorophyte (*Chlorococcum sp.*). To address similar issues, there is an increasing use of quantitative molecular analysis to provide insights on the composition and metabolic role of benthic microbial communities (e.g. Ravenschlag *et al.* 2001).

The current study aims to assess the impacts of the fully established biofilm at the tailings – water interface and to assess the oxidation status of the submerged tailings in the Louvicourt field cells, nine years after placement. The study integrates geochemical, mineralogical and biological data to provide an overall assessment of the long-term performance of the shallow water cover. Geochemical changes were monitored by determining porewater and tailings chemistry seven years after the last measurements were completed. Samples of the biofilm, the oxidized surface layer of tailings and the deeper tailings were analyzed for total metal content and solid-phase partitioning using sequential chemical extractions. The same samples were subjected to detailed mineralogical analysis by SEM-based image analysis to clarify the extent of oxidation of various minerals at different depths and to elucidate the mechanisms involved in the metal leaching process. Finally, molecular biological tools were used to characterize the microbial community associated with the biofilm and to provide the first step in mapping their potential influence on key geochemical processes affecting metal fluxes within this system.

MATERIALS AND METHODS

Site description. Louvicourt Mine was an underground Cu/Zn mine located about 15 km east of Val d'Or, Québec. It was in operation between July 1994 and July 2005. Grain size measurements indicated that the tailings are mainly composed of particles in the silt and fine sand fractions (Li and St-Arnaud, 2000). The tailings consist of silicate, sulphide, carbonate and oxide minerals. The dominant sulphide is pyrite, with chalcopyrite, sphalerite and galena present in trace quantities. Silicate minerals include quartz, muscovite, ferroan clinochlore, plagioclase and K-feldspar. Magnesian siderite and ankerite (or ferroan dolomite) were identified as the dominant carbonate minerals (Li and St-Arnaud, 2000). About 55% of the tailings resulting from the separation of Cu and Zn concentrates by flotation were used as underground back fill. The remaining 45% of the tailings were disposed directly underwater in a 1.5 x 10^6 m^2 man-made reservoir. During its operation, 6.62 millions tons of tailings were disposed of in the impoundment, which has a capacity of 4.7 Mm^3. The outflow from the impoundment was treated when required by liming. The treated water was routed through a polishing pond, where suspended sediments settled, before being discharge to the Colombière River (see Appendix A for site map). Discharge was annual, occurring sporadically from the spring to the beginning of the following winter, and was in compliance with provincial and federal discharge limits during its operation.

Two experimental cells (21 x 21 x 3 m deep) were constructed at the Louvicourt Mine in 1996 at a site adjacent to the tailings impoundment (see Appendix A for site plan and site pictures). The tailings were placed directly underwater and a water cover of 0.3 m was maintained by periodic refilling until the field cells were decommissioned in August 2005. Therefore, the studied tailings had never been exposed to air. The 0.3 m depth was selected as the minimum depth that would prevent tailings resuspension. The original plan was to use the experimental cells to test the addition of a sand or an organic layer on the tailings at the closure. However, studies conducted under the MEND Project 2.12.1 have indicated that the addition of a protective layer is not desirable (MEND 2002) and *in situ* tests were never conducted. Since 1998, a photosynthetic biofilm had gradually developed over the submerged tailings. Given that the tailings submerged in Experimental Cell #1 were highly heterogeneous (MEND 2001), the current study was limited to the more homogeneous Cell #2. In July 2005, the established biofilm had a thickness of about 1 cm. At that time, three peepers were inserted in the tailings submerged in Cell #2. After a two-week equilibration period, geochemical sampling was conducted over a period of two days and included microprofiles across the overlying water–tailings interface, the sampling and retrieval of peepers and finally collection of biofilm/tailings cores.

pH and oxygen microprofiles. A micro-manipulator, consisting of a hand-operated micrometer attached to a tripod support inserted into the tailings, was used to lower the oxygen and pH electrodes incrementally across the interface. Along with the micrometer readings, the microsensor's tip position (a white dot painted close to the sensor's tip) was followed visually with the aid of a mask and a snorkel. In this way, the position of the electrode's tip could be determined relative to the tailings-water interface with a precision of ±0.5 mm. Oxygen micro-profiles were measured *in situ* using Clark-type oxygen micro-electrodes with a guard cathode (Unisense, Denmark; OX10; outer tip diameter <20 µm) and a picoampere meter (Unisense,

Denmark; PA2000). A two-point calibration was made prior to the measurements with water purged with either air or nitrogen. The pH micro-profiles were obtained with glass combination micro-electrodes from Orion Research Inc. (No. 9803BN), which were also fixed to the end of the micro-manipulator (see Appendix A for a picture of the set up). The first two oxygen and pH micro-profiles were obtained about 3.5 and 2.0 hours before sunset on July 18. The last oxygen and pH micro-profiles were measured the next day in full sunlight, 6.5 hours before sunset. The micro-manipulator was deployed at different points within the cell, to obtain the three distinct micro-profiles.

In situ **dialysis.** Water samples were collected with *in situ* samplers (porewater peepers; 1 cm vertical resolution; Gelman HT-200 polysulfone membrane, 0.2 μm nominal pore size) similar to those described by Carignan and Tessier (1985). The Plexiglas components of the peepers were kept under an N_2 atmosphere for a minimum of 15 d (Carignan *et al.* 1994), prior to filling the compartments with Milli-Q water (> 18 MΩ·cm). The assembled peepers were then further deoxygenated under a N_2 atmosphere for at least 48 h, and were also maintained under N_2 during transport to the field site. At the sampling site, peepers were inserted vertically into the tailings at three locations (10-15 m apart), using a small boat. Once in place, the peepers extended 7-9 cm above the tailings-overlying water interface; the remaining 21-23 cm were within the tailings. They were allowed to equilibrate for two weeks; no major outflow events occurred during this period.

After the equilibration period, the peepers were retrieved, rinsed with the overlying water from the cell and sampled immediately. The whole process of sampling each peeper generally took <15 min (See Appendix A for a picture of the sampling set up). Samples for dissolved sulphides (ΣH_2S) determinations were processed first to minimize losses of this unstable analyte. Samples for ΣH_2S and inorganic carbon analysis (1.5 mL) were obtained from the compartments of one of the vertical rows with N_2-purged syringes. The first 1.0 mL was injected through a septum into pre-washed 3 mL amber glass bottles, which had been purged with N_2 and contained 40 μL of N,N'-dimethyl-p-phenylenediamine sulphate (2.7 mM in 6 M HCl) and 40 μL of $FeCl_3$ (5.55 mM in 6 M HCl). These samples were maintained at 4°C in the dark during their transport to the laboratory. The remaining 0.5 mL in the syringes was injected through rubber septa into 3 mL helium-purged and pre-acidified (20 μL 10% HCl) glass vials. A second set of subsamples of approximately 0.5 mL was also retrieved from the same row of compartments with a micropipette and injected into 1.5 mL pre-washed polypropylene tubes for Cl^- and SO_4^{2-} analyses. Finally, the remaining 2 mL were collected in pre-combusted glass bottles for dissolved organic carbon (DOC) measurements. Samples of 3 mL for metals were then collected from the compartments of the second vertical row by piercing the peeper membrane with a micropipette fitted with an acid-cleaned tip; these samples were injected into pre-washed and pre-acidified (40 μL 10 % HNO_3 Anachemia ultrapur) vials. Since in 1998 porewater metals in at depth below 2.5 cm were less than 0.01, 0.2 and 5 μg L^{-1} for Cd, Cu and Zn respectively (Vigneault *et al.* 2001); porewater samples for metals were not collected at depth greater than 5.5 cm in this study. The remaining 1 mL was removed with a syringe for immediate pH measurement, using a combination glass micro-electrode and a portable pH meter. The absence of pH electrode drift was confirmed after sampling each peeper using a solution buffered at pH 7.00.

ΣH_2S were measured within 24 h of collection, by colorimetry (660 nm; Cline, 1969) in a 1 cm flowcell (Lachat Quikchem FIA+ 8000 series). Standard solutions for the calibration curve were prepared in the laboratory at the time of sampling. Cl^- and SO_4^{2-} concentrations were determined with an ion chromatography system equipped with a conductivity detector (DX-100 Gradient Chromatography Systems, Dionex, CA). An AS14 column with an AG14 pre-column and an injection loop of 25 µL were used. DOC was measured with a total carbon analyzer (TOC-V CSH, Shimadzu, Kyoto, Japan). Dissolved inorganic carbon (DIC) was determined by gas chromatography, GC, with a flame ionization detector equipped with a methanizer (CombiPal 3800, Varian, Mississauga, ON). Cu, Zn and Cd were analyzed by inductively coupled plasma mass spectroscopy, ICP-MS with a collision cell (XSeries, Thermo Electron Corporation, Winsford, UK). Other elements were measured by inductively coupled plasma atomic emission spectroscopy, ICP-AES (Vista, Varian, Mississauga, ON) using cesium chloride as an ionization suppressant and yttrium as an internal standard.

Diffusive fluxes across the tailings - overlying water interface. Diffusive fluxes of species "i" across the tailings-water interface, J_i, were calculated according to Fick's law, neglecting porewater advection:

$$J_i = -\Phi \, \tau \, D_i \, \frac{dC_i}{dx}$$

where Φ is the porosity of the tailings, τ the tortuosity, D_i the molecular diffusion coefficient and dC_i/dx is the concentration gradient. The porosity value for settled tailings of 0.4 and a tortuosity value of 0.2 were obtained from an earlier study by Li and St-Arnaud (2000) on the same tailings. Diffusion coefficients were obtained from Li and Gregory (1974) and corrected for the overlying water temperature, 27°C, according to Zhang and Davison (1995). The O_2 concentration gradients were calculated from the slope of the micro-profiles in the biofilm/tailings between 97% and 0% air saturation. O_2 diffusivity was obtained from Broecker and Peng (1974). For trace metals and anions fluxes, tracer diffusion coefficients were obtained from Li and Gregory (1974) and the mean concentrations at +0.5 cm in the overlying water and at –0.5 cm in the biofilm/tailings were used to calculate the concentration gradients.

Sequential extractions on biofilm and tailings. Following peeper retrieval, 3 cores were collected close to the peeper sampling sites, with Plexiglass coring tubes (10 cm inside diameter). The tubes were tightly closed and handled with care to minimize any perturbation of the tailings during their transport to shore. The cores were immediately extruded using a piston extruder under nitrogen to prevent oxidation (see Appendix A for a picture of the extrusion set up). Three layers were collected separately from each core: the biofilm, the uppermost 0.5 cm of tailings and 4.5 to 5 cm deep tailings (See Appendix A for a picture of a collected core). The biofilm samples were placed in a 250 mL HDPE bottle, half-filled with overlying water from the cell. The tailings samples were placed in sample bags (118 mL, Nasco Whirl-Pak®) which were then placed in larger bags filled with anoxic tailings. All samples were stored at -86°C until analysis. Before analysis, the samples were thawed, shaken gently for 30 min and then centrifuged at 12 000 g for 30 min to remove excess water. Metals in the biofilm or tailings (Cd, Cu, Zn, Mn, Fe, Ni and Pb) were partitioned into operationally defined fractions by extracting

the sample sequentially according to the methods of Tessier *et al.* (1989). Sequential extractions were conducted in parallel on a marine sediment reference material for trace metals (MESS-3, National Research Council of Canada, Ottawa, ON). For Cd, Cu and Zn, the sums of each fraction was 93 ± 1% of the expected values (Appendix B). These extractions were developed for natural oxic lake sediments and their application to biofilm or mine tailings is not straightforward, given the differences in composition between lake sediments, biofilm and mine tailings. Dold (2003) reported, for example, that secondary Cu-sulphides were dissolved along with organic phases in the oxidation step with hydrogen peroxides. Nevertheless, this sequential fractionation procedure yields results that are roughly indicative of the lability of the metals in the biofilm and submerged tailings and will allow a comparison between the 1996, 1998 and 2005 findings.

Mineralogical analysis. Subsamples of the solids from two selected tailings cores (C2 and C3) subjected to sequential extraction were examined for their mineralogical composition using a variable-pressure scanning electron microscope (VP-SEM) equipped with an energy-dispersive X-ray (EDX) analyzer. The subsamples stored at $-86^{o}C$ were depleted of their moisture content by drying overnight under vacuum in a freeze-drier. A portion of each homogenized sample was mounted as loose grains onto a circular aluminum stub (2.54 cm in diameter) with a matching double-sided carbon tape. The loose-grain mount was placed in the sample chamber of the VP-SEM and examined under the operating conditions of 20 pa air pressure, 20 keV accelerating voltage and a working distance of 21 mm. X-ray maps of As, Ca, Cd, Cu, Fe, Pb, S and Zn were first acquired over a couple of randomly selected areas of the loose-grain mount at low magnification (100X) to reveal the general distribution and abundance of these elements as well as to locate minerals of particular interest such as sulphides for more detailed analysis. The primary purpose of mineralogical analysis involved in this project was not to quantify any particular mineral phases but to detect indications of subaqueous chemical weathering and, where possible, to assess the relevant reaction mechanisms. The morphology, texture and composition of minerals of interest located by preliminary X-ray mapping were further investigated at higher magnification using secondary and back-scattered electron imaging, *in situ* EDX analysis and more refined X-ray mapping.

Molecular biology analysis. DNA was extracted from a biofilm sample, amplified, cloned and sequenced in order to identify the micro-organisms present in the biofilm and potentially infer their contribution to the observed chemical and mineralogical observations. On August 5, 2005, Louvicourt Mine personnel collected another sample of the biofilm in Cell #2. The sample was received on August 8 at CANMET-MMSL and subsampled using 6 mL syringes with cut-off tips as mini-cores. The biofilm samples were stored at $-86°C$ until their analysis at McMaster University. Genomic DNA from environmental samples was isolated using the PowerSoil DNA Isolation Kit (MO BIO Laboratories, Inc.) and subsequently amplified using PCR primer pairs 533F/1492R and 515F/1391R. PCR products were incubated at $94°C$ for 3 min, followed by 30 cycles at $55.5°C$ for 1 min, $72°C$ for 1.5 min and $94°C$ for 30 sec, followed by a single $55.5°C$ step for 1 min and a final $72°C$ elongation step for 12 min. Each 50 µL reaction contained 1X *Taq* Buffer with $(NH_4)_2SO_4$, 0.2 mM each dNTP, 2.5 mM $MgCl_2$ [4 mM $MgCl_2$ for Louvicourt gDNA], 0.4 µM each primer, 1.25 units of *Taq* polymerase and 1 µL of gDNA template [diluted 1:10 for Louvicourt gDNA]. *Taq* polymerase amplified PCR products were extracted and purified from a 0.9% agarose gel using the MinElute Gel Extraction Kit

(Qiagen) and TOPO cloned with the TOPO TA Cloning Kit for Sequencing (Invitrogen). Colonies were cultured overnight in LB medium (1% tryptone, 0.5% yeast extract, 0.5% NaCl) containing 100 µg/mL Carbenicillin and the plasmid DNAs were isolated with QIAprep Spin Miniprep Kit (Qiagen) and sequenced. A total of 27 clones were sequenced. Isolated sequences were then identified via the BLAST databank (http://www.ncbi.nlm.nih.gov/BLAST/) for nearest genomic neighbours. Sequences with greater than 95% similarities to known clones were identified.

RESULTS AND DISCUSSION

pH and dissolved oxygen microprofiles. Photosynthetic activity within the established biofilm had major impacts on pH and oxygen vertical distribution below the interface with the overlying water. There was significant production of oxygen within the biofilm giving rise to maximum dissolved oxygen concentrations a few mm below the interface (Figure 1). For example, the maximum dissolved oxygen concentration was observed at -3 mm below the biofilm interface at the highest luminosity. However, oxygen penetration was still limited to the first -5 mm to -14 mm into the biofilm/tailings depending on the luminosity conditions (Figure 1). Similar to dissolved oxygen, porewater pH was strongly affected by the photosynthetic activity of the biofilm, with a marked initial pH increase within the first 10 mm of biofilm/tailings. At -20 mm below the interface, pH was down to 7.1 compared to 8.8 in the overlying water (Figure 2). The overlying water pH measured with the semi-microelectrode, 8.8 $\pm$ 0.1, was confirmed by a measurement with a standard pH probe, 8.8 (data not shown). The effects of photosynthesis on both dissolved oxygen and pH increased with ambient luminosity. At the end of the day, no oxygen production was observed at the lowest luminosity, i.e. 5700 Lux (Figure 1). Similarly, a much smaller pH increase was observed at the lowest luminosity compared to the two higher luminosities (Figure 2). The impacts of biofilm photosynthetic activity on oxygen and pH profiles at Louvicourt were similar to those observed in natural sediments with a micro-algal cover. Ploug *et al.* (1999) reported a similar large increase in dissolved oxygen and increase in pH in the biofilm as compared to the overlying water within a colony of *Phaeocystis sp.*.

Even in the presence of intense photosynthetic activity, anoxic conditions were still observed in the tailings porewater, except for the first few mm of tailings. While the thickness of the biofilm was estimated to be 1.5 cm for the 3 cores that were collected, anoxia was observed at a maximum of 1.4 cm below the biofilm-overlying water interface. This suggests that the anoxia actually developed within the biofilm and that no or very little oxygen actually reached the tailings below the biofilm. The 2005 oxygen flux, (1.0 ± 0.2) x 10^{-11} mol cm^{-2} s^{-1}, was about 20 times higher than that measured in 1997 in the absence of photosynthetic periphyton, (1.7 ± 0.2) x 10^{-12} nmol cm^{-2} s^{-1} (Vigneault *et al.*, 2001) but still about 400 times less than the oxygen flux reported for the Louvicourt tailings in humidity test cells, 3.6 x 10^{-9} mol cm^{-2} s^{-1} (MEND 2000). Based on similar micro-scale oxygen profiles, Elberling and Damgaard (2001) reported an *in situ* oxic zone of 9 mm below the tailings–overlying water interface for 1 year old tailings deposited directly underwater at the Nanisivik Mine, NWT, Canada. This is within the 5 to 14 mm observed for the Louvicourt tailings. They also measured in the laboratory an oxygen flux of 4.5 x 10^{-11} mol cm^{-2} s^{-1} for these tailings, which is comparable to the consumption rate for the Louvicourt tailings. However, based on the estimated thickness of the biofilm and on the oxygen microprofile the increased consumption of oxygen between 1998 and 2005 is likely related to consumption of oxygen within the biofilm (i.e. respiration and organic matter decomposition) rather than tailings oxidation. Furthermore, the presence of a biofilm might also be beneficial since it could hamper tailings resuspension, which will increase the tailings oxygen consumption. For example, Yanful and Verma (1999) observed a ten-fold increase in submerged tailings oxygen consumption in a column experiment as a result of an increase of about four times in the water cover agitation speed.

Porewater pH. The porewater pH depression observed in the deeper section of the microprofile at the mm scale was also observed at the cm scale, with a minimal pH value of 7.3 at -1.5 cm (Figure 3). Below this peak, the pH increased to about 7.8 at -4.5 cm, and remained constant for the deeper pore water. The overlying and porewater pH measured on the subsamples collected by *in situ* dialysis over 2 weeks were lower than the instantaneous measurements of the pH micro-profiles (see above). The overlying water pH measured on the *in situ* dialysis samples were 8.4 ± 0.2 while the instantaneous measurements were 8.8 (Figures 2 and 3). This suggests that the overlying and pore-water pH fluctuates daily depending on the photosynthetic activity. The overlying water pH measured for the microprofile at the lowest luminosity (at the end of the day) was also lower than the pH measured for the microprofiles with the higher luminosity (Figure 2). Therefore the relatively high pH in the overlying water is likely related to photosynthetic activity in addition to the residual buffering capacity of the tailings porewater. In 1998, it was also observed that the tailings became a source of H^+ to the overlying water at night time (Vigneault *et al.* 2001). Finally, since there was no evidence of peeper misplacement or displacement, the lower pH in one of the three peepers (open circles in Figure 3) was likely related to tailings/porewater spatial heterogeneity within the experimental cell. Spatial heterogeneity was expected for the porewater and was also observed for major cation concentrations (Figure 4). The observed differences in pH in the overlying water are however surprising and in contrast with the relatively homogenous major cation concentrations, SO_4^{2-} and DOC (Figure 4 and 5). Given the strong influence of photosynthetic activity observed with the pH microprofiles, it is possible that the heterogeneous distribution of overlying water pH is related to limited mixing in the water cover and spatial variation of the photosynthetic activity within the experimental cell. At depths >6 cm below the interface with the water cover, porewater pH had always been constant and the average pH dropped from 9.5 in 1996 to 8.5 in 1998 (Vigneault *et al.* 2001) and to about 7.8 in 2005. In addition, the observed minimal pH closer to the interface slightly decreased from pH 7.75 ± 0.06 in 1998 (Vigneault *et al.* 2001) to 7.5 ± 0.1 in 2005. Therefore, the porewater pH values are affected by the photosynthetic activity but also by a gradual depletion of the porewater buffering capacity.

Porewater major cations and anions. Nine years after the construction of the experimental cells, the tailings were still acting as a source of dissolved solids for the overlying water since the porewater was still enriched with major cations and major anions (Figure 4 and 5). Ca, Mg, sodium and K concentrations in the pore water at -5.5 cm were 2-3 times higher than those in the overlying water (Figure 4). Porewater concentrations increased sharply with depth except for Ca between -3.5 and 5.5 cm, and to some extent for Mg, for which the concentrations appeared to level off in the deepest part of the profiles. It should be noted however, that the porewater Cl^- and SO_4^{2-} concentrations decreased by factors of 10 and 2.5, respectively, between 1996 and 2005. For Cl^-, the average concentration at the deepest part of the profiles (-14.5 cm in 1996 and 1998 and -13.5 cm in 2005) decreased from 25 ± 5 mg L^{-1} in 1996 to 8 ± 1 mg L^{-1} in 1998 (Vigneault *et al.* 2001) and to only 2.4 ± 0.4 mg L^{-1} in 2005. The flux of Cl^- to the overlying water could not be calculated in 2005 as the concentrations in the overlying water and for first one cm of pore water were below the detection limit of 0.6 mg L^{-1}. For SO_4^{2-}, the concentration decreased from 380 ± 10 mg L^{-1} in 1996 to 330 ± 30 mg L^{-1} in 1998 (Vigneault *et al.* 2001) and to 150 ± 30 mg L^{-1} in 2005. As in 1998, the SO_4^{2-} profile alone did not indicate any diagenetic sulphide production by SO_4^{2-} reduction, a phenomenon that has been observed at other mine sites (Martin *et al.* 2003). Nevertheless, an increase in dissolved ΣH_2S concentrations and a

concomitant decrease in dissolved Fe concentrations are observed in the deeper portion of the porewater profiles (Figure 7 and 8, respectively). In contrast to 1998 (Vigneault *et al.* 2001), no SO_4^{2-} peak was observed concomitant to the pH minimum observed at -1.5 cm in the 2005 profiles. The calculated SO_4^{2-} flux to the overlying water however remained similar in 2005 compared to 1998, (-1.9 ± 0.5) x 10^{-13} mol cm^{-2} s^{-1} compared to (-1.7 ± 0.5) x 10^{-13} mol cm^{-2} s^{-1} (Vigneault *et al.* 2001). In the earlier study, Vigneault *et al.* (2001) also noted that the SO_4^{2-} flux remained unchanged between 1997 and 1998 (unlike the case with Cl$^-$).

Compared to the overlying water, pore water was also enriched in dissolved inorganic and organic carbon. DIC concentrations at about -5 cm in the pore water were similar in 1998 and 2005 (17 ± 3 mg L^{-1} (Vigneault *et al.* 2001) and 23 ± 2 mg L^{-1} respectively) (Figure 5). As observed for pH (Figure 3), there were significant differences in DIC concentrations in the overlying water. As for pH, spatial variation in photosynthetic activity and limited mixing in the water cover could explain these variations. Although the tailings were still a source of inorganic carbon to the overlying water, the porewater concentrations increased with depth in 2005, while they decreased with depth in 1998. The opposite trend was observed for organic carbon. While the shape of DOC concentration profiles remained similar, the concentrations at -5.5 cm greatly increased from about 3 mg L^{-1} in 1998 (unpublished data, INRS-Eau) to 34 mg L^{-1} in 2005 (Figure 5). The absorptivity of dissolved organic matter in the overlying water and in the porewater was much higher than that for the leachate from the filtration membrane (Figure 6). Therefore, the elevated DOC concentrations were not related to contamination from the HT Tuffryn filtration membrane used in the peepers. The difference in DOC concentration between the overlying water and the pore water was small and the production of large quantities of DOC within the tailings was unlikely. It is assumed that organic carbon was produced in the overlying water and in the biofilm, and that flushing of the water cover reduced the overlying water concentrations. Porewater advection could have also contributed to the slightly higher concentrations of organic carbon in the pore water compared to the overlying water.

Porewater ΣH$_2$S, Fe and Mn. Porewater ΣH$_2$S concentrations observed in 2005 were much lower than those previously observed. ΣH$_2$S concentrations increased with depth below -1.5 cm in the tailings (Figure 7). This coincides with the depth at which the tailings porewater became anoxic. The ΣH$_2$S profiles indicate spatial heterogeneity with one of the three peepers having non-detectable ΣH$_2$S concentrations at -7.5 cm and deeper in the tailings. The maximum observed concentration was 0.09 μM at -13.5 cm. This is far less than the concentration measured at similar depth in 1998, 1.3 ± 0.3 μM (Vigneault *et al.* 2001). As a result of the anoxic conditions, dissolved Fe, and also dissolved Mn concentrations increased in the tailings porewaters, achieving a maximum at -2.5 cm (Figure 8). Porewater profiles for Fe and Mn remained similar to those previously observed. The maximum dissolved Fe concentration in 2005 was 0.5 ± 0.1 mg L^{-1} (Figure 7) compared to 0.4 ± 0.2 in 1998 (Vigneault *et al.* 2001). Similarly, the maximum dissolved Mn concentrations in 2005 and 1998 were 0.38 ± 0.08 mg L^{-1} and 0.18 ± 0.07, respectively. Above this peak, Fe and Mn were most likely removed from porewater by oxidation and the precipitation of oxy-hydroxides. Deeper in the tailings, Fe concentrations decreased, presumably through the precipitation as sulphides.

In contrast to Fe, it is unlikely that Mn precipitated as sulphide deeper in the porewater. Ion Activity Products (IAP) were compared with the solubility products of Mn solid phases to

identify possible processes that could explain the disappearance of this metal from interstitial waters at depths >2.5 cm in the tailings. Ion activities were calculated with the computer code WHAM VI (Tipping 1998) from the 1998 measured concentrations, assuming that the DOC is composed exclusively of fulvic acid with a carbon content of 50% (i.e. using the DOC concentration as the fulvic acid concentration). The original WHAM VI thermodynamic database was modified to include a thermodynamic constant for HS^- (see Huerta-Diaz *et al.* 1998). The IAP calculations suggest that the porewater was strongly under-saturated with respect to Mn sulphide or carbonate. As suggested by Huerta-Diaz *et al.* (1998) for two Canadian Shield lakes, the adsorption of Mn to FeS(s) and the co-precipitation of Mn with FeS(s) could be responsible for the observed trapping of dissolved Mn below 2.5 cm in the tailings, rather than the precipitation of distinct Mn sulphide or carbonate solid phases.

Porewater trace metals. Cu, Zn and Cd were generally mobilized within the first 2 cm of tailings (Figure 9). The higher dissolved Zn and Cd concentrations observed in one of the three peepers may be related to higher levels in the tailings at this location of the experimental cell. The tailings acted as a source of trace metals with relatively low fluxes to the overlying water of $(-8 \pm 5) \times 10^{-17}$, $(-7 \pm 3) \times 10^{-17}$ and $(-4 \pm 2) \times 10^{-19}$ mol $cm^{-2} \cdot s^{-1}$ for Cu, Zn and Cd, respectively (Table 1). Simultaneously, Cu diffused out of tailings to the overlying water, although there was no evidence of Cu flux to the overlying water in 1998. However, the fluxes for Zn and Cd to the overlying water were an order of magnitude lower than those obtained in 1998. The maximum Cd and Zn porewater concentrations were similar in 1998 and 2005, i.e. about 0.4 and 30 µg L^{-1} for Cd and Zn respectively. Aside from the flux of Cu to the overlying water, an important change in the porewater profiles was that for all three metals the porewater concentrations were still detectable at -5.5 cm in the tailings (Figure 9), i.e. higher than 0.3, 0.4 and 0.4 µg L^{-1} for Cd, Cu and Zn, respectively. In contrast, the trace metal concentrations in the porewater deeper than 3.5 cm were all below the detection limits in 1998 (Vigneault *et al.* 2001), which were 0.01, 0.2 and 5 µg L^{-1} for Cd, Cu, and Zn, respectively. The higher dissolved Cu, Zn and Cd concentrations were likely related to the observed lower pH and lower ΣH_2S concentrations which favour the solubility of metal sulphides.

Nevertheless, it should be noted that the Cu, Cd and Zn fluxes observed in 2005 at Louvicourt were several orders of magnitude lower than the fluxes reported at other sites (e.g. Heath Steele Mine (Gravel and Poirier 2006), Lago Junin, Peru (Martin *et al.* 2001) or Detour Lake Mine (Martin *et al.* 2003)). For the 1.05×10^6 m^2 tailings impoundment and assuming a water cover of 1 m with a 1 year residence time, metal concentrations in the overlying water resulting from the diffusive fluxes would be in the order of 2, 1 and 0.01 µg L^{-1} for Cu, Zn and Cd, respectively. These concentrations are well below discharge limits for mine effluents (e.g. Metal Mining Effluent Regulations). Furthermore, such concentrations are equal to or lower than water quality guidelines for the protection of aquatic life for the measured hardness of the overlying water (CCME 2006), i.e. 2, 30 and 0.8 µg L^{-1} for Cu, Zn and Cd, respectively. The estimated Cd concentration, 0.01 µg L^{-1}, is also lower than the interim guideline of 0.017 µg L^{-1} proposed by the CCME (2006).

Sequential chemical extractions on the biofilm and submerged tailings. The analysis of Cd, Cu and Zn in solid samples of the biofilm and tailings provides further insight into the fate of these metals. First, it should be noted that the total concentrations were similarly elevated in

the biofilm, the surface tailings and anoxic tailings for Cd and Zn (Table 2). For Cu however, the biofilm and surface tailings were impoverized compared to the anoxic tailings, 750 ± 100 mg kg[1] compared to 1070 ± 10 mg kg^{-1} for the surface tailings and 1420 ± 50 mg kg^{-1} for the deeper tailings. The elevated concentrations of metals in the biofilm were likely related to the entrapment of tailings particles and secondary oxide precipitates. Since metal contents were expressed as dry weight, the elevated metal concentrations could also be related to some extent to density of the biofilm, i.e. to its elevated water content compared to the tailings. For all three metals the total concentrations in the surface tailings were similar to the levels measured in 1996 and 1998 (Vigneault *et al.* 2001). Cd and Zn were clearly more labile in the biofilm than in the tailings. Only 6.6% of the total Cd was associated with the residual and oxidizable fractions (fractions 5 and 6) compared to 39% and 60% for the surface and anoxic tailings respectively (Table 2). The same trend was observed for Zn, with 20% of the total concentrations in the biofilm being found in the residual and oxidizable fractions and with 65% and 63% for the surface tailings and the anoxic tailings respectively (Table 2). For Cd and Zn, the two most important fractions in the biofilm were the acid-exchangeable (fraction 2) and the reducible fraction presumably associated with Mn-oxyhydroxides (fraction 4). This was not the case for Cu, which remained predominantly associated with organics and sulphides (Dold 2003) (fractions 5 and 6), i.e. 81%, 98% and 90% of the total concentration for the biofilm, the surface tailings and the anoxic tailings respectively.

From 1996 to 2005, Cd in the surface tailings became more concentrated in the more labile solid fractions while Cu and Zn moved to the less labile fractions. Over the seven year period, Cd has tended to move from the more refractory to the more labile fractions. Exchangeable Cd (fraction 1) was higher in 2005 compared to 1996 (Figure 10). The relative proportion of Cd in the more labile fractions (fractions 1 to 4) was also higher in 1998 compared to 1996 (Figure 10). However, it is assumed that these fractions effectively trapped the Cd since the overall flux of Cd to the overlying water greatly decreased from 1998 to 2005 (Table 1). In contrast, the portion of metals in the more labile fractions (fractions 1 to 4) for Cu, and to a lesser extent for Zn, decreased from 1996 to 2005 (Figure 10). The proportion of Cu associated with the less labile fractions (fractions 4 and 5) increased from 90% in 1996 and to 93% in 1998 (Vigneault *et al.* 2001), and to 98% in 2005. In contrast, a switch to a net efflux of Cu to the overlying water was observed in 2005 (Table 1). Complexation of Cu by the elevated porewater organic carbon concentrations (Figure 5) likely contributed to the elevated total dissolved Cu concentrations, which would have increased the diffusive flux to the overlying water. The assumption that there was important complexation of Cu in the dissolved phase is supported by estimations with WHAM VI which indicate that free Cu activity in the tailings porewater would be roughly four orders of magnitude lower if organic carbon was excluded from the calculations.

Mineralogical analysis of the biofilm and submerged tailings. Although the sampled solids, especially those associated with the biofilm layer, were locally heterogeneous in their mineralogical make-up, a general change in mineralogy was apparent with depth. There was a gradual depletion of sulphides towards the water/tailings interface. Pyrite was by far the most abundant sulphide mineral occurring in the samples examined. It showed an increasing degree of alteration with decreasing depth to Fe oxyhydroxide, which dominated the Fe-containing minerals in the biofilm layer. In contrast, fresh pyrite was more abundant than partially weathered material in the 4.5-5.0 cm samples. However, grain morphology appeared to play a

very significant role in pyrite weathering. For example, Figure 11 shows a euhedral pyrite grain at the tailings-biofilm interface in the form of pyritohedron that remained intact while other subhedral to anhedral grains in the same sample invariably showed some degree of alteration to Fe oxyhydroxide.

Two other sulphides, sphalerite and chalcopyrite, were confirmed to occur in the tailings profiles in trace amounts, except in the biofilm layer. Sphalerite typically occurs as isolated grains that show varying extents of dissolution (Figure 12). Rarely, it is also found as intensively corroded grains associated with pyrite (Figure 13). Chalcopyrite typically occurs as very small (<5 μm across) anhedral grains either by itself or associated with pyrite and sphalerite (Figure 14). In several general X-ray maps of selected areas, Cu was found spatially associated with Fe, S and Zn, suggesting that it may substitute for Fe and Zn in pyrite and sphalerite, respectively, or it may occur as chalcopyrite as widely dispersed, submicroscopic exsolved blebs in the two sulphides. Other minerals identified in the cursory probing of the loose-grain mounts by means of EDX analysis included quartz, chlorite, mica (muscovite + biotite), carbonates (calcite and ankerite), Fe oxyhydroxide, apatite and traces of pyrrhotite. The identification of these minerals is mainly based on their composition (i.e. elemental ratios) and crystal shape, where evident. A complete set of electron images, X-ray maps and EDX spectra acquired in the mineralogical analysis is provided in Appendix C.

The observation of intensively corroded sphalerite in contact with pyrite suggests that galvanic interaction may have been operative in the sulphide oxidation process. Remnant sphalerite not in contact with pyrite is usually characterized by a more angular crystal outline, suggestive of less aggressive dissolution (Figures C18, C26 and C27 in Appendix C). Given that sphalerite has a considerably lower electrode potential than pyrite (Kwong *et al.* 2003; Hita *et al.* 2006), it is conceivable that the current reduced Zn efflux to the overlying water compared to the last sampling event seven years ago was caused by the progressively decreasing dominance of preferential dissolution of sphalerite. In the last seven years, most of the sphalerite in contact with pyrite was weathered out, such that only isolated, fully liberated grains remained. It is not clear if the apparent galvanic interaction between pyrite and sphalerite observed at depths depleted in oxygen (Figure 1) was caused by oxidants other than dissolved oxygen (Sato 1992) or if the observed texture was a relic snapshot of the weathering process prior to the complete depletion of dissolved oxygen in the tailings. Chalcopyrite also has a comparable but slightly lower electrode potential than pyrite (Kwong *et al.* 2003). The chalcopyrite-sphalerite couple could also have also contributed to the greater Zn efflux observed soon after the installation of the field cells. With the gradual depletion of the pyrite-sphalerite and chalcopyrite-sphalerite galvanic couples, the interaction between pyrite and chalcopyrite became more prominent despite the relatively small difference in electrode potential between the galvanic pair. This interaction could have led to the small efflux of Cu to the overlying water detected in the recent monitoring study.

Molecular biology analysis of the biofilm. As shown in Table 3, the diversity of the Louvicourt biofilm community based on 27 identified sequences was fairly high, which indicated a robust biofilm community. Phylogenetic results can give some insight into likely metabolic function based on similarities to known organisms (from BLAST and ARB databases), although these are inferred only based on closest known relatives in the databank. However, the results are

consistent with a foodchain that includes a strong, and diverse phototrophic component of different organisms from a number of bacterial groups (Chloroflexi, Cytophagales (Bacteriodetes), and cyanobacteria), which comprised approximately 26% (7 clones) of the total number of clones sequenced (27; Figure 15). A very enigmatic Bacterial group, the Planctomycetales, comprised 33% (9 clones) of the total clone library diversity of the biofilm (Figure 15). The Planctomycetales show divergent morphology and ultrastructure compared to both Bacteria and Archea and while widely spread in aquatic and soil environments, their possible metabolic function is not widely described. However, they are implicated in methanogenic consortia (CO_2 reduction to CH_4) as well as involved in anaerobic ammonia oxidation and lithotrophy. In addition, a variety of heterotrophs, decomposing fungi (2 clones), chemoorganoheterotrophy (1 clone), as well as a Eukaryotic amoebic grazer (1 clone) also occurred (Table 3, Figure 15). There were 7 clones which comprised 26% of the community, whose function could not be ascertained. These clones included members of Proteobacteria (3 clones), Acidobacteria, (3 clones) a newly described division of Bacteria widely found in acidic environments, as well as one Verrumicrobia clone. The Verrumicrobia clone occurs within a recently described phylum of bacteria that are not yet well described, although known strains commonly form symbiotic relationships with Eukaryotic organisms.

These results confirm that photosynthesis carried out by a variety of phototrophic organisms drove the high oxygen saturation observed in the biofilms during lighted periods. During non-lighted periods, when respiration dominates, methanogenesis and/or anaerobic ammonia oxidation or lithotrophy (carried out by the Planctomycetales) might have occurred. The aerobic heterotrophs, the amoeba grazer and the fungi would likely migrate within the biofilm over diel periods associated with fluctuating oxygen conditions and might be responsible for recycling organic wastes as well as controlling bacterial populations. It is interesting to note that a fairly high proportion of acidophilic organisms, the Acidobacteria (3 clones, 9%; Table 3, Figure 15), still occurred within the biofilm despite the current high pH levels. Many of the identified sequences are consistent with environmental organisms known to be metal tolerant.

CONCLUSIONS

Overall assessment of the long term performance of the shallow water cover. The mineralogical and chemical data indicate that mobilisation of trace metals occurred in the surface tailings but that the overlying biofilm effectively trapped the released metals. Several independent observations suggest that the high concentrations of dissolved oxygen prevalent at the water-tailings interface led to the oxidation of the first few mm of the surface tailings. The porewater profiles exhibit peaks of dissolved metals and the mineralogical analysis provide evidence of oxidation affected by galvanic interactions within the surface tailings. While oxidation might have extended to as much as 1-2 cm below the water-tailings interface, the biofilm itself was about 1.5 cm thick. However, Cd and Zn fluxes to the overlying water decreased significantly from 1998 to 2006. In parallel, the mineralogical analyses revealed a high abundance of Fe-oxyhydroxide in the biofilm layer and surface tailings, and high concentrations of Cd and Zn were found by sequential extraction in the biofilm in the more labile fractions (fractions 1 to 4). The mobilized Cd and Zn were therefore likely captured by adsorptive processes within the biofilm. The sequential extractions and indirectly the mineralogical analyses suggest, however, that Cu was associated with organic matter in the biofilm. This accounts for the very small net release of metals to the overlying water, which is estimated to have little impact on the overlying water quality and has allowed discharge at the outflow within prescribed limits.

It should be noted that the system had not reached equilibrium after nine years of operation. The tailings still acted as a net source of dissolved solids to the overlying water. Furthermore, significant differences were observed between the 1998 and 2005 in the deeper portion of the porewater profiles. Notably, porewater pH and ΣH_2S concentrations decreased from 1998 to 2005. This could have led to the observed increase in the porewater Cu, Cd and Zn concentrations. These changes suggest that with time the system would continue to evolve towards more natural conditions with near-neutral pH and lower major cation concentrations and that the biofilm would further contribute to the development of anoxic conditions with the decomposition of organic matter produced by the autotrophic organisms.

Finally, the pH and oxygen microprofiles and the molecular biology analysis indicate that the biofilm was a highly dynamic system in terms of vertical stratification and temporal variation. The biofilm acted both as a source and a sink of H^+ and oxygen and had a diverse and robust microbial food web that included photosynthesizers, decomposers, and grazers from a variety of microbial groups. During the day, oxygen was produced within the biofilm and the depth of oxygen penetration varied greatly depending on the luminosity conditions. At the same time, the OH^- production associated with photosynthetic activity greatly increased the pH. Respiration within the biofilm consumed the oxygen at night time and potentially methanogenesis and/or anaerobic ammonia oxidation could occur (insights from molecular biological characterization of biofilm community structure) along with bulk respiration. The biofilm/tailings also became a source of H^+ to the overlying water at night. Compared to a deeper water cover, which does not allow sufficient light to reach the tailings surface, it can be assumed that biofilm development in a shallow water cover is beneficial since it will protect tailings from resuspension, trap mobilized metals before they reach the overlying water and allow a more

rapid formation of an organic layer over the tailings that will contribute to maintenance of anoxic conditions.

Recommended future work. While current study results demonstrate that a water cover over "fresh" reactive tailings that have been colonized by a superficial biofilm act as a geochemical barrier to long-term oxidation, a number of questions remain unanswered. Given the observed physical characteristics of the biofilm, it was assumed that the biofilm would limit or even prevent wind-induced tailings resuspension. However, this was not evaluated under the objectives of the current study. It would be useful for future impoundment design to quantify the protective effect of tailings-water interfacial biofilm development, especially over the entire tailings impoundment. The effect of water depth was also not the focus of the current study. However, it is conceivable that the presence of a biofilm layer could compensate for the increased potential for resuspension in shallow water covers, which is the main disadvantage of limiting the depth of overlying water. This study was conducted on the Louvicourt Mine experimental cells and assumed that the collected data could be extrapolated to the actual tailings impoundment. However, physical and geochemical conditions in the actual Louvicourt impoundment or at other sites will vary, and the extent to which such factors as pH, oxygen, water clarity, influence of biofilm development, biofilm stability and biofilm protection from tailings metal loss need to be evaluated. It would be useful, for example, to investigate the effect of variable depths on the capacity of periphyton to colonize the tailings, the nature of the biofilm communities involved and their relative abilities to maintain tailings as metal sink.

These questions are also linked to the most interesting applied outcome of this study. Namely, using engineered biofilm layers to limit oxidation by artificially promoting the growth of periphyton at the surface of submerged tailings. The collected data indicate that under the conditions evaluated, a fully established biofilm consumes oxygen and traps dissolved metals. Thus, under the physical and geochemical conditions of this study, biofilm promotion would be beneficial for tailings management. However, conditions that affect biofilms such as available light and nutrients availability should be evaluated for biofilm development. Furthermore, a better understanding of the mechanisms involved in the interactions between the biofilm microbial community and trace metals could allow a proper selection of microbial species that would maximize the beneficial impacts of the engineered biofilm layer.

ACKNOWLEDGEMENTS

REFERENCES

Broecker, W.S. and Peng, T.-H. 1974. Gas exchange rates between air and sea. Tellus **26**: 21-34.

Carignan, R., St-Pierre, S., and Gächter, R. 1994. Use of diffusion sampler in oligotrophic lake sediments: Effects of free oxygen in sampler material. Limnol. Oceanogr. **39**: 468-474.

Carignan, R. and Tessier, A. 1985. Zn deposition in acid lakes: The role of diffusion. Science **228**: 1524-1526.

CCME. 2006. Canadian Water Quality Guidelines for the Protection of Aquatic Life – Summary Table Update 6.0.1. Canadian Council of the Ministers of the Environment, Winnipeg, Manitoba.

Cline, J.D. 1969. Spectrophotometric determination of hydrogen sulfide in natural waters. Limnol. Oceanogr. **14**: 454-458.

Dold, B. 2003. Speciation of the most soluble phases in a sequential extraction procedure adapted for geochemical studies of Cu sulfide mine waste. J. Geochem. Explor. **80**: 55-68.

Elberling, B. and Damgaard, L.R. 2001. Microscale measurements of oxygen diffusion and consumption in subaqueous sulfide tailings. Geochim. Cosmochim. Acta **65**: 1897-1905.

García-Meza, J.V., Barrangue, C., and Admiraal, W. 2005. Biofilm formation by algae as a mechanism for surviving on mine tailings. Environ. Toxicol. Chem. **24**: 573-581.

Gravel, J. and Poirier, P. 2006. Heath Steele Tailings Area: Field Assessment Miramichi, New Brunswick. SNC-Lavalin Environment Inc. No. M-6817 (603508).

Hita, R., Torrent, J., and Bigham, J.M. 2006. Experimental oxidative dissolution of sphalerite in the aznalcóllar sludge and other pyritic matrices. J. Environ. Quality **35**: 1032-1039.

Huerta-Diaz, M.A., Tessier, A., and Carignan, R. 1998. Geochemistry of trace metals associated with reduced sulfur in freshwater sediments. Appl. Geochem. **13**: 213-233.

Kwong, Y.T.J., Swerhone, G.W., and Lawrence, J.R. 2003. Galvanic sulfide oxidation as a metal-leaching mechanism and its environmental implication. Geochem. Explor. Environ. Anal. **3**: 337-343.

Li, M., and St-Arnaud, L. 2000. Reactivity assessment and subaqueous oxidation rate modelling for Louvicourt tailings - Final Report. MEND Report No. 2.12.1.d, Natural Resources Canada. CANMET. Mine Environment Neutral Drainage Program. Ottawa, ON, Canada.

Li, Y.H. and Gregory, S. 1974. Diffusion of ions in sea water and in deep-sea sediments. Geochim. Cosmochim. Acta **38**: 703-714.

Martin, A.J., Jambor, J.L., Pedersen, T.F., and Crusius, J. 2003. Post-depositional behavior of Cu in a metal-mining polishing pond (East Lake, Canada). Environ. Sci. Technol. **37**: 4925-4933.

Martin, A.J., McNee, J.J., and Pedersen, T.F. 2001. The reactivity of sediments impacted metal-mining in Lago Junin, Peru. J. Geochem. Explor. **74**: 175-187.

MEND 1990. A preliminary assessment of subaqueous tailings disposal in Mandy Lake. Mine Environment Neutral Drainage Program, Natural Resources Canada, Ottawa, Ontario, MEND Project 2.11.1a-d.

MEND 1991. A preliminary biological and geological assessment of subaqueous tailings disposal in Benson Lake, British Columbia. Mine Environment Neutral Drainage Program, Natural Resources Canada, Ottawa, Ontario, MEND Project 2.11.1c-a.

MEND 2000. Reactivity assessment and subaqueous oxidation rate modeling for Louvicourt tailings. Mine Environment Neutral Drainage Program, Natural Resources Canada, Ottawa, Ontario, MEND Project 2.12.1d.

MEND 2001. Subaqueous disposal of reactive mine tailings at Louvicourt Mine test cells: geochemical sampling and analysis. Mine Environment Neutral Drainage Program, Natural Resources Canada, Ottawa, Ontario, MEND Project 2.12.1c.

MEND 2002. Evaluation of man-made subaqueous disposal option as a method for controlling the oxidation of sulphide minerals. Synthesis Report. Mine Environment Neutral Drainage Program, Natural Resources Canada, Ottawa, Ontario, MEND Project 2.12.1a.

Ploug, H., Stolte, W., Epping, E.H.G. and Jorgensen, B.B. 1999. Diffusive boundary layers, photosynthesis, and respiration of the colony-forming plankton algae, *Phaeocystis sp.* Limnol. Oceanogr. **44**: 1949-1958.

Ravenschlag, K., Sahm, K., and Amann, R. 2001. Quantitative molecular analysis of the microbial community in marine arctic sediments (Svalbard). Appl. Environ. Microbiol. **67**: 387-395.

Sato, M. 1992. Persistency-field Eh-pH diagram for sulfides and their application to supergene oxidation and enrichment of sulfide ore bodies. Geochim. Cosmochim. Acta **56**: 3133-3156.

Tessier, A., Campbell, P.G.C., and Bisson, M. 1979. Sequential extraction procedures for the speciation of particulate trace metals. Anal. Chem. **51:** 301-312.

Tessier, A., Carignan, R., Dubreuil, B., and Rapin, F. 1989. Partitioning of Zn between the water column and the oxic sediments in lakes. Geochim. Cosmochim. Acta **53**: 1511-1522.

Tipping, E. 1998. Humic ion-binding model VI: an improved description of the interactions of protons and metal ions with humic substances. Aquat. Geochem. **4**: 3-48.

Vigneault, B., Campbell, P.G.C., Tessier, A., and De Vitre, R. 2001. Geochemical changes in sulfidic mine tailings stored under a shallow water cover. Water Res. **35**: 1066-1076.

Wallmann, K., Kersten, M., Gruber, J., and Forstner, U. 1993. Artifacts in the determination of trace metal binding forms in anoxic sediments by sequential extraction. Intern. J. Environ. Anal. Chem. **51**: 187-200.

Warren, L.A. 2005. Biofilms and metal geochemistry: the relevance of micro-organism induced geochemical transformations. In: Gadd, G.M., Semple, K.T. and Lappin-Scott, H.M. (Eds.) Micro-organisms and Earth Systems- Advances in Geomicrobiology. Cambridge University Press, Cambridge, pp. 11-34.

Yanful, E.K. and Verma, A. 1999. Oxidation of flooded mine tailings due to resuspension. Can. Geotech. J. **36**: 826-845.

Zhang, H. and Davison, W. 1995. Performance characteristics of diffusion gradients in thin films for the *in situ* measurement of trace metals in aqueous solution. Anal. Chem. **67**: 3391-3400.

Table 1. Comparison of calculated diffusive flux for dissolved trace metals across the tailings – overlying water interface in 2005 (this study) with fluxes obtained in August 1998 (Vigneault *et al.* 2001). Positive fluxes indicate an ion that diffuses from the overlying water into the tailings, whereas negative fluxes correspond to diffusion out of the tailings into the overlying water. Values are mean $\pm$ SD, n = 4 (1998) and n = 3 (2005).

Metal	Diffusive Flux (mol $\cdot$ cm^{-2} $\cdot$ s^{-1})	
	Aug. 1998	July 2005
Cu	(9 ± 5) x 10^{-17}	(-8 ± 5) x10^{-17}
Zn	(-6 ± 2) x 10^{-16}	(-7 ± 3) x 10^{-17}
Cd	(-4 ± 2) x 10^{-18}	(-4 ± 2) x 10^{-19}

Table 2. Sequential extraction of metals from biofilm, surface tailings (upper 0.5 cm of tailings) and anoxic tailings (4.5 to 5.0 cm deep tailings) with (1) $MgCl_2$, (2) acetate buffer at pH 5, (3) $NH_2OH \cdot HCl$ at room temperature, (4) $NH_2OH \cdot HCl$ at 96°C, (5) H_2O_2 and (6) HF, HNO_3 and $HClO_4$. Value are mean ± SD, n = 3.

Fraction	Solid-phase concentrations of metal (mg · kg^{-1})								
	Cu in Biofilm	Cu in Surface tailings	Cu in Anoxic tailings	Cd in Biofilm	Cd in Surface tailings	Cd in Anoxic tailings	Zn in Biofilm	Zn in Surface tailings	Zn in Anoxic tailings
1 (%)	12.7 ±0.6 (1.69)	0.6 ±0.2 (0.05)	0.17 ±0.03 (0.014)	1.4 ±0.3 (16)	1.06 ±0.04 (13.4)	0.15 ±0.03 (1.9)	29 ±7 (1.2)	13 ±1 (0.54)	1.4 ±0.3 (0.058)
2 (%)	90 ±10 (12)	13 ±1 (1.3)	129 ±23 (10)	2.9 ±0.5 (33)	1.7 ±0.1 (21)	1.9 ±0.3 (24)	600 ±100 (26)	320 ±30 (13)	420 ±80 (18)
3 (%)	5 ±5 (0.7)	5 ±3 (0.5)	0.5 ±0.5 (0.04)	0.3 ±0.3 (4)	0.30 ±0.03 (3.8)	0.17 ±0.01 (2.1)	100 ±100 (4)	56 ±5 (2.2)	44 ±4 (1.9)
4 (%)	36 ±4 (4.8)	8.8 ±0.8 (0.83)	0.65 ±0.09 (0.052)	3.5 ±0.2 (40)	1.8 ±0.4 (22)	1.0 ±0.3 (12)	1150 ±90 (48)	500 ±100 (21)	390 ±90 (17)
5 (%)	500 ±70 (67)	500 ±100 (46)	950 ±30 (77)	0.5 ±0.1 (6)	2.1 ±1.0 (27)	4.5 ±0.3 (56)	150 ±30 (6.4)	500 ±200 (20)	1060 ±70 (45.4)
6 (%)	100 ±50 (14)	500 ±100 (52)	150 ±30 (13)	<0.05 (<0.6)	1.0 ±0.3 (12)	0.3 ±0.3 (4)	300 ±100 (14)	1100 ±100 (45)	420 ±80 (18)
Total	700 ±100	1070 ±10	1420 ±50	9 ±1	7.9 ±0.3	8.1 ±0.4	2400 ±300	2500 ±40	2350 ±70

Table 3. Micro-organisms identified in a biofilm sample (collected August 8, 2005) based on the molecular biology analysis and inferred metabolisms. Results show sequence identification from BLAST, with greater than 95% similarity to known sequences in the databank. Inferred or known metabolism was given, where possible.

Organism	*#clones*	*inferred/known metabolism*
Proteobacteria	1	uncultured bacterium clone I-4
Alphaproteobacteria	2	uncultured S-N(0)-25B related to Rhodobacter sp. EMB174 (phototroph),
		AKYG679 recovered from soil adjacent to silage storage bunker
Planctomycetales	9	clone SM1A02 Angel Terrace, Mammoth Hotsprings, Yellowstone, 6 clones YCC52
		geothermal spring (Tibet), UASB_TL4 from methanogenic consortium, uncultured
		clone AKYG1739
		(aquatic bacteria, unique combinations of morphological and ultrastructural properties
		such as membrane-bound nucleus, budding replication lack of peptidoglycan in cell wall)
		involved in methane cycle - methanogens; autotrophs (lithotrophs)
		also in anaerobic ammonium oxidation (removes ammonia from waste waters)
Chloroflexi	4	anoxygenic photosynthesizers, filamentous, facultatively aerobic
(Eubacteria; class Chloroflexi)		hypersaline microbial mat clone 01D2Z74, 3 clones uncultured AKYH1397
Bacteroidetes	2	Cytophagales/green sulphur bacteria clone 500M1 H6
		uncultured bacterium Saprospiraceae mostly aerobic chemoorganoheterotrophs
Acidobacteria	3	new division of Bacteria - widely occurring in acidic environments - function not really well known
Cyanobacteria	2	phototrophs, uncultured clone 100M2_A2, clone 100M2_H9
Verrucomicrobia	1	clone 1hac19
		recently described phylum of bacteria - some form symbiotic relationships with Eukaryotes
		widely spread soils/waters
Acanthamoeba castellanii mitochondrion	1	free living amoeba (Eukaryote)
Paecilomyces sp	1	Fungus
Acremonium	1	hyphomycete - filamentous fungus clone KR21-2
Total Clones	*27*	
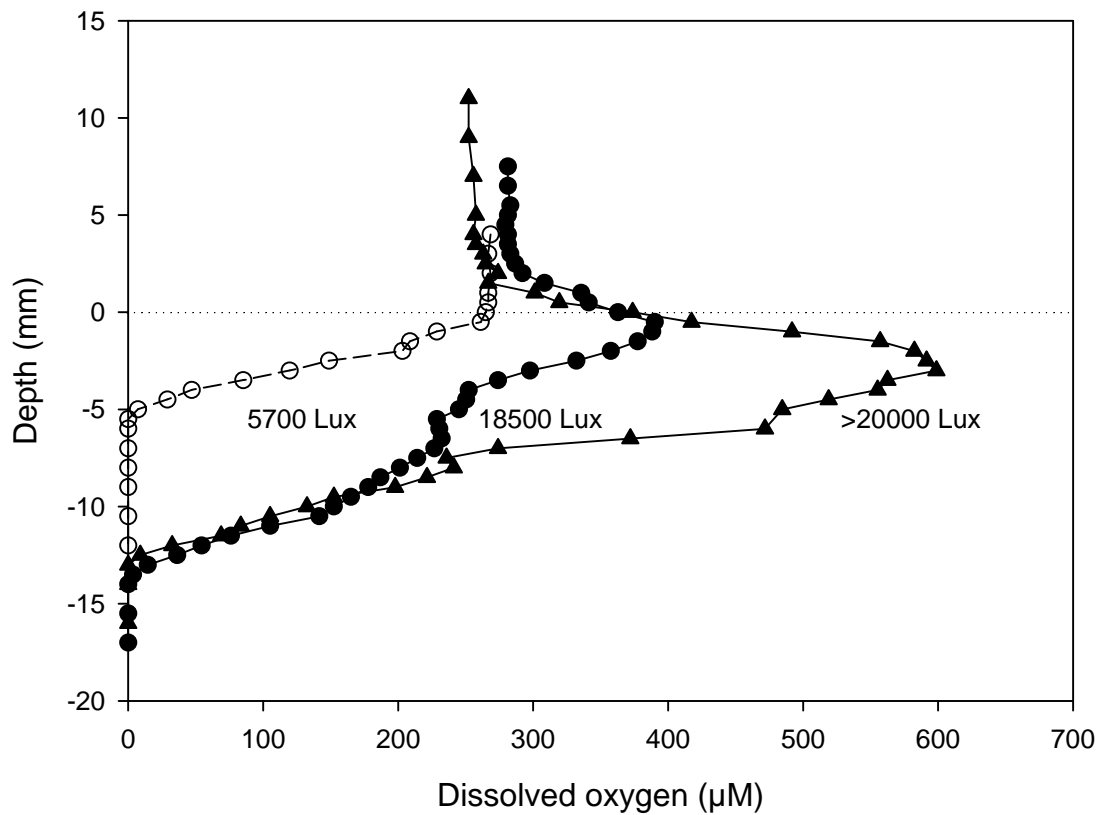
Figure 1   Porewater oxygen microprofiles (0.5 mm vertical resolution) sampled using an oxygen microelectrode. The horizontal broken line indicates the biofilm/tailings-overlying water interface. Each curve was obtained under different light conditions, 6.5, 3.5 and 2.0 hours before sunset (with measured luminosity of > 20000, 18500 and 5700 Lux respectively).
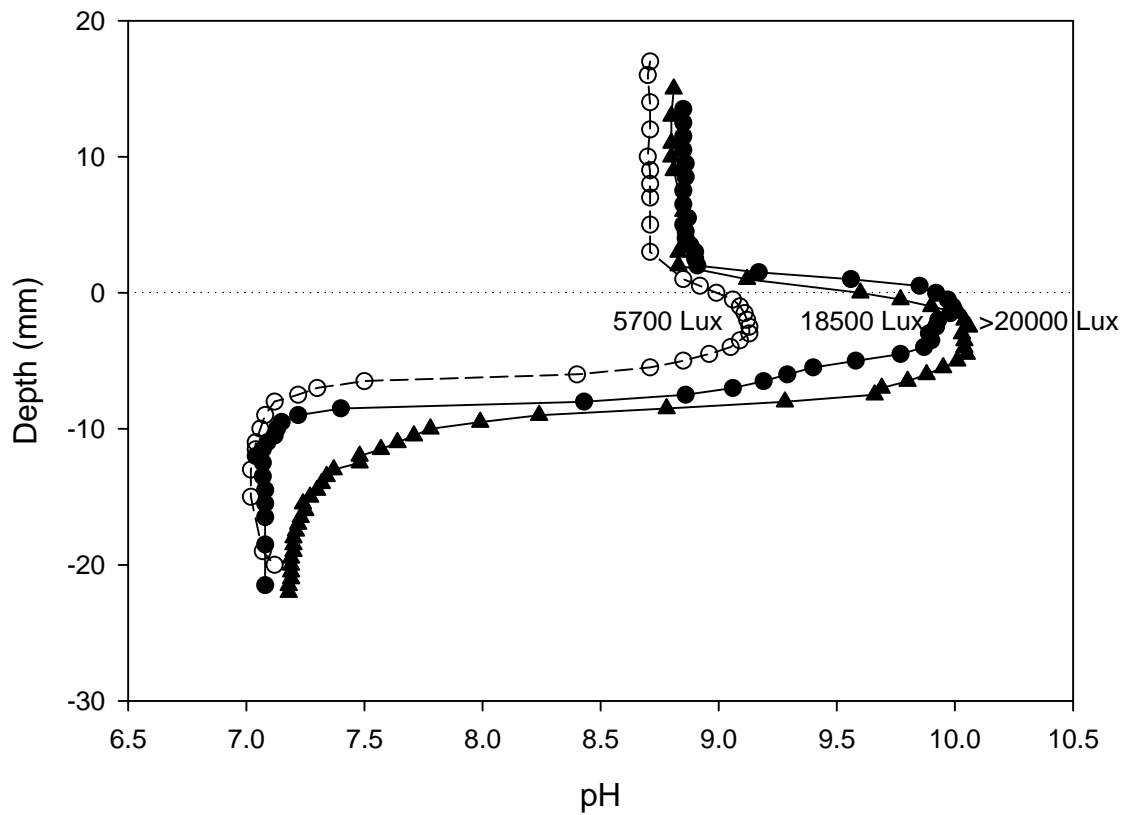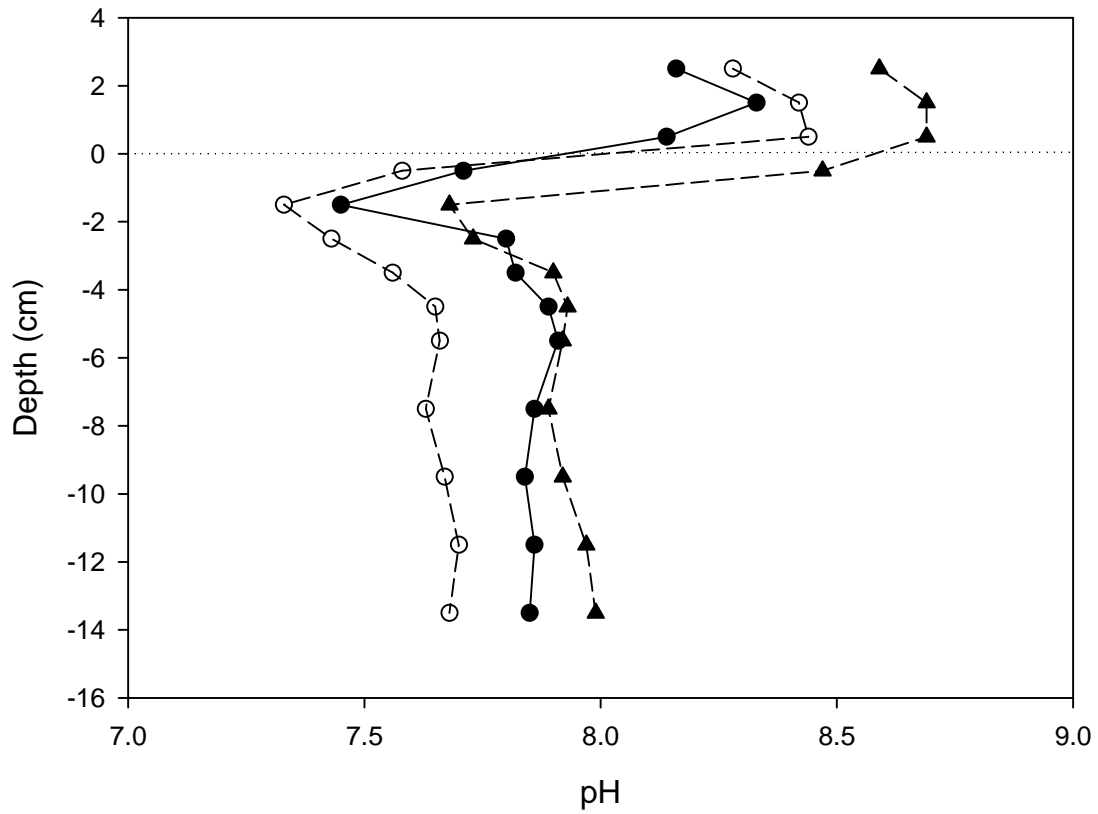
Figure 2   Porewater pH microprofiles (0.5 mm vertical resolution) sampled using a semi-micro pH electrode. The horizontal broken line indicates the biofilm/tailings-overlying water interface. Each curve was obtained at different light conditions, 6.5, 3.5 and 2.0 hours before sunset (with measured luminosity of > 20000, 18500 and 5700 Lux respectively).

Figure 3   Porewater pH profiles as sampled by *in situ* dialysis (1 cm vertical resolution). The horizontal broken line indicates the biofilm/tailings-overlying water interface. Each curve is from an individual peeper inserted into the tailings and allowed to equilibrate for 2 weeks.
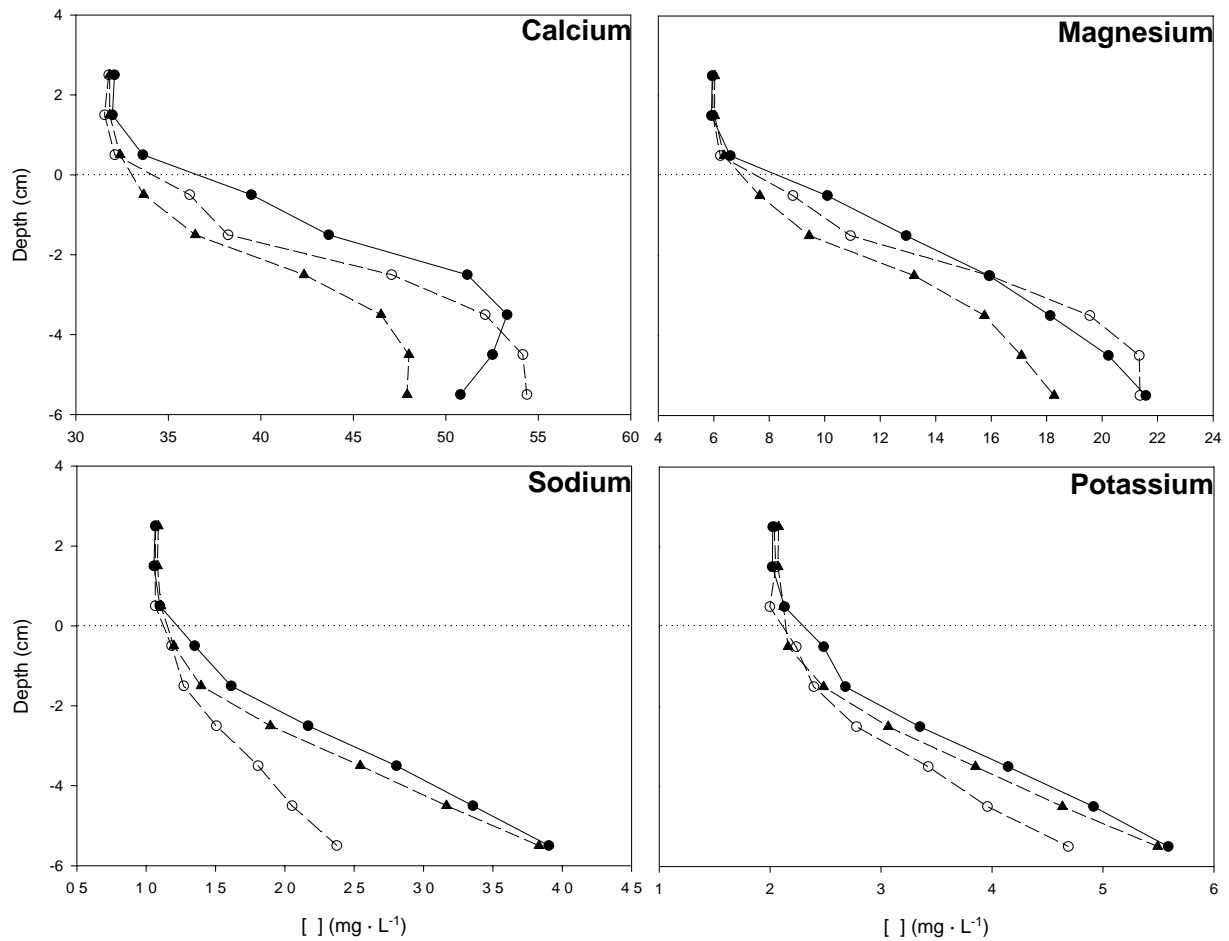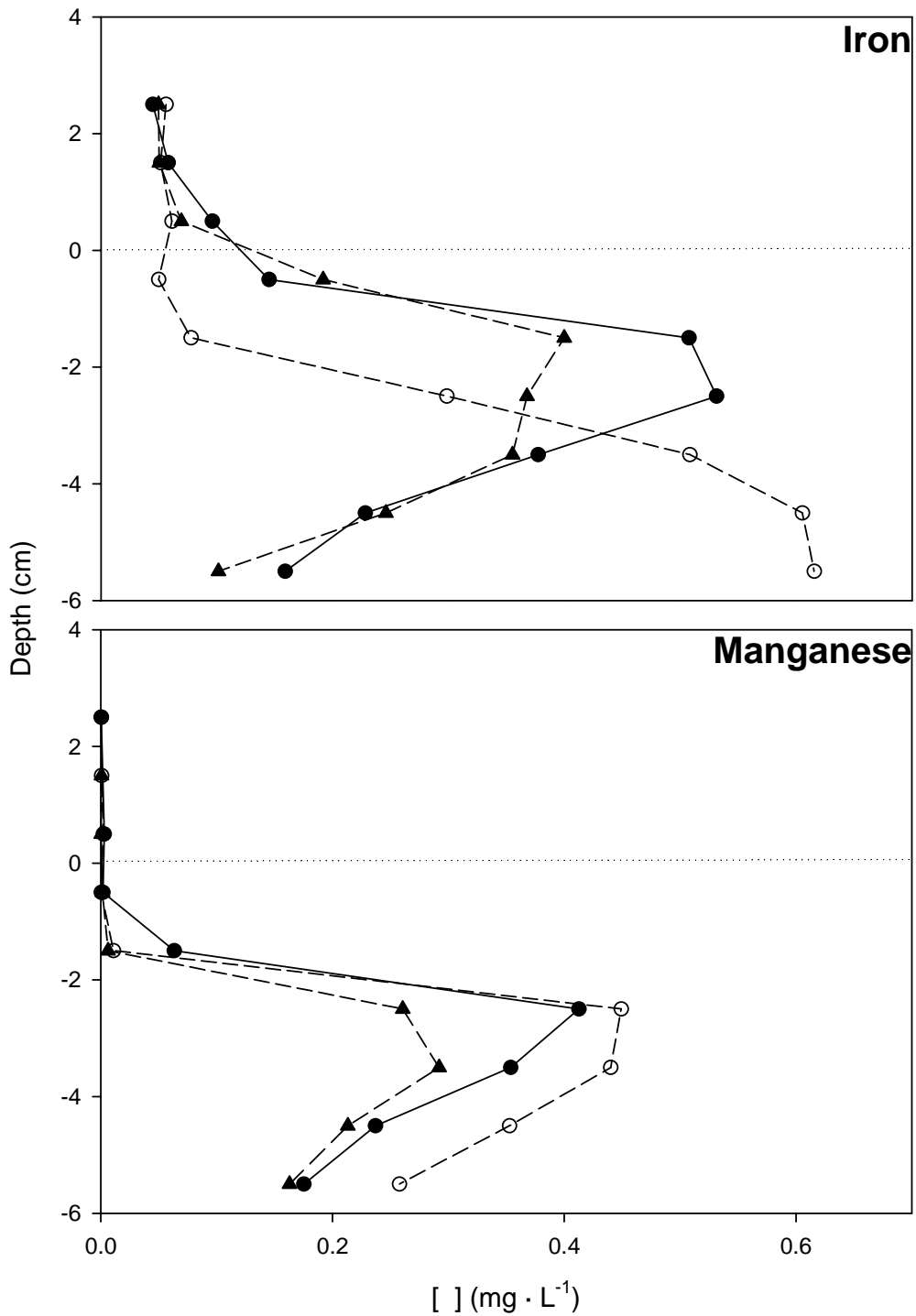
Figure 4   Porewater Ca, Mg, Na and K profiles as sampled by *in situ* dialysis (1 cm vertical resolution). The horizontal broken line indicates the biofilm/tailings-overlying water interface. Each curve is from an individual peeper inserted into the tailings and allowed to equilibrate for 2 weeks.
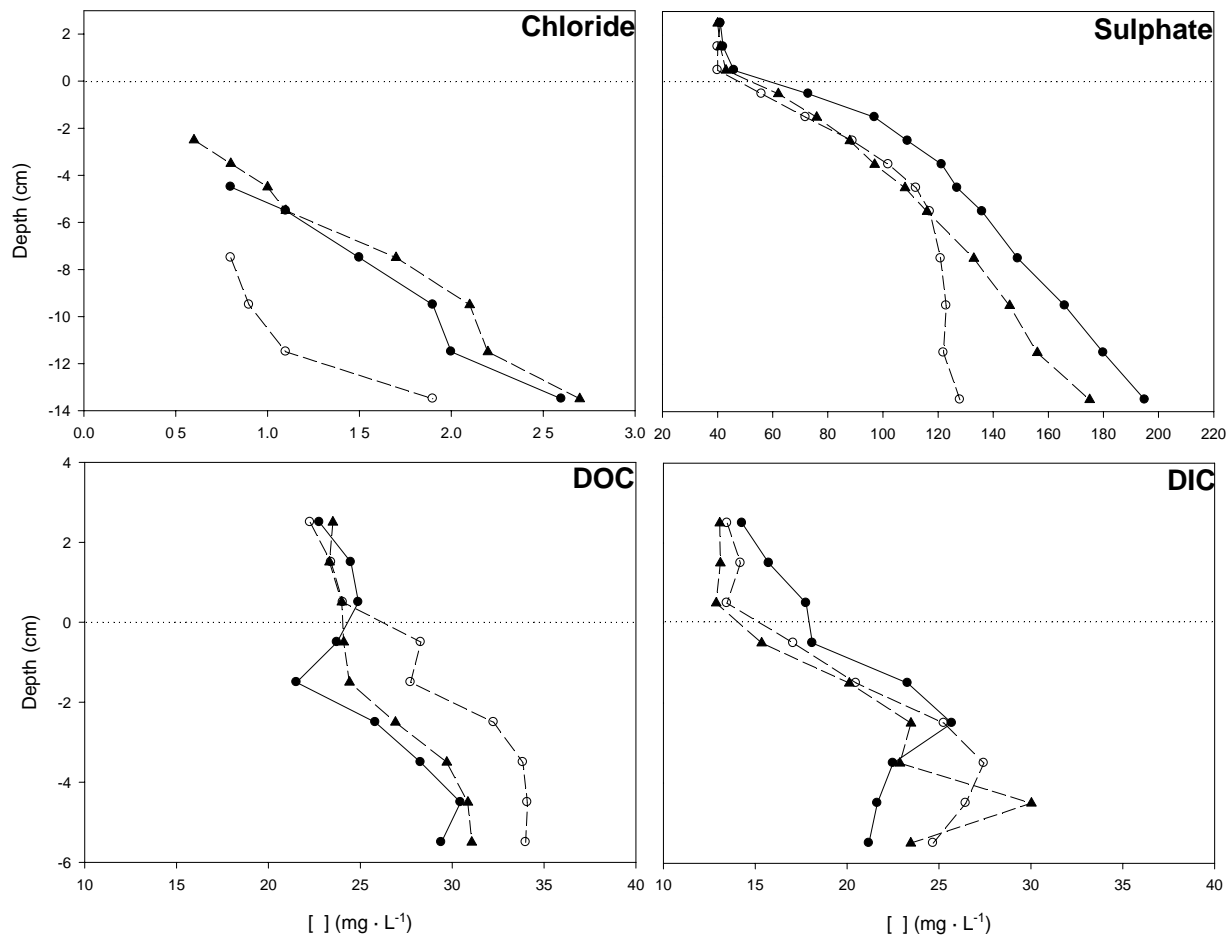
Figure 5   Porewater Cl⁻, SO₄²⁻, dissolved organic carbon (DOC), and dissolved inorganic carbon (DIC), profiles as sampled by *in situ* dialysis (1 cm vertical resolution; detection limit for Cl⁻ = 0.6 mg · L⁻¹). The horizontal broken line indicates the biofilm/tailings-overlying water interface. Each curve is from an individual peeper inserted in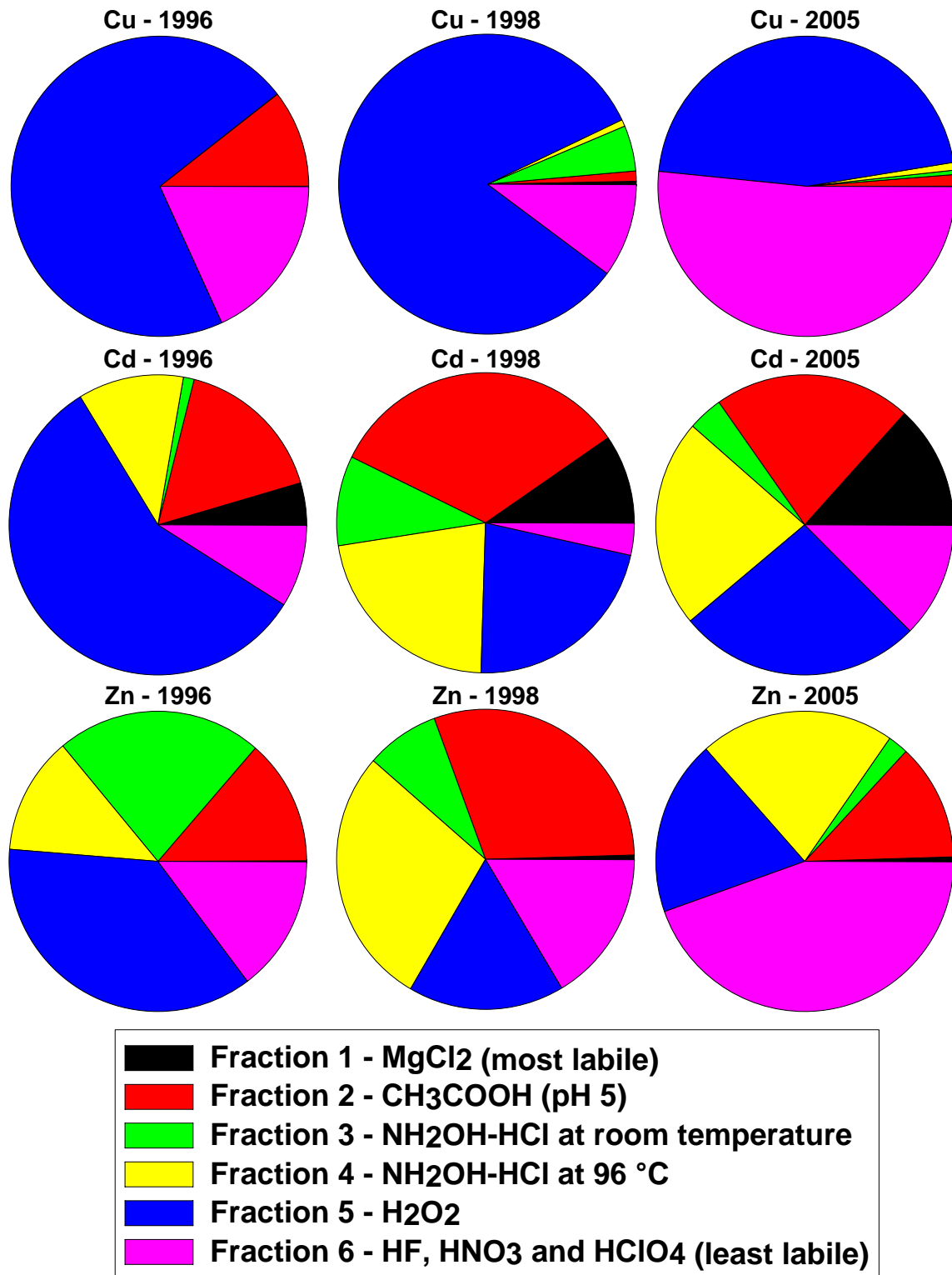to the tailings (and allowed to equilibrate for 2 weeks). In the overlying water and for first centimetres of pore water, Cl⁻ is below the detection limit of 0.6 mg L⁻¹.
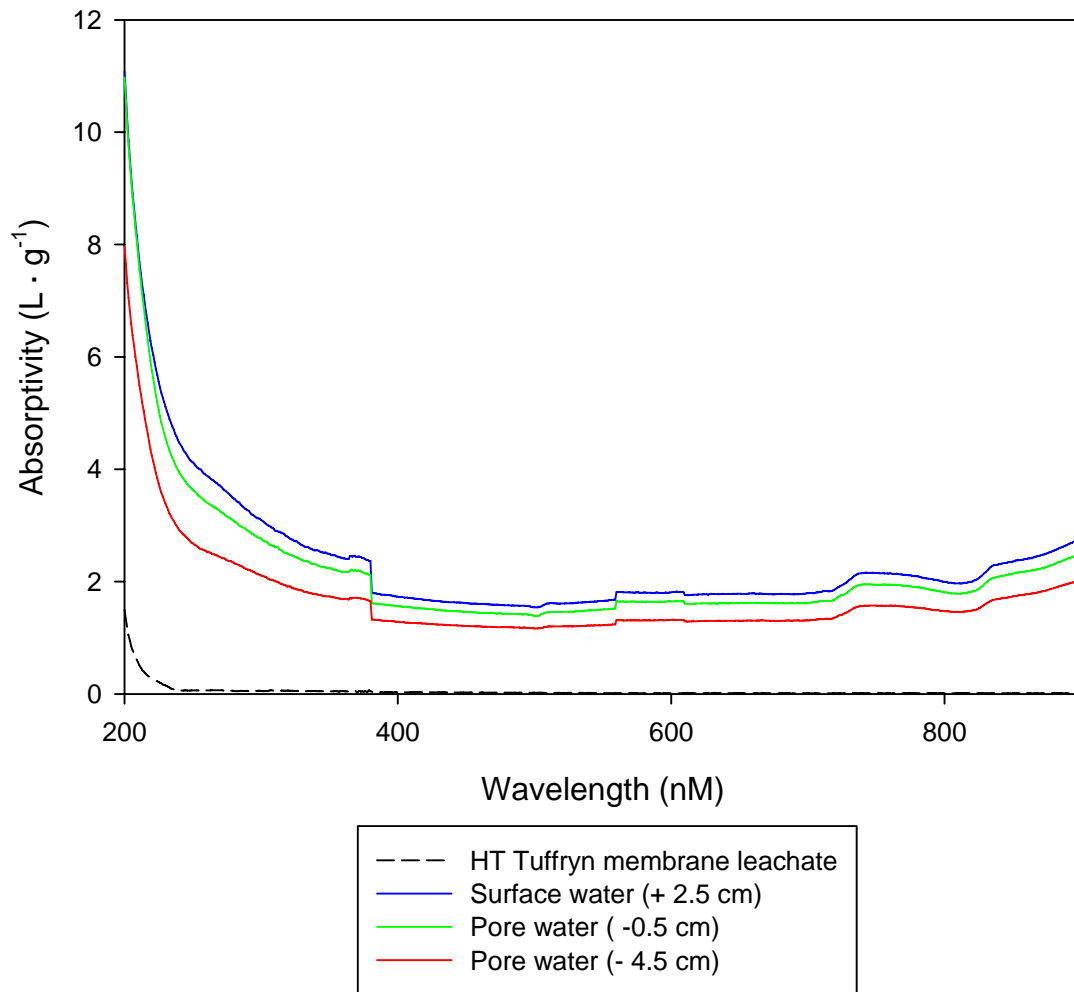
Figure 6   UV-visible absorptivity scan for surface water (2.5 cm above the biofilm –
overlying water interface) and porewater (0.5 and 4.5 cm below the biofilm –
overlying water interface) samples collected by *in situ* dialysis. The absorptivity
is the measured absorvance normalized for the DOC concentration, i.e. the
absorbance divided by the DOC concentration in g L^{-1}. Each curve is the average
for the 3 peepers inserted into the tailings and allowed to equilibrate for 2 weeks.
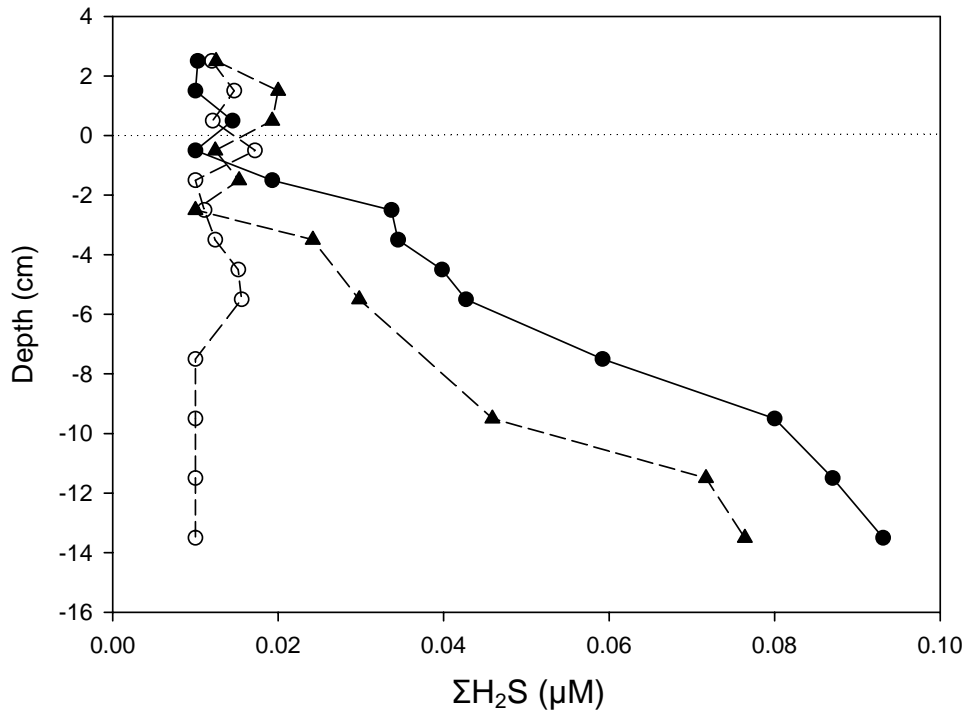
Figure 7   Porewater ΣH_2S profiles as sampled by *in situ* dialysis (1 cm vertical resolution; detection limit = 0.01 μM). The horizontal broken line indicates the biofilm/tailings-overlying water interface. Each curve is from an individual peeper inserted into the tailings and allowed to equilibrate for 2 weeks.

Figure 8   Porewater dissolved Fe and Mn profiles as sampled by *in situ* dialysis (1 cm vertical resolution; detection limit for Mn = 0.001 mg L^{-1}). The horizontal broken line indicates the biofilm/tailings-overlying water interface. Each curve is from an individual peeper inserted into the tailings and allowed to equilibrate for 2 weeks.
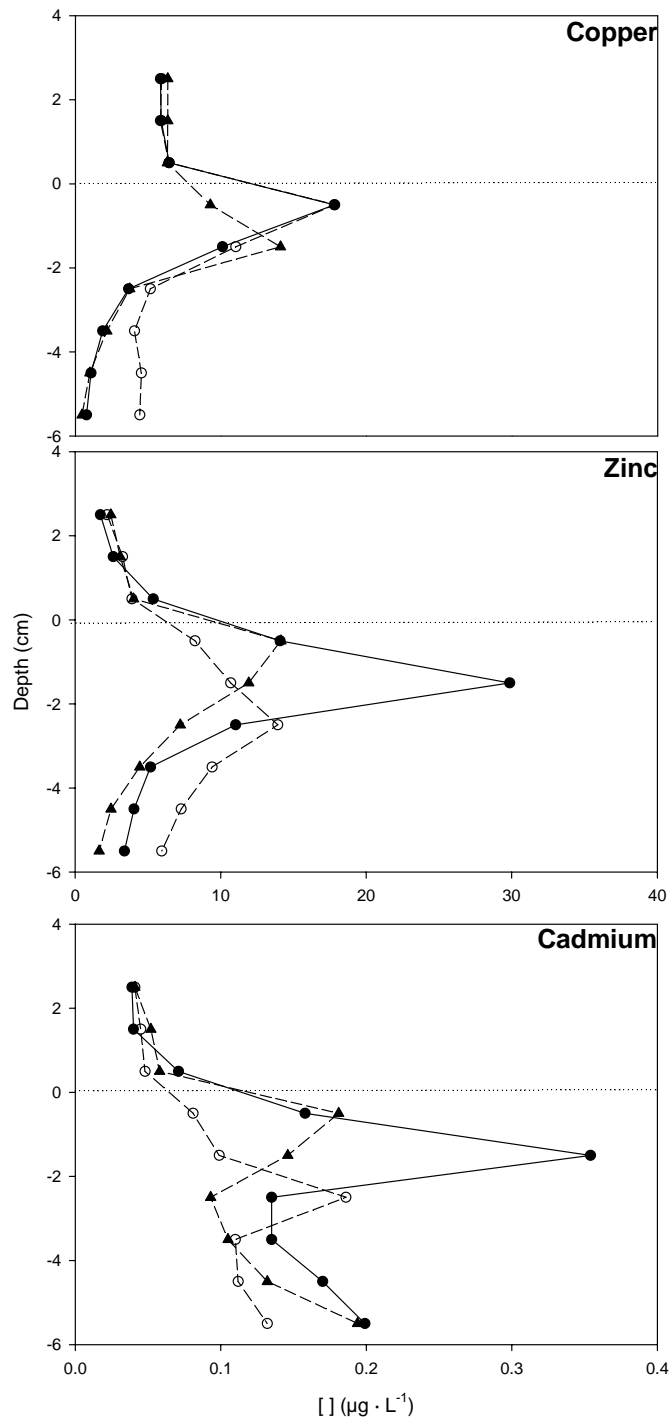
Figure 9   Porewater dissolved Cu, Zn and Cd concentration profiles as sampled by *in situ* dialysis (1 cm vertical resolution). The horizontal broken line indicates the biofilm/tailings-overlying water interface. Each curve is from an individual peeper inserted into the tailings and allowed to equilibrate for 2 weeks.

Fraction 1 - MgCl2 (most labile)
Fraction 2 - CH3COOH (pH 5)
Fraction 3 - NH2OH-HCl at room temperature
Fraction 4 - NH2OH-HCl at 96 °C
Fraction 5 - H2O2
Fraction 6 - HF, HNO3 and HClO4 (least labile)

Figure 10   Changes in metal partitioning in the uppermost 0.5 cm layer of submerged tailings from 1996 to 2005. Data from 1996 and 1998 are from Vigneault *et al.* (2001). In 2005, the biofilm was sampled separately from the surface tailings.
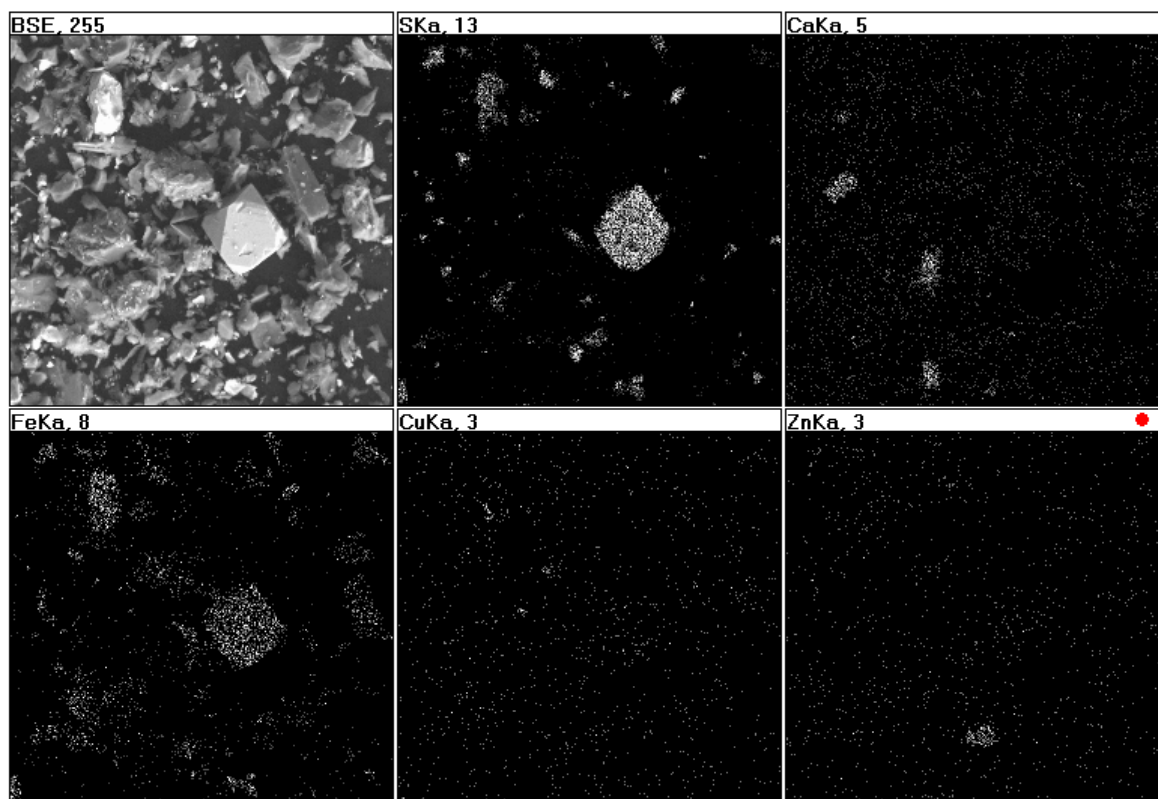
Figure 11   Backscattered electron image (BSE, top left) and the associated X-ray maps of surface tailings from C2 that show an intact pyritohedron surrounded by several remnant pyrite grains altered to various extents to Fe-oxyhydroxide (evident from comparing the Fe and S X-ray maps).
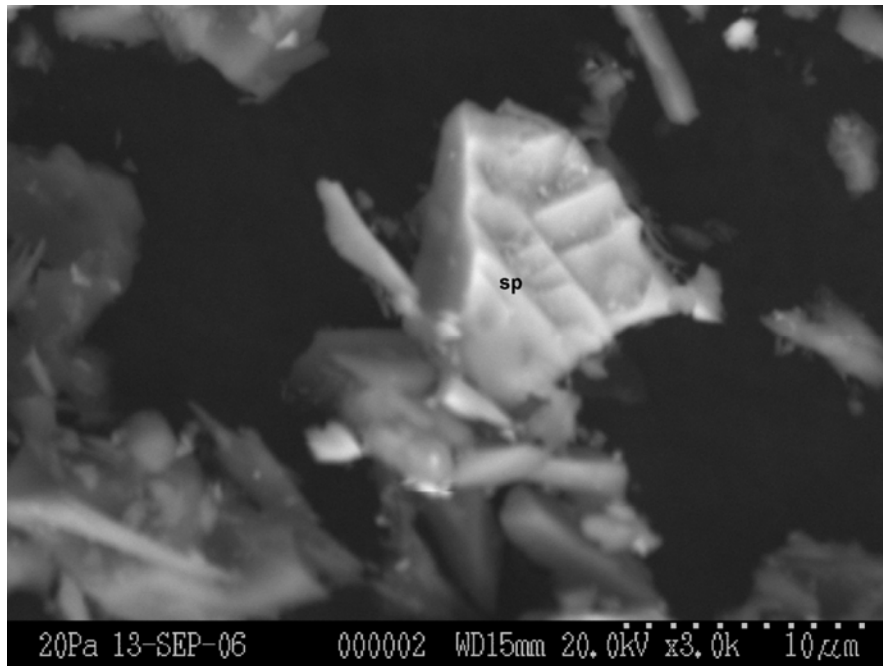
Figure 12   Backscattered electron image showing a fully liberated sphalerite (sp) grain detected in the 4.5-5.5 interval of C3 tailings profile with prominent dissolution features.
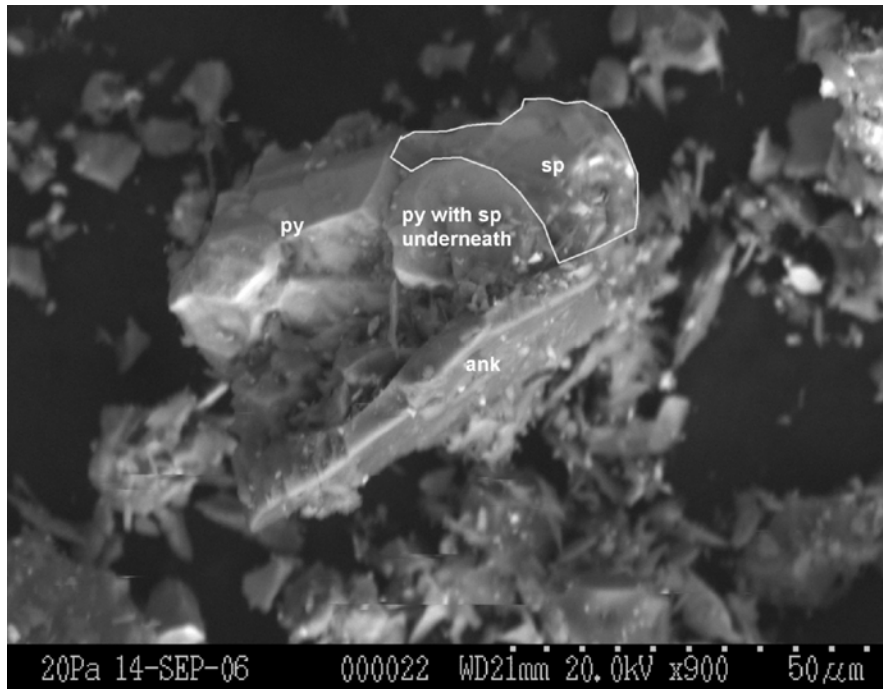
Figure 13   Backscattered electron image showing partially dissolved sphalerite (sp) adjacent to pyrite (py). The sample under examination is from tailings profile C2, 4.5-5.5 cm.
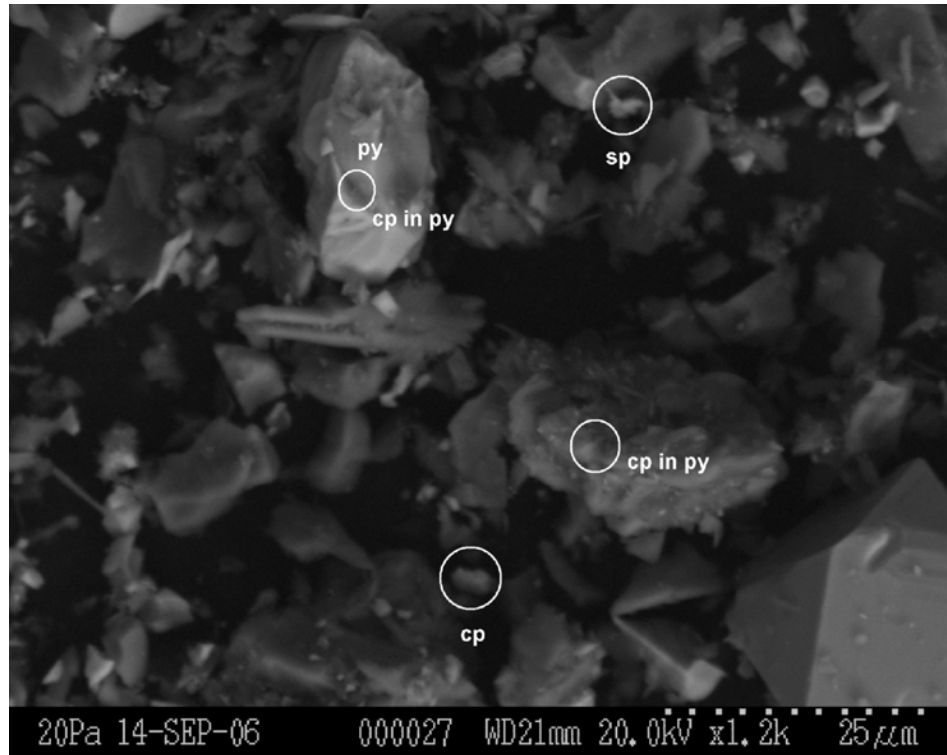
Figure 14   Backscattered electron image of a selected area of the C2 surface tailings (0.0-0.5 cm) showing the occurrence of chalcopyrite (cp) as separate grains and as inclusions in pyrite (py).

Upper panel legend:
- Proteobacteria
- Alphaproteobacteria
- Acidobacteria
- Verrucomicrobia
- Planctomycetales
- Chloroflexi
- Cytophagales
- Cyanobacteria
- Saprospiraceae
- Acamthamoeba
- Paecilomyces
- Acremonium

Lower panel legend:
- unknown function
- methanogenic consortium; lithotrophs, anaerobic NH4 oxidation
- Phototrophs
- chemoorganoheterotrophs
- grazer
- fungus-decomposer

Figure 15   Louvicourt biofilm community phylogenetic diversity (27 clones, upper panel) and inferred metabolic function occurring within the biofilm community (lower panel).

APPENDIX A – Site Plan and Site Pictures
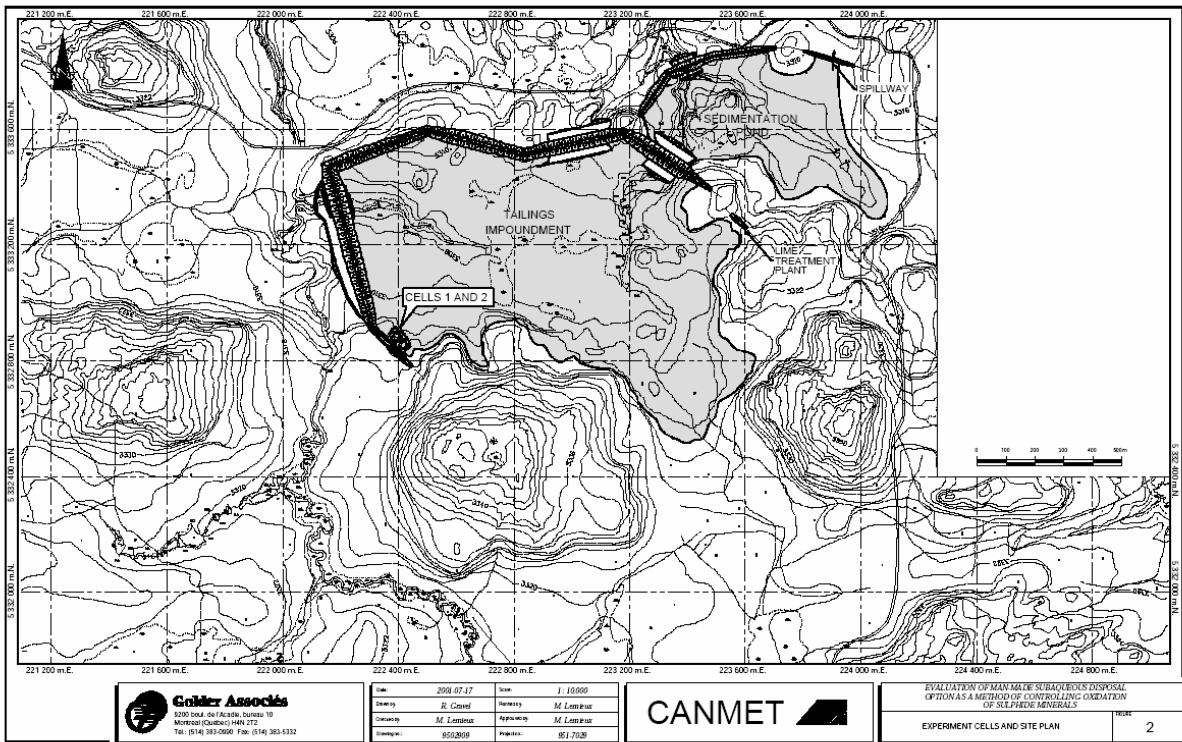
Experiment cells and site plan (above, from Golder Associés) and 1996 picture of the two experimental cells with the tailings impoundment in the background (Dr. Peter Campbell, INRS-ETE).

Aerial view of the Louvicourt Mine polishing pond and tailings impoundment (Aur Resources).

Experimental Cell #2 in July 2005 where the sampling for the current study was conducted (CANMET-MMSL).

Set-up for the *in situ* measurement of pH microprofile (CANMET-MMSL).

Set-up for the sampling of the peepers used for the *in situ* dialysis (CANMET-MMSL).

Set up for the extrusion of the collected cores using a piston extruder under nitrogen to prevent oxidation.

Core collected in July 2005 from Experimental Cell #1 with the biofilm, the surface tailings (brown) and the deeper anoxic tailings (grey).

APPENDIX B – Analytical Results

PROJECT#: 603066 Caracterisation geochimique des residus minieres

CERTIFICATE #: 12586
DATE RECEIVED: 04/08/2005
CL ENT No.: 126

CL ENT NAME: Vigneault Bernard 555 Booth Street Ottawa K1A 0G1

		ANALYTE / RESULT**	
SAMPLE#	SAMPLE DESCRIPTION	Cl	SO4
116277	BLANC1	<0 06 ppm	<0.5 ppm
116278	BLANC2	<0 06 ppm	<0.5 ppm
116279	BLANC3	<0 06 ppm	<0.5 ppm
116280	D1-1	<0 06 ppm	4.1 ppm
116281	D2-1	<0 06 ppm	4.1 ppm
116282	D3-1	<0 06 ppm	4 ppm
116283	D1-2	<0 06 ppm	4.2 ppm
116284	D2-2	<0 06 ppm	4 ppm
116285	D3-2	<0 06 ppm	4.1 ppm
116286	D1-3	<0 06 ppm	4.6 ppm
116287	D2-3	<0 06 ppm	4 ppm
116288	D3-3	<0 06 ppm	4.3 ppm
116289	D1-4	<0 06 ppm	7.3 ppm
116290	D2-4	<0 06 ppm	5.6 ppm
116291	D3-4	<0 06 ppm	6.2 ppm
116292	D1-5	<0 06 ppm	9.7 ppm
116293	D2-5	<0 06 ppm	7.2 ppm
116294	D3-5	<0 06 ppm	7.6 ppm
116295	D1-6	<0 06 ppm	10.9 ppm
116296	D2-6	<0 06 ppm	8.9 ppm
116297	D3-6	0 06 ppm	8.8 ppm
116298	D1-7	<0 06 ppm	9.1 ppm
116299	D2-7	<0 06 ppm	10.2 ppm
116300	D3-7	0 08 ppm	9.7 ppm
116301	D1-8	0 08 ppm	12.7 ppm
116302	D2-8	<0 06 ppm	11.2 ppm
116303	D3-8	0.1 ppm	10.8 ppm
116304	D1-9	0.11 ppm	13.6 ppm
116305	D2-9	<0 06 ppm	11.7 ppm
116306	D3-9	0.11 ppm	11.6 ppm
116307	D1-10	0.15 ppm	14.9 ppm
116308	D2-10	0 08 ppm	12.1 ppm
116309	D3-10	0.17 ppm	13.3 ppm
116310	D1-11	0.19 ppm	16.6 ppm
116311	D2-11	0 09 ppm	12.3 ppm
116312	D3-11	0 21 ppm	14.6 ppm
116313	D1-12	0 2 ppm	18 ppm
116314	D2-12	0.11 ppm	12.2 ppm
116315	D3-12	0 22 ppm	15.6 ppm
116316	D1-13	0 26 ppm	19.5 ppm
116317	D2-13	0.19 ppm	12.8 ppm
116318	D3-13	0 27 ppm	17.5 ppm

**Note: Results given in ppm units correspond to mg/L (for liquids) and ug/g for solids. .

Note: values marked '<' were found to be below the reliable reporting limit shown.
Analytical methods applied are on the sheet 'Method Report'

Analytical Service Group	Approved by: Chemist	05/08/2005
555 Booth St		
Ottawa , Ontario	Approve Date:	05/08/2005
K1A 0G1	Issue Date :	05/08/2005

Note: Dilution factor for major anions was 10, except for D1-7 which was 13.333.

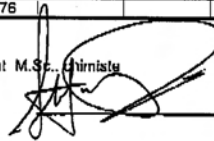Université du Québec
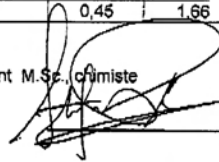Institut National de la recherche scientifique

INRS-ETE

RAPPORT D'ANALYSE

NOM: Laboratoire des mines et des sciences minérales de CANMET
ADRESSE: Ressources naturelles Canada
            555 Booth. Ottawa, Ontario, Canada   Date: 2005-12-20
            K1A 0G1
ATT: Bernard Vigneault

Échantillon		CID mM	S2- µmole/L				
Louvl bl-1		< 0.01	0,001				
Louvl bl-2		< 0.01	0,023				
Louvl bl-3		< 0.01	0,017				
D.1.1		1,19	0,010				
D.1.2		1,31	0,008				
D.1.3		1,48	0,015				
D.1.4		1,51	0,008				
D.1.5		1,94	0,019				
D.1.6		2,14	0,034				
D.1.7		1,87	0,035				
D.1.8		1,80	0,040				
D.1.9		1,76	0,043				
D.1.10			0,059				
D.1.11			0,080				
D.1.12			0,087				
D.1.13			0,093				
D.2.1		1.12	0,012				
D.2.2		1,18	0,015				
D.2.3		1,12	0,012				
D.2.4		1,42	0,017				
D.2.5		1,71	0,009				
D.2.6		2,10	0,011				
D.2.7		2,29	0,012				
D.2.8		2,20	0.015				
D.2.9		2,06	0,016				
D.2.10			-0,067	différence entre échantillon et blanc			
D.2.11			-0,087	différence entre échantillon et blanc			
D.2.12			-0.100	différence entre échantillon et blanc			
D.2.13			-0,109	différence entre échantillon et blanc			
D3.1		1,09	0,013				
D3.2		1.09	0.020				
D3.3		1.07	0,019				
D3.4		1,28	0,012				
D3.5		1,68	0,015				
D3.6		1,95	0,008				
D3.7		1,90	0,024				
D3.8		2,50	n.a.*	*: un pic dû à une bulle d'air surévalue le résultat			
D3.9		1,95	0,030				
D3.10			n.a.*				
D3.11			0,046				
D3.12			0,072				
D3.13			0,076				

Les résultats sont certifiés par: Stéfane Prémont M.Sc. Chimiste

Université du Québec
Institut National de la recherche scientifique

INRS-ETE

RAPPORT D'ANALYSE

NOM:	Laboratoire des mines et des sciences minérales de CANMET		
ADRESSE:	Ressources naturelles Canada		
	555 Booth. Ottawa, Ontario. Canada	Date:	2005-12-20
	K1A 0G1		
ATT:	Bernard Vigneault	**Analyses par ICP-MS**	

Échantillon				Cu (µg/L)	Zn (µg/L)	Cd (µg/L)	
Louvi bl-1				< 0.16	0,89	0,002	
Louvi bl-2				< 0.16	0,75	0,002	
Louvi bl-3				< 0.16	0,84	0,002	
D.1.1				5,84	1,74	0,039	
D.1.2				5,90	2,62	0,040	
D.1.3				6,44	5,37	0,071	
D.1.4				17,79	14,08	0,158	
D.1.5				10,11	29,66	0,354	
D.1.6				3,66	11,03	0,135	
D.1.7				1,88	5,18	0,135	
D.1.8				1,07	4,05	0,170	
D.1.9				0,76	3,39	0,199	
D.2.1				5,91	2,21	0,041	
D.2.2				5,84	3,26	0,045	
D.2.3				6,42	3,91	0,048	
D.2.4				17,81	8,24	0,081	
D.2.5				11,02	10,69	0,099	
D.2.6				5,15	13,93	0,186	
D.2.7				4,06	9,42	0,110	
D.2.8				4,53	7,29	0,112	
D.2.9				4,42	5,96	0,132	
D3.1				6,35	2,46	0,041	
D3.2				6,34	3,10	0,052	
D3.3				6,31	4,02	0,058	
D3.4				9,26	14,14	0,181	
D3.5				14,09	11,93	0,146	
D3.6				3,73	7,23	0,093	
D3.7				2,16	4,44	0,105	
D3.8				0,99	2,47	0,132	
D3.9				0,45	1,66	0,194	

Les résultats sont certifiés par: Stéfane Prémont M.Sc. chimiste

CHIMISTE
STÉFANE PRÉMONT
QUÉBEC

Université du Québec
Institut National de la recherche scientifique

INRS-ETE

RAPPORT D'ANALYSE

NOM: Laboratoire des mines et des sciences minérales de CANMET
ADRESSE: Ressources naturelles Canada
556 Booth, Ottawa, Ontario, Canada
K1A 0G1
ATT: Bernard Vigneault

DATE: 2005-12-20

Echantillon	Al (mg/L)	Ca (mg/L)	Cd (mg/L)	Cu (mg/L)	Fe (mg/L)	K (mg/L)	Mg (mg/L)	Mn (mg/L)	Na (mg/L)	Ni (mg/L)	Pb (mg/L)	Zn (mg/L)
Leuvl bt-1	<0.004	<0.008	0,0005	<0,0004	<0.002	3,04	<0,001	<0,001	0,01	<0,002	<0,01	<0,0004
Leuvl bt-2	<0.004	<0.008	0,0003	<0,0004	<0.002	3,04	<0,001	0,01	0,01	<0,002	<0,01	<0,0006
Leuvl bt-3	<0.004	0,009	<0,0003	0,0014	<0.002	3,04	<0,001	0,003	0,01	<0,002	<0,01	<0,0004
D1.1	0,013	32,09	<0,0003	0,0054	0,045	2,02	5,94	1,07	1,07	<0,002	0,01	0,0013
D1.2	0,018	31,98	<0,0003	0,0065	0,058	2,02	5,92	<0,001	1,06	<0,002	0,01	0,0028
D1.3	0,018	33,62	<0,0003	0,0072	0,090	2,13	6,60	0,003	1,10	<0,002	0,01	0,0052
D1.4	0,024	39,49	0,0004	0,0167	0,145	2,48	10,09	0,002	1,35	<0,002	0,01	0,0140
D1.5	0,047	43,67	0,0004	0,0099	0,507	2,68	12,94	0,084	1,61	<0,002	0,01	0,0320
D1.6	0,056	51,17	<0,0003	0,0039	0,531	3,35	15,92	0,413	2,17	<0,002	0,01	0,0114
D1.7	0,043	53,32	<0,0003	0,0014	0,377	4,14	18,13	0,354	2,80	<0,002	0,01	0,0068
D1.8	0,031	52,53	<0,0003	0,0014	0,228	4,91	20,23	0,237	3,35	<0,002	0,01	0,0041
D1.9	0,030	50,79	0,0005	0,0015	0,159	5,39	21,57	0,176	3,80	<0,002	0,01	0,0035
D2.1	0,018	31,77	<0,0003	0,0066	0,058	2,04	5,95	0,001	1,07	<0,002	0,01	0,0022
D2.2	0,017	31,55	<0,0003	0,0053	0,052	2,06	5,97	0,001	1,07	<0,002	0,01	0,0026
D2.3	0,018	32,11	<0,0003	0,0072	0,061	2,00	6,24	0,002	1,07	<0,002	0,01	0,0064
D2.4	0,019	36,15	<0,0003	0,0128	0,050	2,23	8,85	0,001	1,18	<0,002	0,01	0,0078
D2.5	0,021	38,23	0,0003	0,0119	0,078	2,39	10,93	0,011	1,27	<0,002	0,01	0,0078
D2.6	0,049	47,07	<0,0003	0,0040	0,299	2,78	15,94	0,449	1,51	<0,002	0,01	0,0144
D2.7	0,077	52,13	<0,0003	0,0037	0,508	3,43	18,56	0,440	1,81	<0,002	0,01	0,0110
D2.8	0,088	54,17	0,0003	0,0049	0,505	3,96	21,34	0,353	2,05	<0,002	0,01	0,0075
D2.9	0,064	54,40	<0,0003	0,0049	0,516	4,69	21,37	0,258	2,39	<0,002	0,01	0,0081
D3.1	0,017	31,63	<0,0003	0,0054	0,050	2,08	6,04	<0,001	1,09	<0,002	<0,01	0,0021
D3.2	0,015	31,63	<0,0003	0,0063	0,050	2,07	6,03	0,001	1,08	<0,002	0,01	0,0024
D3.3	0,017	32,39	<0,0003	0,0058	0,069	2,12	6,37	0,001	1,11	<0,002	0,01	0,0039
D3.4	0,020	33,87	0,0004	0,0101	0,192	2,16	7,60	0,002	1,20	<0,002	0,02	0,0139
D3.5	0,037	38,46	0,0005	0,0135	0,400	2,48	9,44	0,026	1,40	<0,002	<0,01	0,0122
D3.6	0,032	42,39	<0,0003	0,0033	0,388	3,08	13,22	0,261	1,90	<0,002	0,01	0,0080
D3.7	0,034	46,50	0,0003	0,0024	0,355	3,65	15,76	0,292	2,54	<0,002	0,01	0,0061
D3.8	0,026	48,01	<0,0004	<0,0004	0,246	4,63	17,09	0,213	3,17	<0,002	<0,01	0,0023
D3.9	0,024	47,92	0,0003	0,0007	0,101	5,49	18,27	0,163	3,89	<0,002	<0,01	0,0013

Les résultats sont certifiés par: Stéfane Prémont, M.Sc., chimiste

Somme des fractions pour l'échantillon de contrôle Mess-3

Fractions	Cd 214.43 (µg/g)	Cu (µg/g)	Fe (µg/g)	Mn (µg/g)	Ni (µg/g)	Pb (µg/g)	Zn (µg/g)
Fraction-1	0.06	0.4	1.24	19.05	0.01	0.07	0.18
Fraction-2	0.11	2.2	650	78	1.34	3.88	13.84
Fraction-3a)	0.01	0.1	269	12.8	0.2	0.0	2.07
Fraction 3b)	0.04	2.79	6710	64.5	9.02	4.7	36.6
Fraction-4	< 0.04	5.73	690	12.78	6.09	0	10
Fraction-5	< 0.05	20.0	31437	115.4	24.8	7	84
somme	0.23	31.19	39758.66	302.28	41.44	15.21	147.35
valeurs attendues	**0.24 ± 0.01**	**33.9 ± 1.6**	**43400±1100**	**324 ± 12**	**46.9 ± 2.2**	**21.1 ± 0.7**	**159 ± 8**

Sample ID	Dissolved Organic Carbon (mg/L)
D1.1	22.8
D1.2	24.5
D1.3	24.9
D1.4	23.7
D1.5	21.5
D1.6	25.8
D1.7	28.3
D1.8	30.5
D1.9	29.4
D2.1	22.3
D2.2	23.4
D2.3	24.1
D2.4	28.3
D2.5	27.7
D2.6	32.3
D2.7	33.9
D2.8	34.1
D2.9	34.0
D3.1	23.5
D3.2	23.3
D3.3	24.0
D3.4	24.1
D3.5	24.4
D3.6	26.9
D3.7	29.7
D3.8	30.9
D3.9	31.1

RAPPORT D'ANALYSES: Extractions séquentielles

NOM: Ressources naturelles Canada
ATT: Bernard Vigneault

Projet Louvicourt, échantillons de juillet 2005
analysés en été 2006

Fraction 1- Métaux échangeables:

Échantillon	Cd 214.4 (µg/g)	Cu 324.7 (µg/g)	Fe 238.2 (µg/g)	Mn 257.6 (µg/g)	Ni 231.6 (µg/g)	Pb 220.3 (µg/g)	Zn 206.2 (µg/g)
blanc	< 0.06	< 0.1	< 1.1	< 0.10	< 0.5	< 1.1	< 0.5
B1	1,06	12,5	37,92	31,93	< 0.5	< 1.1	22,94
B2	1,57	12,2	87,76	20,72	< 0.5	< 1.1	37,18
B3	1,43	13,3	43,34	13,18	< 0.5	< 1.1	26,95
R1	1,03	0,9	27,19	50,15	0,27	< 1.1	14,80
R2	1,11	0,4	0,08	88,78	0,32	< 1.1	13,39
R3	1,04	0,5	4,30	49,66	0,17	< 1.1	12,15
S1	0,16	0,1	2,02	14,27	0,28	< 1.1	1,46
S2	0,11	0,2	2,27	11,09	0,27	< 1.1	1,06
S3	0,17	0,2	2,86	13,94	0,27	< 1.1	1,60
limite si dil 8x	0,06	0,1	1,1	0,10	0,5	1,1	0,50

Fraction 2- Métaux liés aux carbonates:

Échantillon	Cd 214.43 (µg/g)	Cu 324.75 (µg/g)	Fe 261.18 (µg/g)	Mn 260.56 (µg/g)	Ni 231.60 (µg/g)	Pb 220.35 (µg/g)	Zn 206.2 (µg/g)
blanc	< 0.05	0,1	< 1	< 0.2	< 0.27	< 1.3	< 0.25
B1	2,40	102,7	175	195,1	1,07	2,8	545
B2	3,37	96,1	360	278,5	1,41	4,1	741
B3	2,93	79,5	182	184,3	1,26	2,7	596
R1	1,60	120,7	559	291,5	1,29	33,4	284
R2	1,68	131,1	733	372,6	1,66	42,2	342
R3	1,82	143,2	508	361,2	1,49	21,9	323
S1	2,06	138,6	1676	132,7	2,25	184,5	461
S2	1,55	103,5	1411	114,8	1,76	137,6	337
S3	2,16	145,6	1707	126,1	2,31	188,5	476
limite si dil 8x	0,05	0,1	1,00	0,20	0,27	1,34	0,25

Les résultats sont certifiés par:
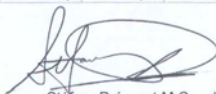
StéfanePrémont M.Sc. chimiste

RAPPORT D'ANALYSES: Extractions séquentielles

Louvicourt, échantillons de juillet 2005
analysés en été 2006

Fraction 3a)- Métaux liés aux oxydes de manganèse:

Échantillon	Cd 214.4 (µg/g)	Cu 324.7 (µg/g)	Fe 261.1 (µg/g)	Mn 257.6 (µg/g)	Ni 231.6 (µg/g)	Pb 220.3 (µg/g)	Zn 213.8 (µg/g)
blanc	< 0.01	< 0.02	< 0.12	< 0.04	< 0.02	< 0.1	< 0.02
B1	0,12	2,77	42	176,3	0,18	0,1	33,4
B2	0,73	10,57	155	1234,1	0,95	0,2	214
B3	0,17	1,87	30	141,8	0,15	0,0	39,2
R1	0,29	4,83	609	561,8	0,65	5,0	52,4
R2	0,27	2,23	690	360,0	0,39	4,4	52,6
R3	0,33	7,82	629	507,4	0,55	3,0	61,4
S1	0,17	0,76	1033	91,5	0,32	14,1	45,9
S2	0,16	0,30	903	81,7	0,25	12,1	40,5
S3	0,18	0,40	1091	93,7	0,36	13,4	47,1
limite si dil 20x	0,01	0,02	0,12	0,04	0,02	0,1	0,02

Fraction 3b) - Métaux liés aux oxydes de fer:

Échantillon	Cd 214.4 (µg/g)	Cu 327.3 (µg/g)	Fe 238.2 (µg/g)	Mn 257.6 (µg/g)	Ni 231.6 (µg/g)	Pb 220.3 (µg/g)	Zn 206.2 (µg/g)
blanc	< 0.04	0,27	1	< 0.4	< 0.09	0,6	0,2
B1	3,31	38,36	21260	1237	4,03	89,1	1080
B2	3,65	30,98	22004	1833	4,95	69,1	1254
B3	3,52	37,58	15862	1225	4,34	48,0	1122
R1	1,61	8,78	20142	605	1,37	165,4	462
R2	1,53	9,61	19836	744	1,44	158,1	463
R3	2,20	8,11	26145	834	1,87	192,2	664
S1	1,03	0,60	18940	1372	1,37	122,1	402
S2	0,66	0,75	17266	1302	1,22	108,3	292
S3	1,29	0,60	20283	1458	1,52	126,7	470
limite si dil 20x	0,04	0,09	1	0,4	0,09	0,5	0,2

Les résultats sont certifiés par:

StéfanePrémont M.Sc. chimiste

RAPPORT D'ANALYSES: Extractions séquentielles

Louvicourt, échantillons de juillet 2005
analysés en été 2006

Fractions 1 + 2 + 3a) + 3b) :   (reprises)

Échantillon	Cd 214.4 (µg/g)	Cu 327.3 (µg/g)	Fe 238.2 (µg/g)	Mn 257.6 (µg/g)	Ni 231.6 (µg/g)	Pb 220.3 (µg/g)	Zn 206.2 (µg/g)
blanc(bis)	< 0.04	0,22	1	< 0.4	< 0.09	0,6	0,2
B1(bis)	6,87	47,25	27688	2003	6,00	131,7	1806
B3 (bis)	7,66	39,58	22595	1823	6,49	80,3	1882

Fraction 4- Métaux liés à la matière organique:

Échantillon	Cd 214.4 (µg/g)	Cu 324.7 (µg/g)	Fe 261.1 (µg/g)	Mn 257.6 (µg/g)	Ni 231.6 (µg/g)	Pb 220.3 (µg/g)	Zn 213.8 (µg/g)
blanc	< 0.04	< 0.16	1,2	0,28	< 0.20	< 1	< 0.2
blanc (bis)	< 0.04	< 0.16	1,5	0,24	< 0.20	< 1	< 0.2
B1 (bis)	0,49	581	11040	333,8	4,70	23	143
B2	0,54	452	20840	221,2	5,84	37	136
B3(bis)	0,61	470	8978	295,5	7,12	27	184
R1	2,77	600	9280	228,5	2,25	26	627
R2	2,57	451	14460	204,1	1,99	26	569
R3	0,97	412	8314	155,9	1,40	28	217
S1	4,27	924	14330	198,1	2,51	19	1008
S2	4,82	979	12834	221,9	2,27	19	1150
S3	4,45	963	14684	125,1	2,45	18	1037
limite si dil 20x	0,04	0,16	1,2	0,16	0,20	1	0,2

Fraction 5 - Métaux contenus dans la matière cristalline:

Échantillon	Cd 214.4 (µg/g)	Cu 324.7 (µg/g)	Fe 261.1 (µg/g)	Mn 260.5 (µg/g)	Ni 231.6 (µg/g)	Pb 220.3 (µg/g)	Zn 213.8 (µg/g)
blanc	< 0.05	< 0.2	7,10	< 0.20	< 0.3	< 1	0,5
blanc(bis)	< 0.05	< 0.2	5,07	0,23	< 0.3	< 1	0,4
B1(bis)	< 0.05	156,1	93973	365,4	14,8	59	438
B2	< 0.05	73,7	49835	323,1	16,2	45	346
B3(bis)	< 0.05	75,0	62566	296,8	17,1	36	236
R1	0,64	422,2	143200	775,0	12,4	46	1032
R2	1,05	602,3	133647	794,8	12,1	54	1048
R3	1,28	625,9	138438	653,9	12,2	56	1270
S1	0,11	123,1	109310	569,0	13,0	25	371
S2	0,65	192,3	131172	899,7	13,8	19	516
S3	0,25	150,9	106957	512,9	12,7	22	388
limite si dil 50x	0,05	0,2	1,00	0,20	0,3	1	0,15

Les résultats sont certifiés par: StéfanePrémont M.Sc. chimiste

APPENDIX C – Results on Mineralogy Acquired by Scanning Electron Microscopy

Core 2 Biofilm layer: The sample contained much fibrous material. A portion enriched in mineral matter was mounted for SEM-EDX analysis. Abundant Fe-oxyhydroxide and minor sulphides were identified.
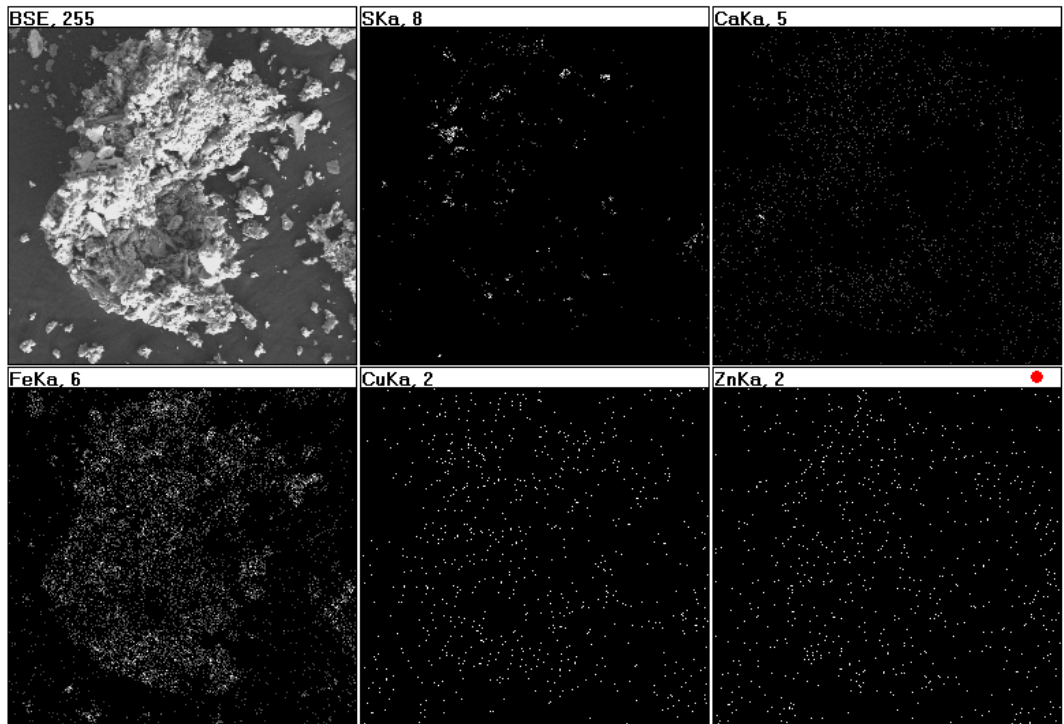
Figure C-1. Backscattered electron image (BSE, upper left) taken at 200X magnification along with the corresponding X-ray maps for S, Ca, Fe, Cu and Zn for a subsample of the biofilm layer from Core 2. The similar appearance between the BSE and X-ray map for Fe reflects the abundance of Fe-oxyhydroxide trapped in the biofilm. The scattered bright spots in the X-ray map for S is indicative of the presence of sulphides.
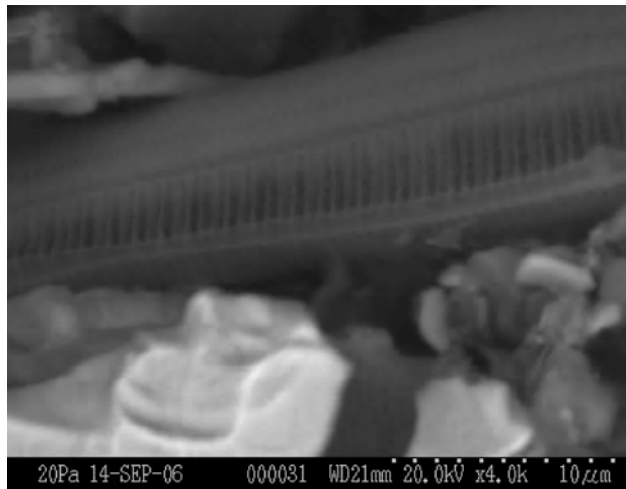
Figure C-2. Enlarged picture of a macrophyte observed in the biofilm layer of Core 2.
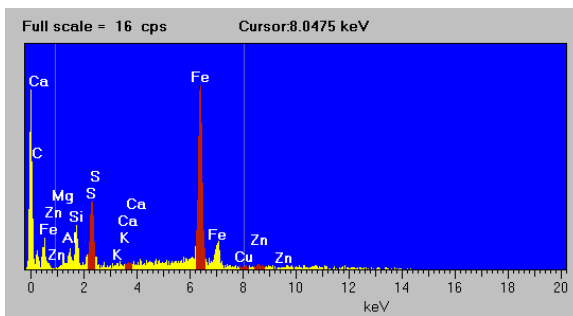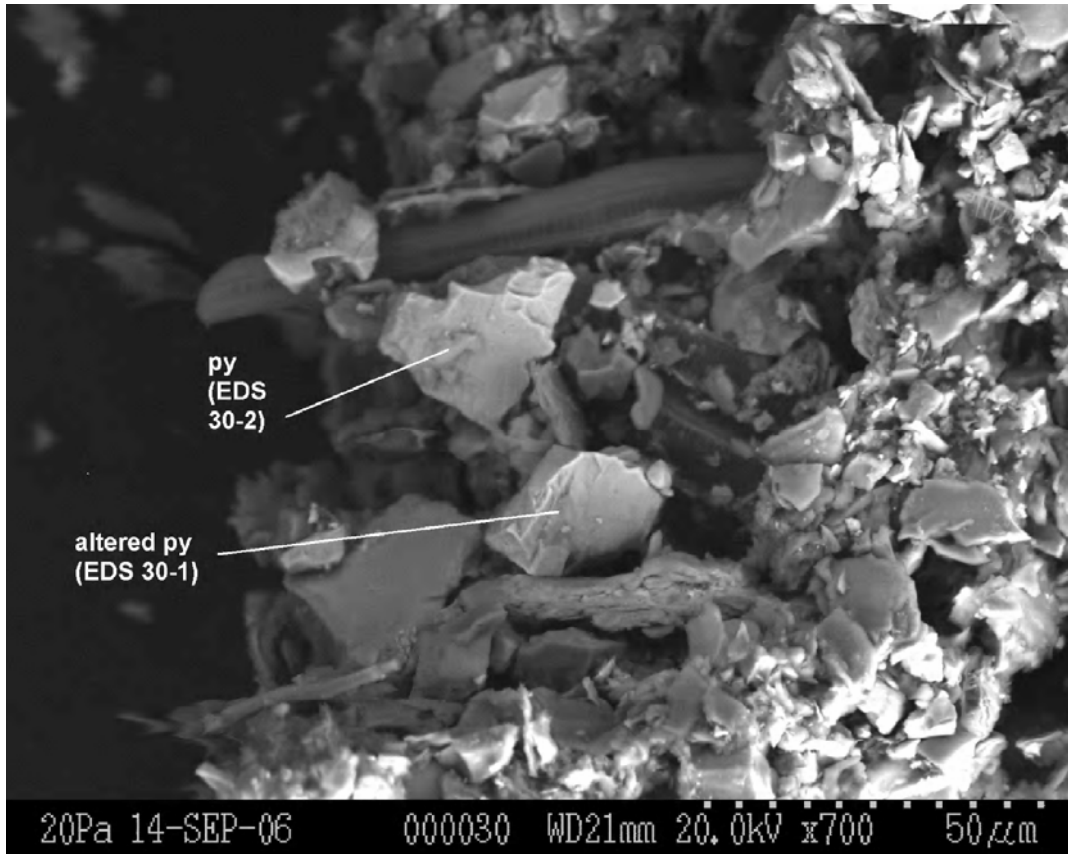
EDS 30-1
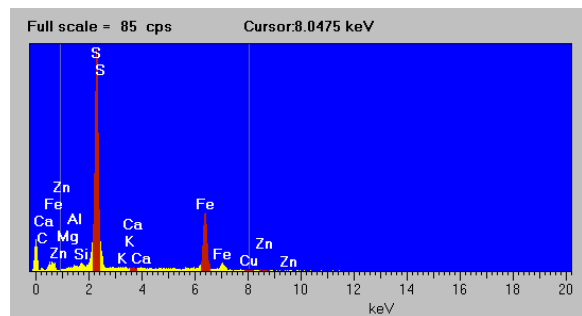
EDS 30-2

Figure C-3. Backscattered electron image (upper picture) of a subsample of the biofilm layer of Core 2 showing the occurrence of pyrite (py) and altered pyrite along with their EDX spectra (lower pictures, EDS 30-1 and EDS 30-2). The higher Fe/S ratio observed in EDS 30-1 is presumably due to the replacement of pyrite by Fe-oxyhydroxide as a result of oxidation.

Core 2, 0.0-0.5 cm: Generally low in sulphides but pyrite in various stage of oxidation and rare grains of chalcopyrite and sphalerite were identified in the subsample.
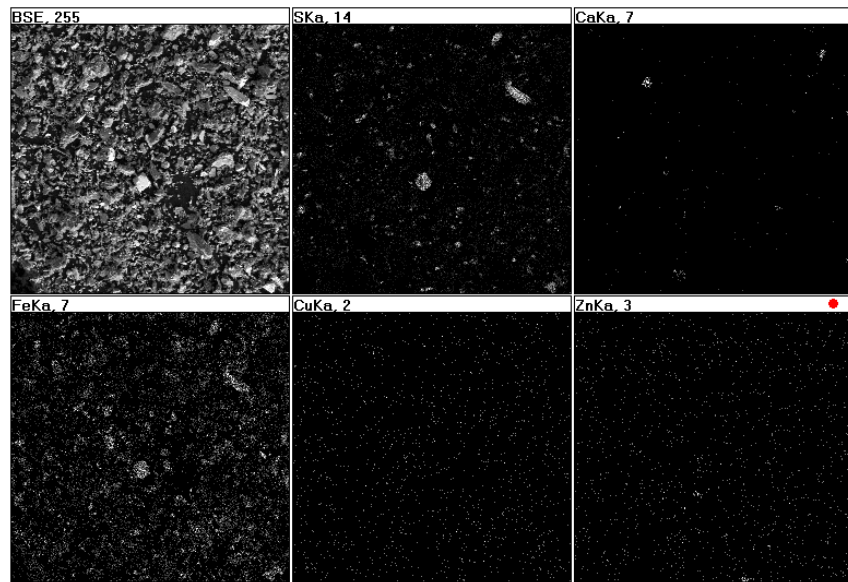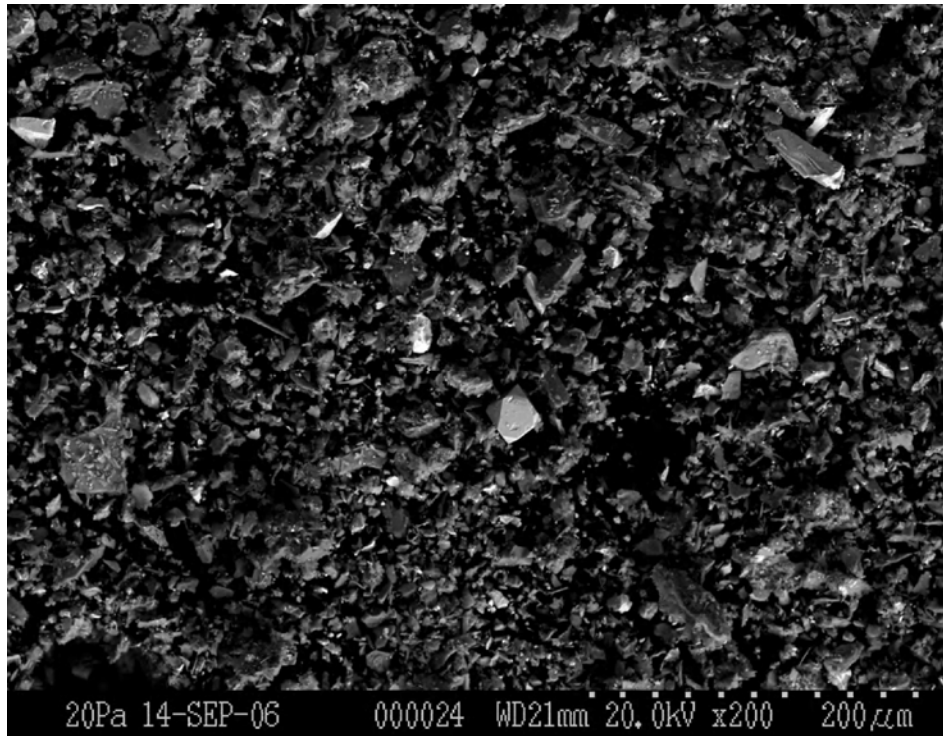
Figure C-4. Backscattered electron image (top picture and upper left corner of bottom picture) of a subsample of Core 2 at 0.0-0.5 cm depth, showing the general morphology of the tailings particles, along with X-ray maps of S, Ca, Fe, Cu and Zn (bottom picture), which aid with locating minerals of interest.
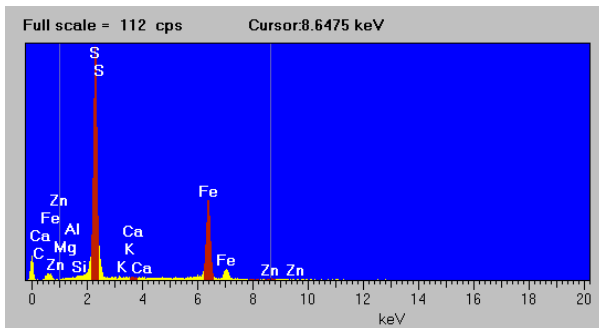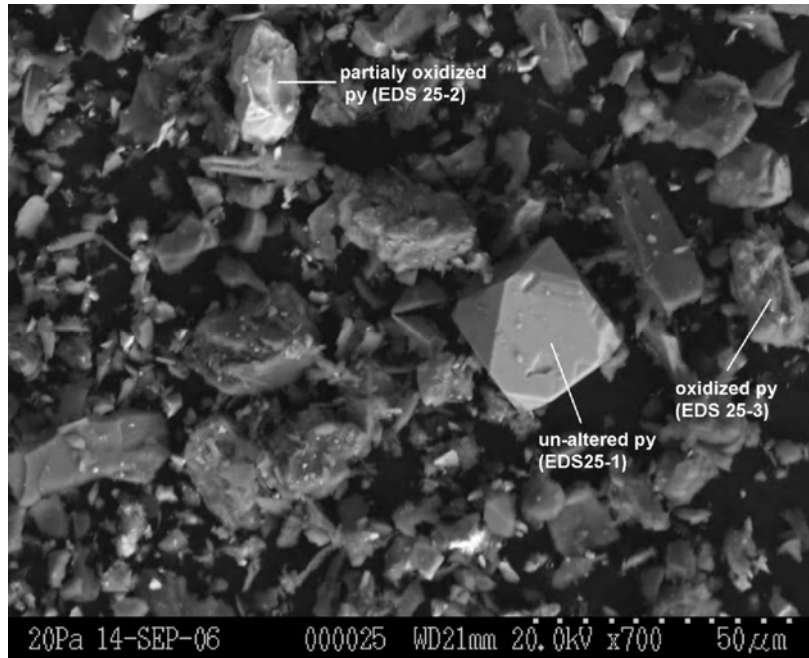
EDS25-1 (unaltered pyrite)

EDS 25-3 (oxidized pyrite)
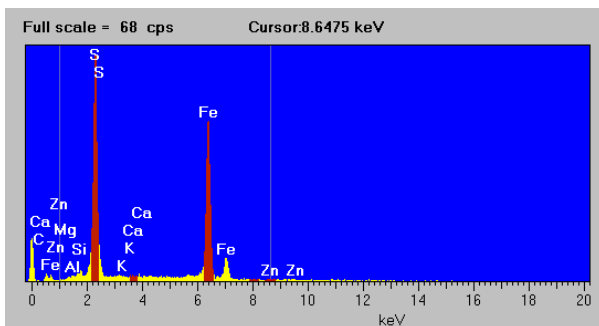
EDS 25-2 (partially oxidized pyrite)
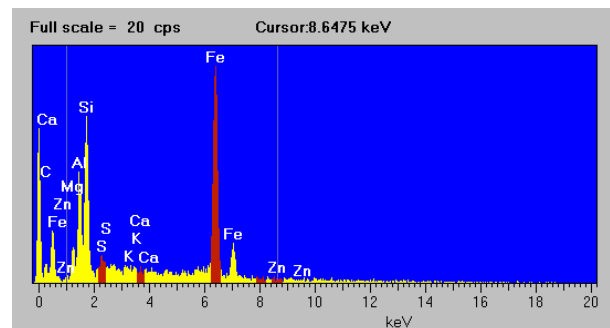
Figure C-5. Backscattered electron image of the centre part of the BSE in Figure C-4 (top picture) showing pyrite altered to various degrees. As demonstrated by the corresponding EDX spectra (bottom pictures), the euhedral grain (EDS 25-1) remains fresh while the deformed grains (EDS 25-2 and 25-3) are more altered with increasing Fe/S ratio.

EDS26-1
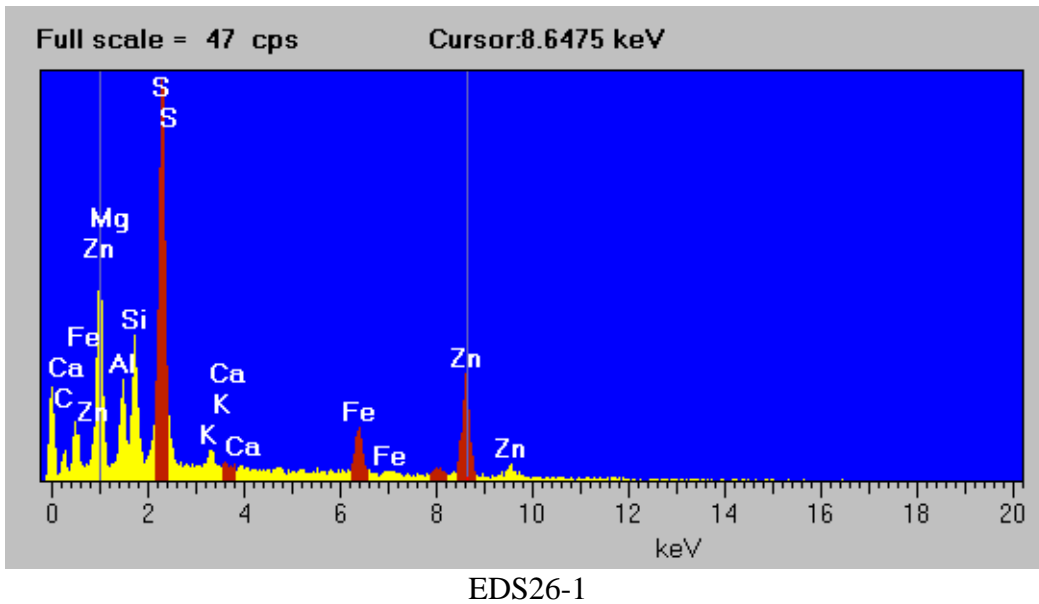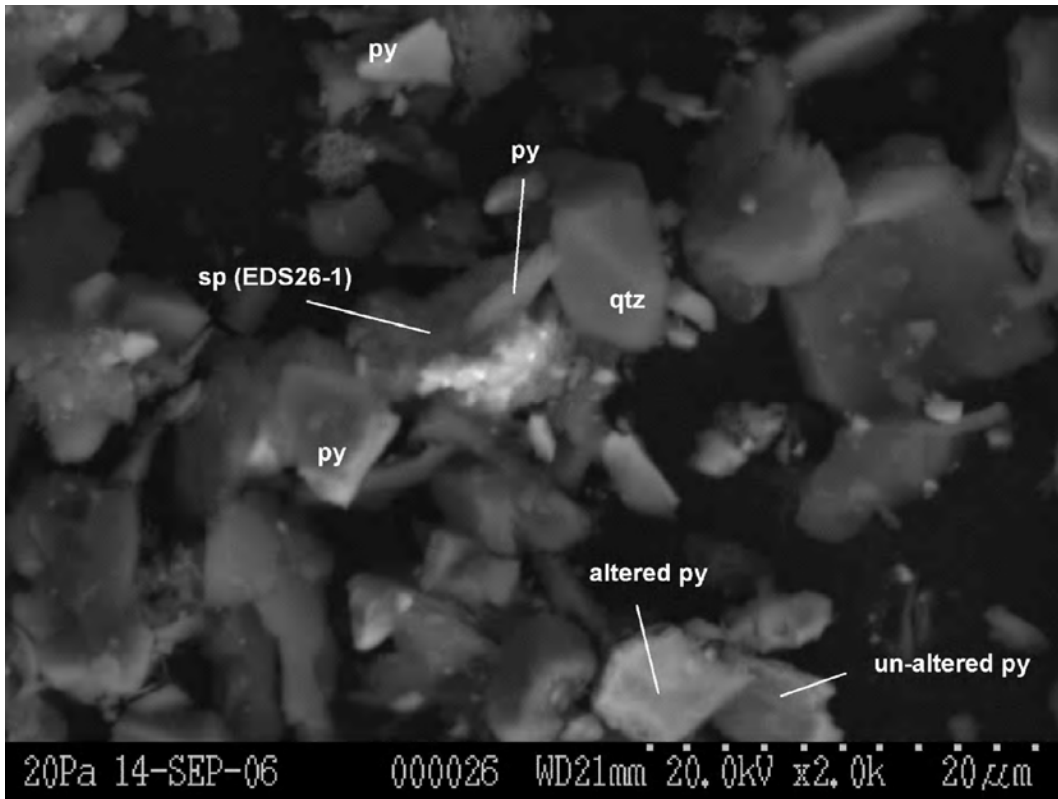
Figure C-6. Backscattered electron image (top) of another portion of the grain mount of Core 2, 0.0-0.5 cm showing the occurrence of pyrite (py) altered to varied extent. The presence of sphalerite (sp) along with pyrite is confirmed by spot EDX analysis (bottom).
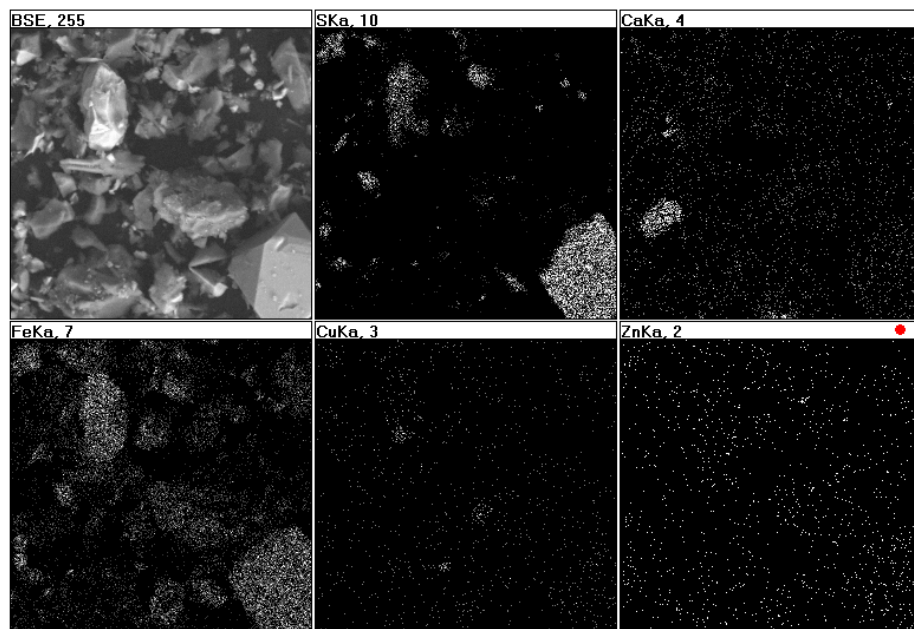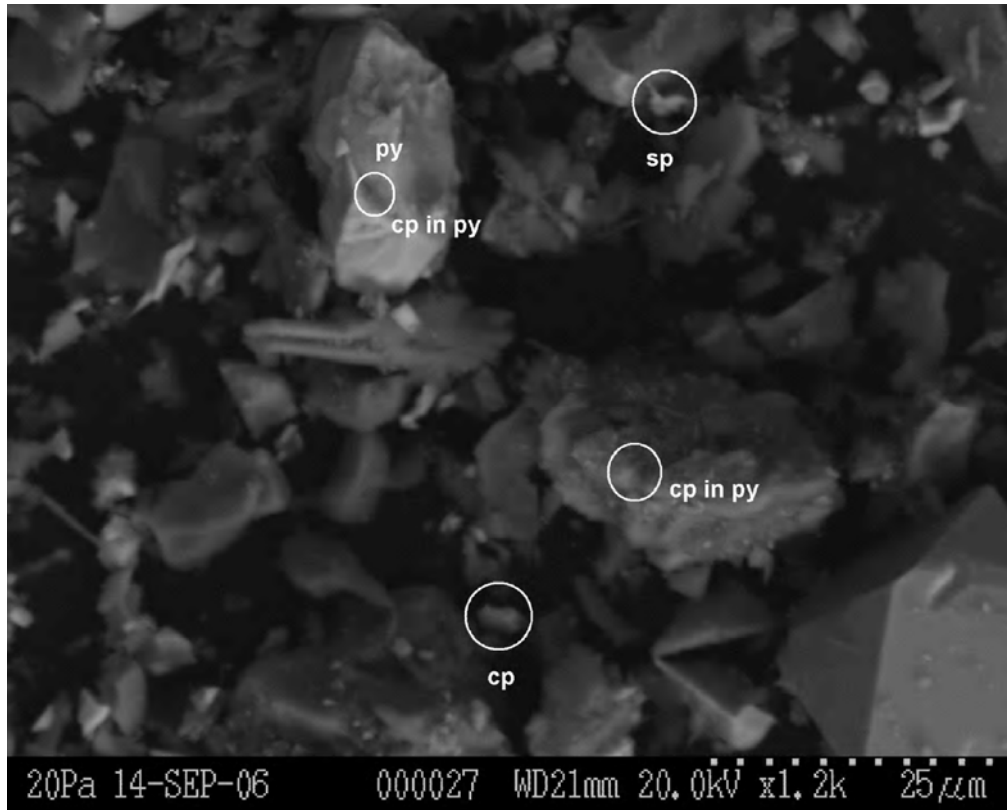
Figure C-7. Backscattered electron image (top) of a subsample of Core 2 at 0.0-0.5 cm depth along with the corresponding X-ray maps for S, Ca, Fe, Cu and Zn showing the occurrence of pyrite (py), chalcopyrite (cp) and sphalerite (sp) and their mutual relationships in the sample.

Core 2, 4.5-5.5 cm: Relatively unaltered pyrite in different forms and shapes were readily observed. Chalcopyrite and sphalerite were also occasionally encountered.
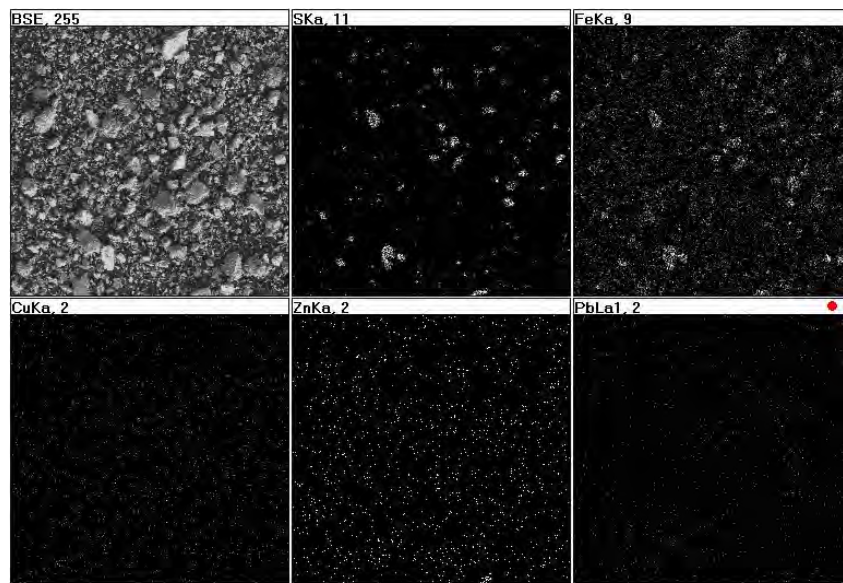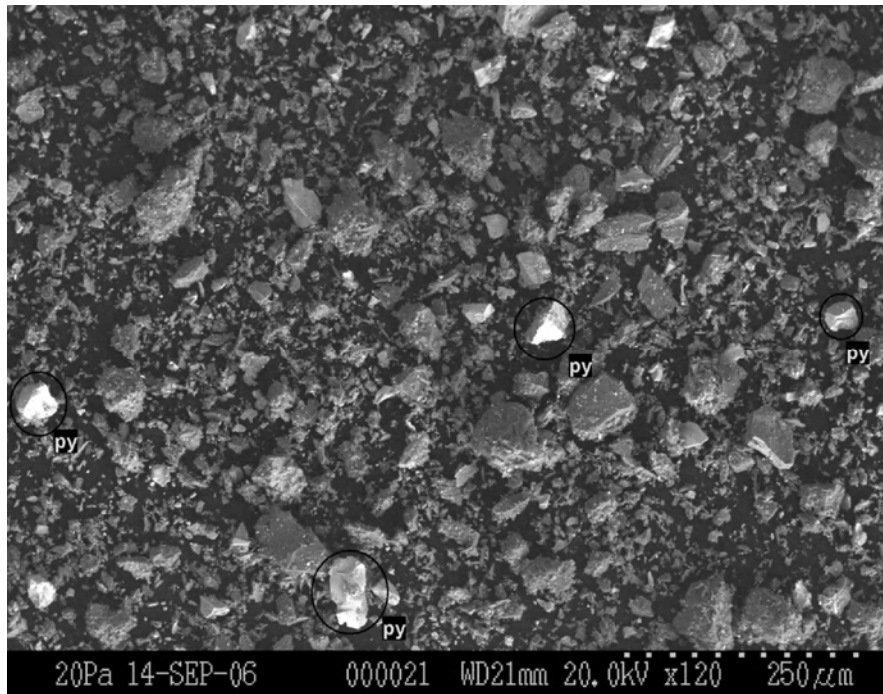
Figure C-8. Backscattered electron image (top) of a selected area of the grain mount for Core 2 at 4.5-5.5 cm depth along with the corresponding X-ray maps for S, Fe, Cu, Zn and Pb (bottom), demonstrating the dominance of relatively fresh pyrite in the sample.
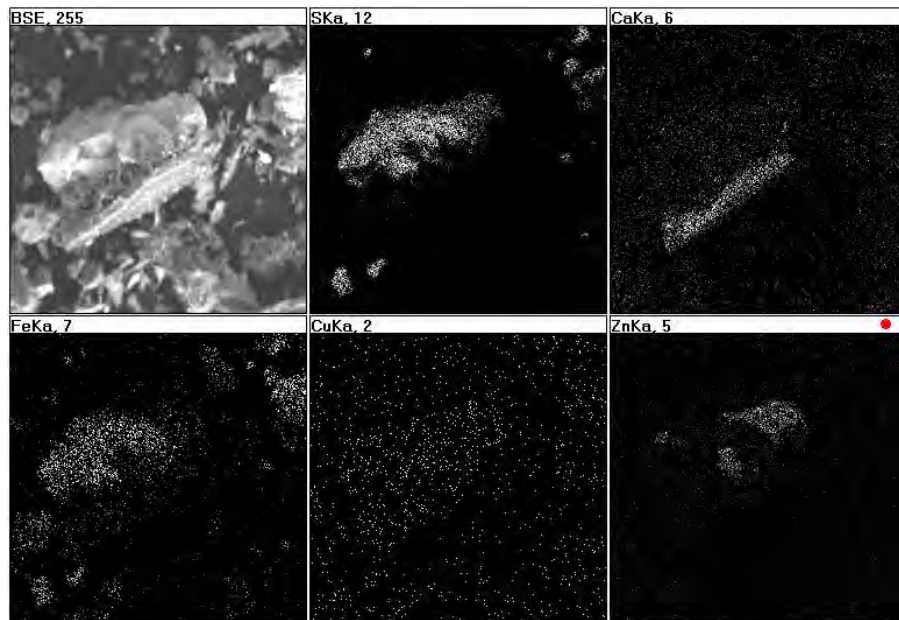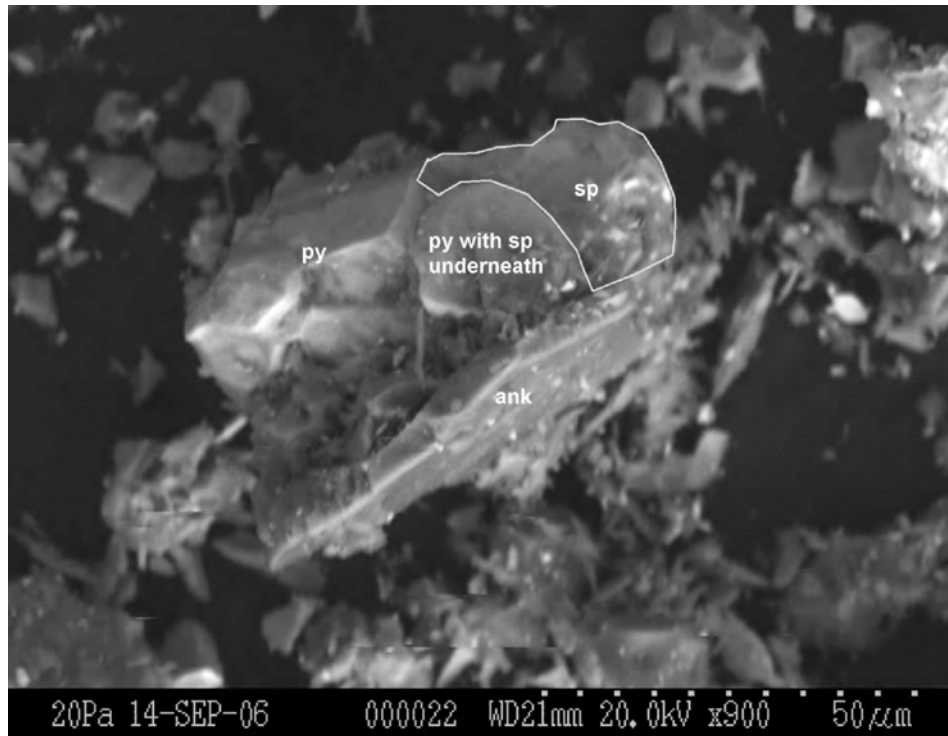
Figure C-9. Backscattered electron image (top) of a pyrite (py)-sphalerite (sp)-ankerite (ank) assemblage in Core 2 at 4.5-5.5 cm depth along with the corresponding X-ray maps for S, Ca, Fe, Cu and Zn (bottom). The texture of the pyrite-sphalerite couple is indicative of galvanic interaction. A comparison of the X-ray map for Cu with those of the other elements suggests a close association of Cu with the sulphide minerals.
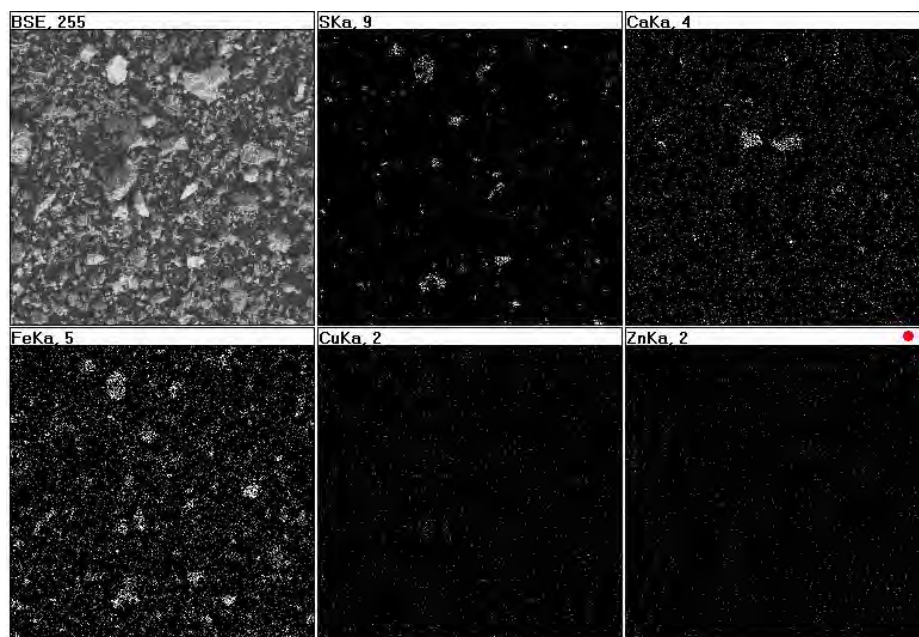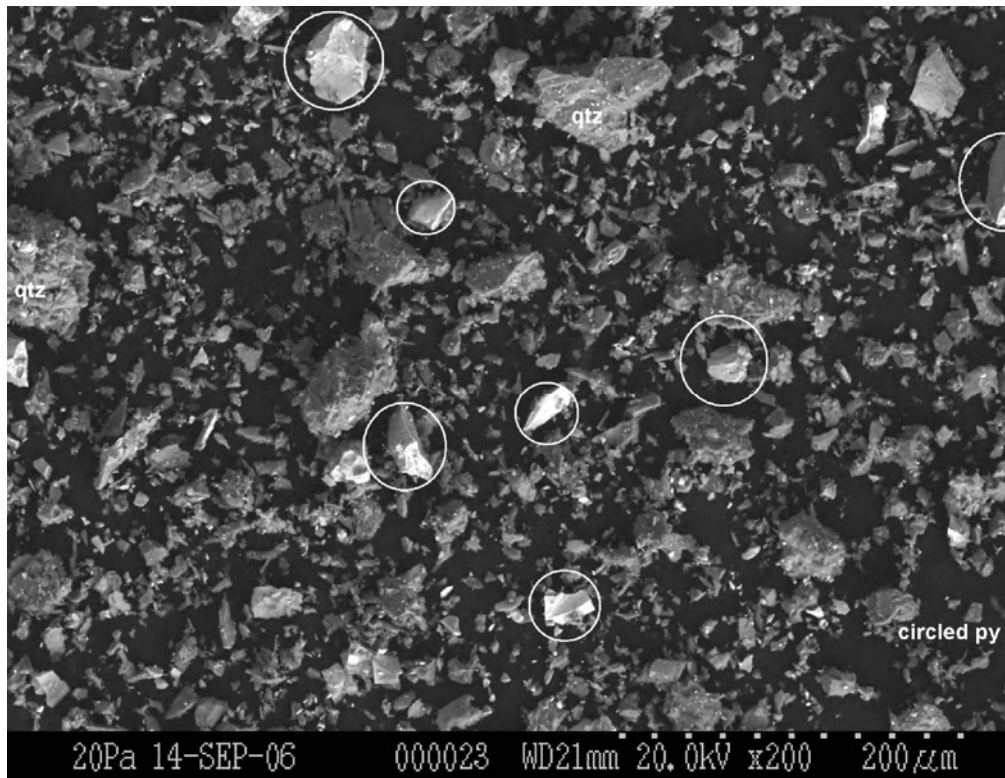
Figure C-10. Backscattered electron image (top) of another selected area in the grain mount of Core 2 at 4.5-5.5 cm depth along with the corresponding X-ray maps for S, Ca, Fe, Cu and Zn (bottom), demonstrating pyrite as the dominant sulphide in the sample.

Core 3 Biofilm layer: The sample was fibrous with notable macrophyte and enriched in Fe-oxyhydroxide. Remnant pyrite was also observed.
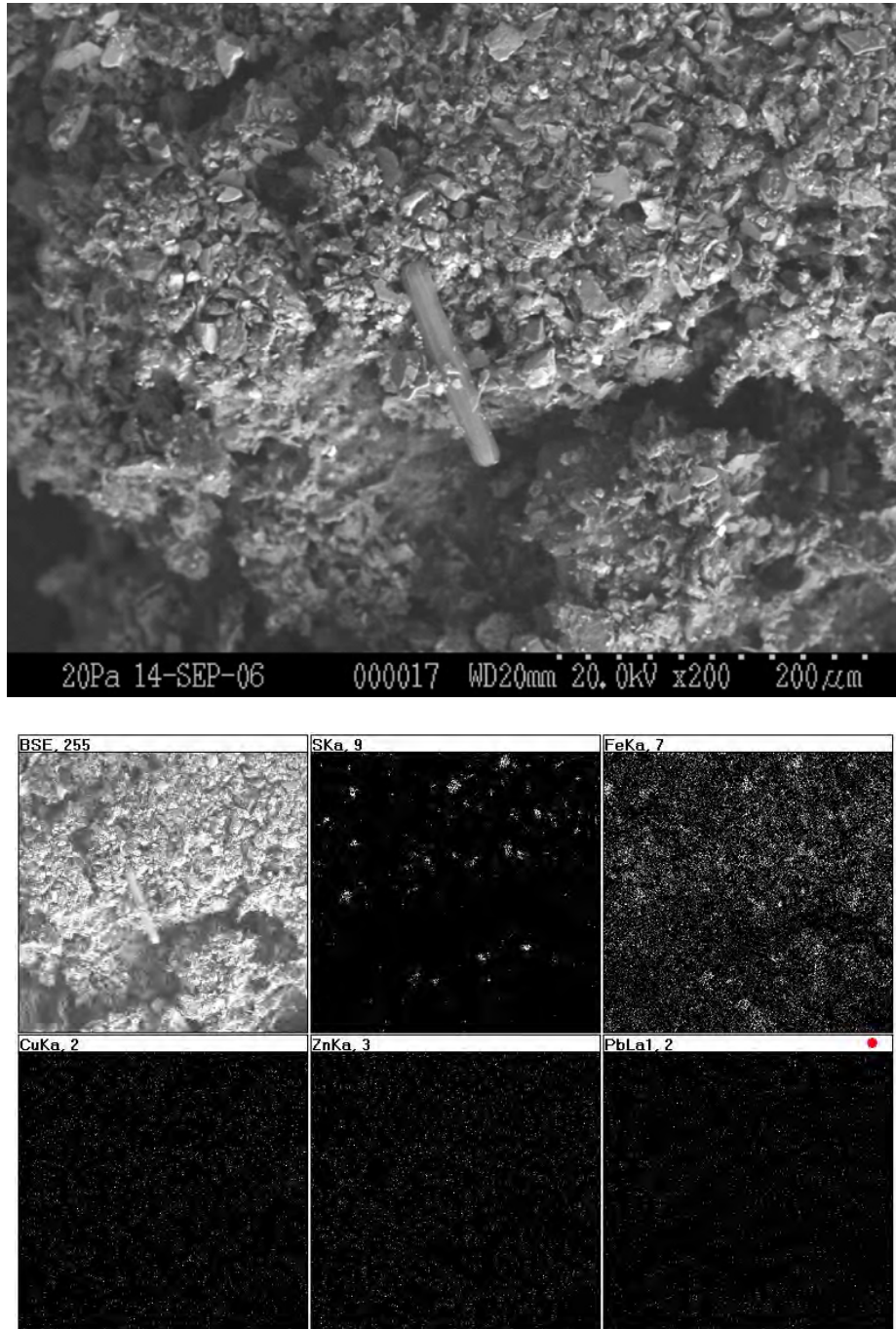
Figure C-11. Backscattered image (top) of a selected area in the grain mount of a subsample of the biofilm layer in Core 3, showing the general texture, along with the corresponding X-ray maps of S, Fe, Cu, Zn and Pb, which demonstrate the abundance of Fe-oxyhydroxide and the occurrence of remnant Fe-sulphide in the sample.
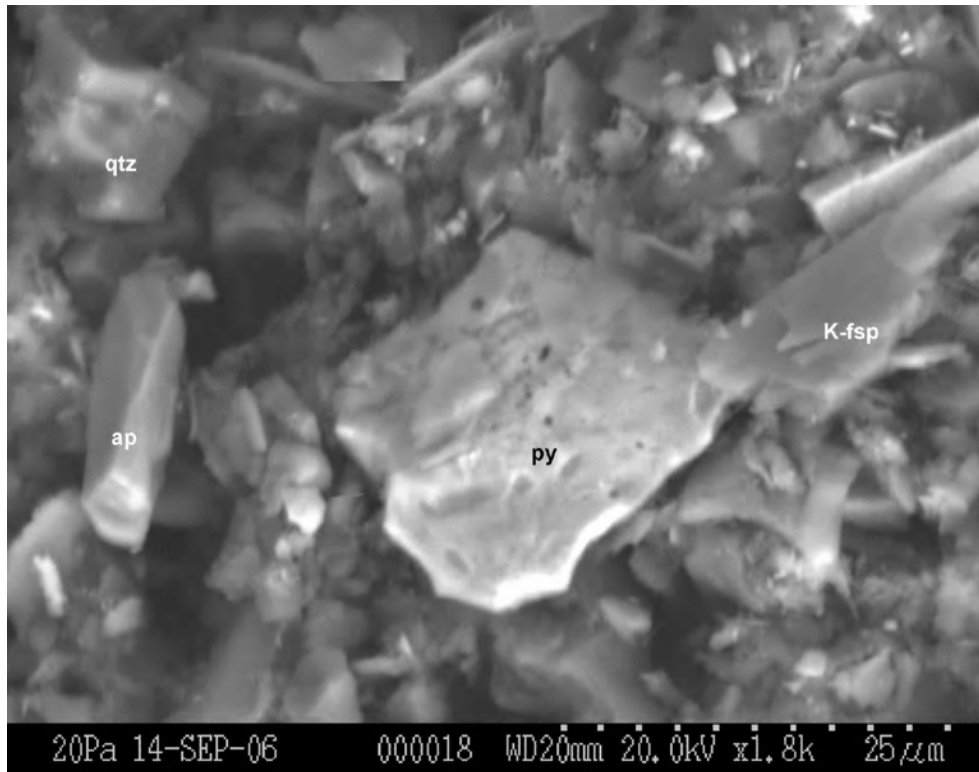
Figure C-12. Backscattered electron image of a partially altered pyrite (py) found in the biofilm layer of Core 3. Other minerals identified include quartz (qtz), K-feldspar (K-fsp) and apatite (ap).
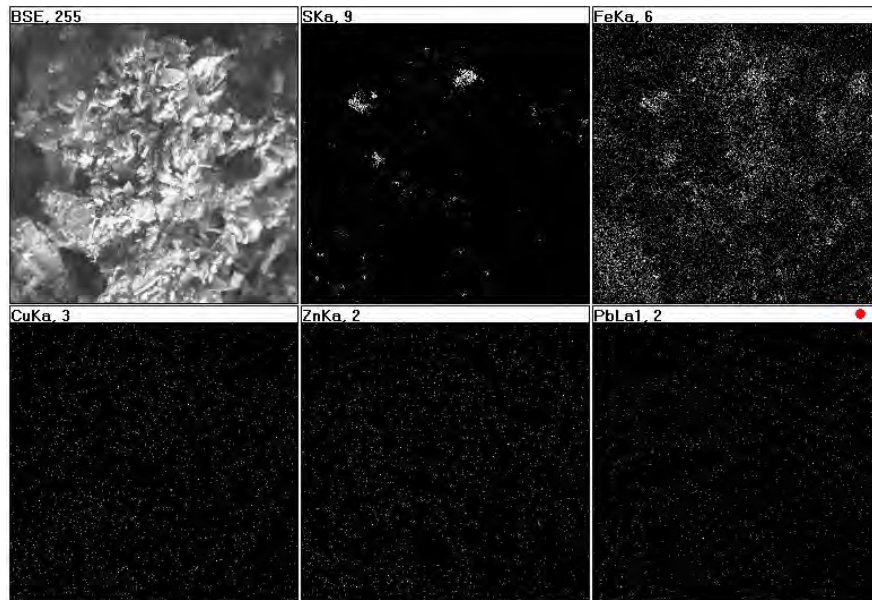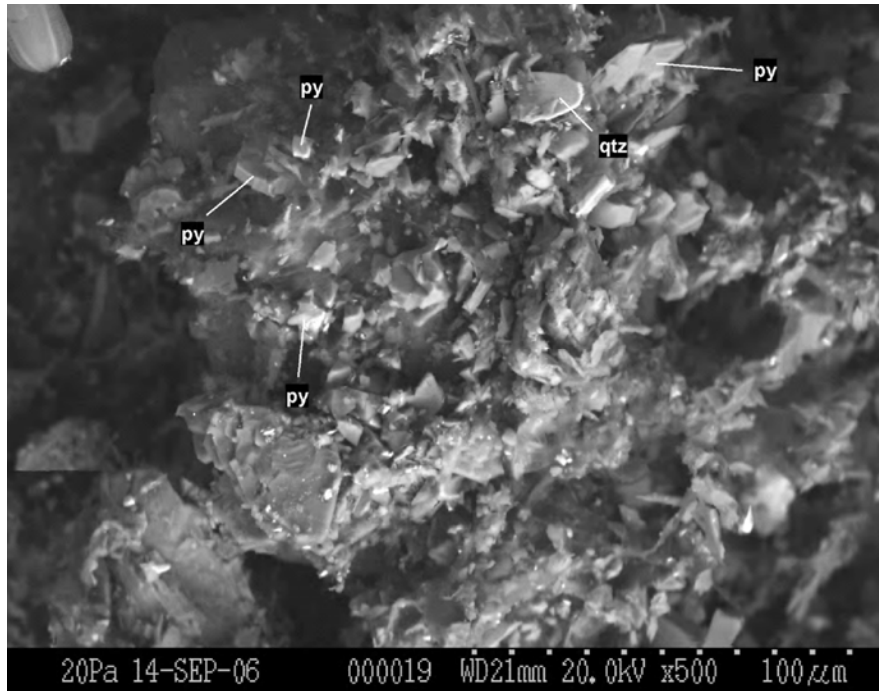
Figure C-13. Backscattered electron image (top) of another area in the grain mount of the biofilm layer from Core 3, showing scattered pyrite (py) with quartz (qtz). The corresponding X-ray maps for S, Fe, Cu, Zn and Pb (bottom), however, indicate that most Fe occurs as Fe-oxyhydroxide. There appears to be little local concentration of Cu, Pb or Zn.
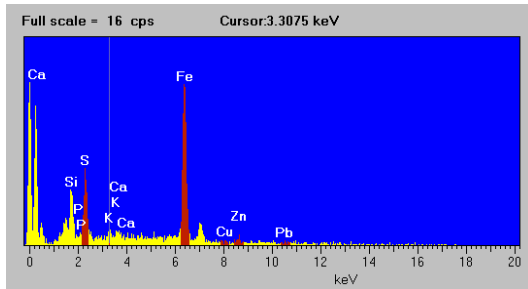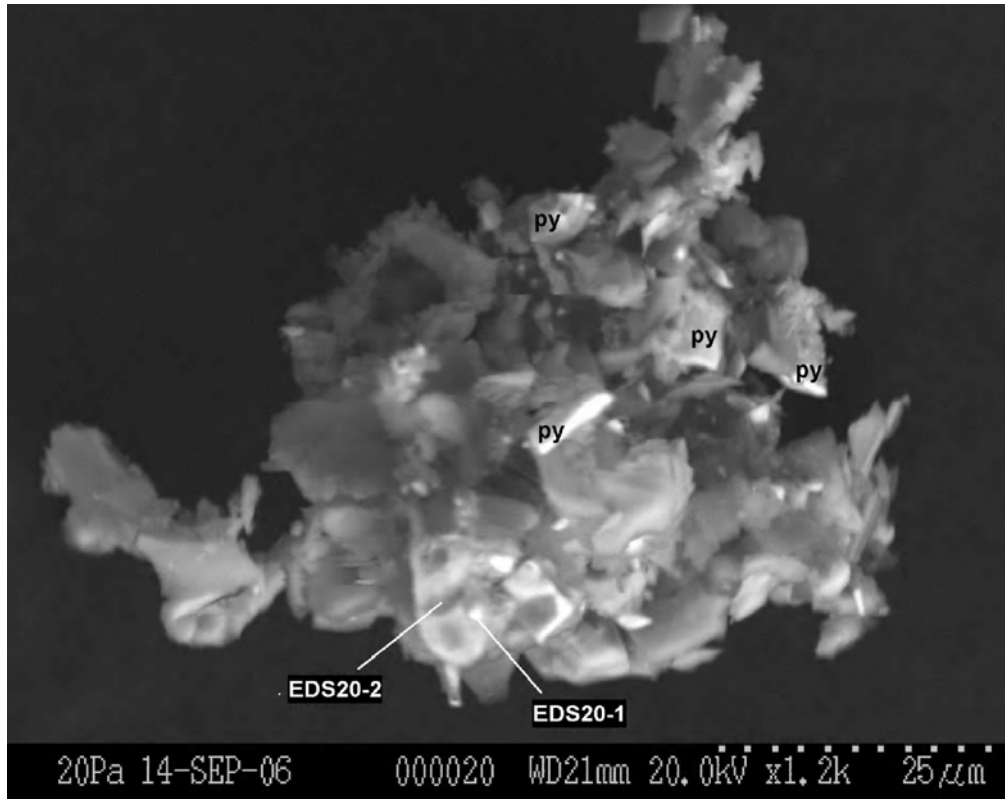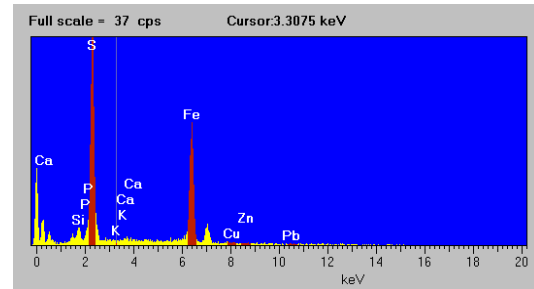
EDS20-1   EDS20-2

Figure C-14. Backscattered electron image (top) of a cluster of remnant pyrite found in the biofilm layer of Core 3. As demonstrated by the EDX spectra (bottom) taken at EDS20-1 and EDS20-2, some of these pyrite grains are partially oxidized, giving rise to a Fe/S ratio significantly different from 1/2.

Core 3, 0.0-0.5 cm: Pyrite altered to various extents was commonly observed. Rare remnants of sphalerite, arsenopyrite and suspected pyrrhotite were also found. Individual Cu sulphide minerals, however, appeared to be absent.
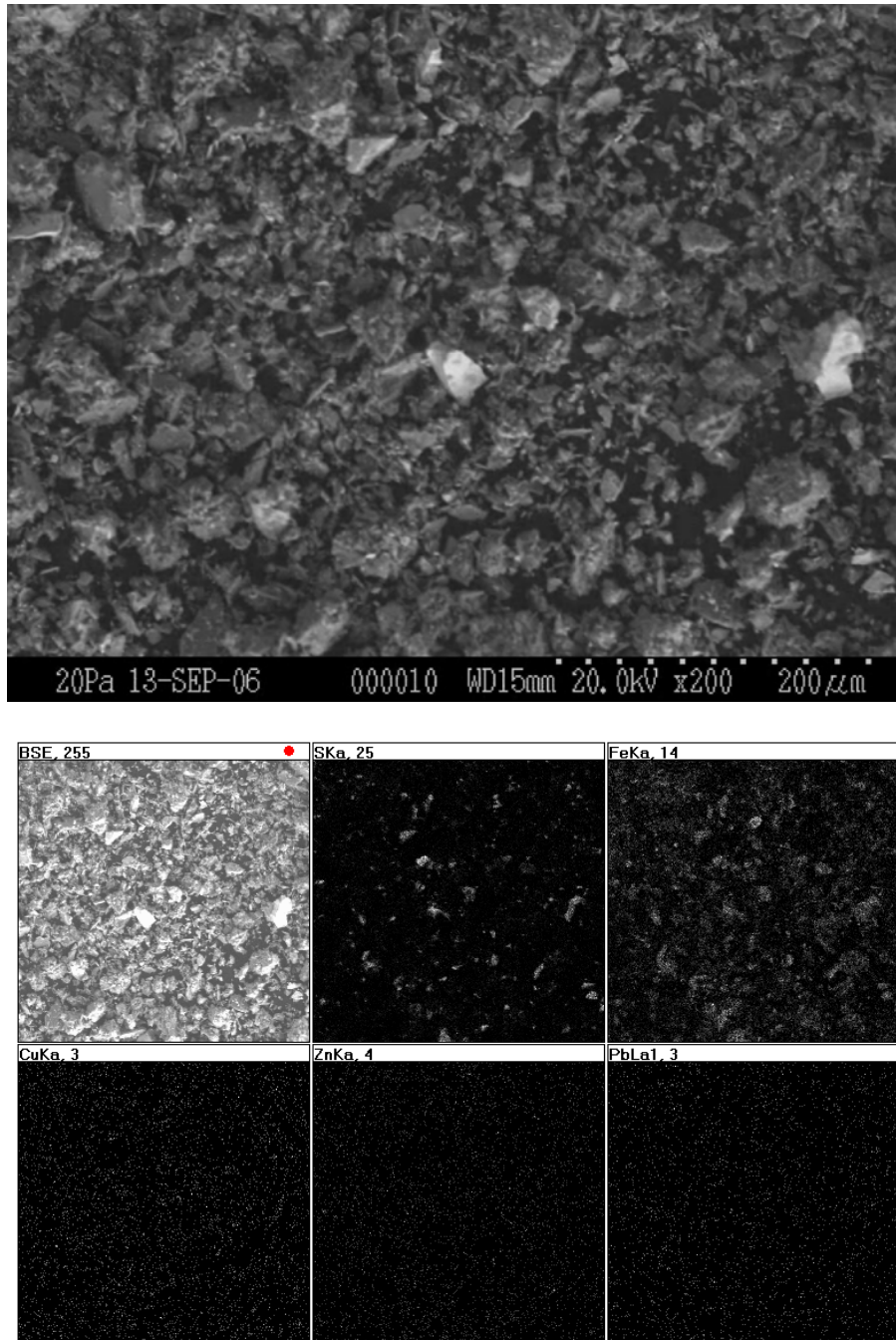
Figure C-15. Backscattered electron image (top) of a selected area in the grain mount of Core 3 at 0.0-0.5 cm depth, showing the general grain morphology, along with the X-ray maps for S, Fe, Cu, Zn and Pb, which reflect the abundance of iron sulphides in the sample.
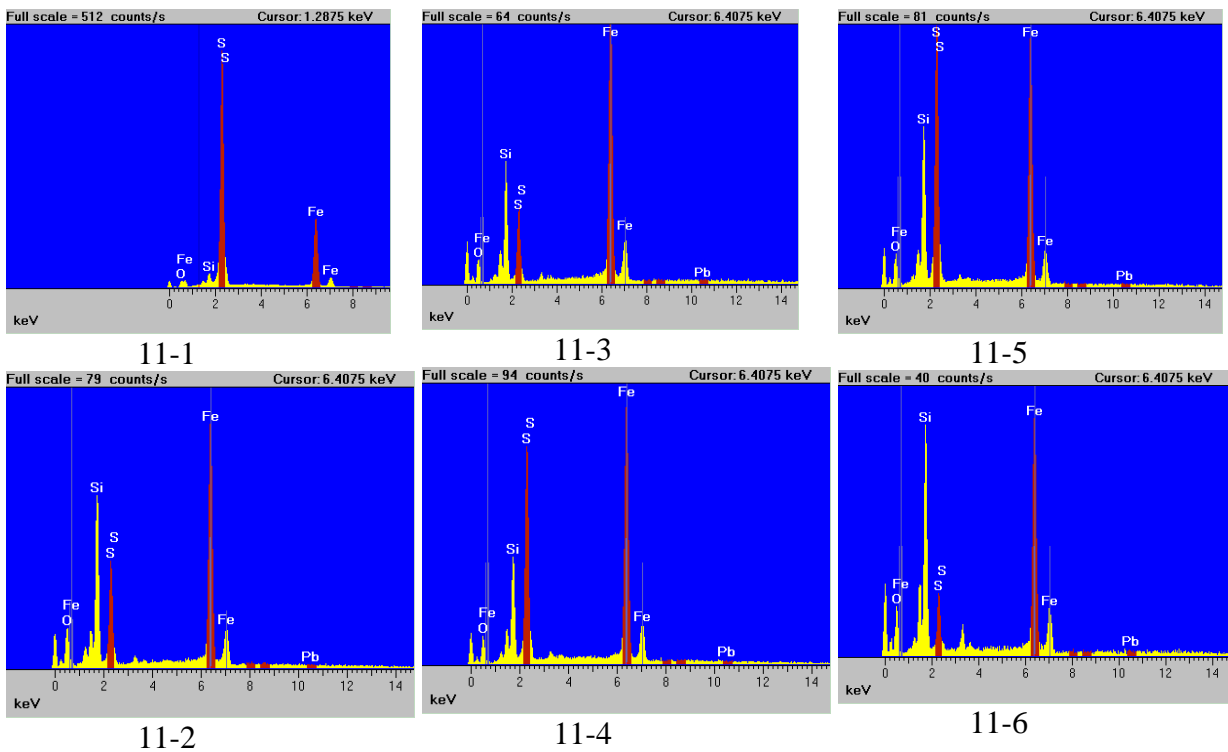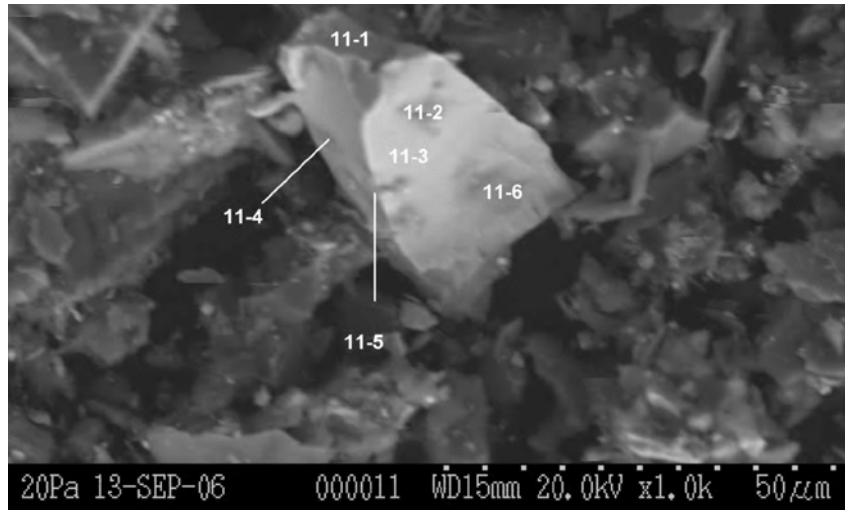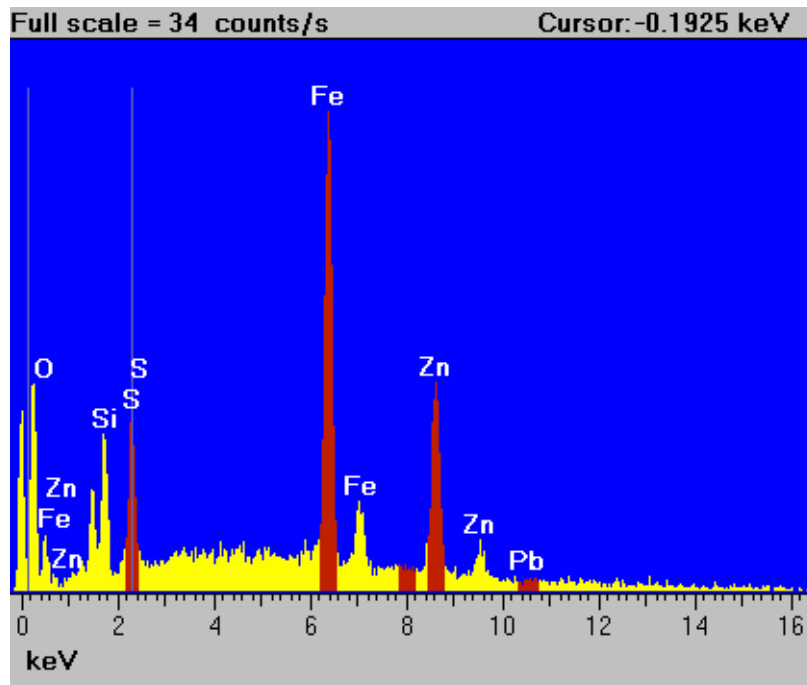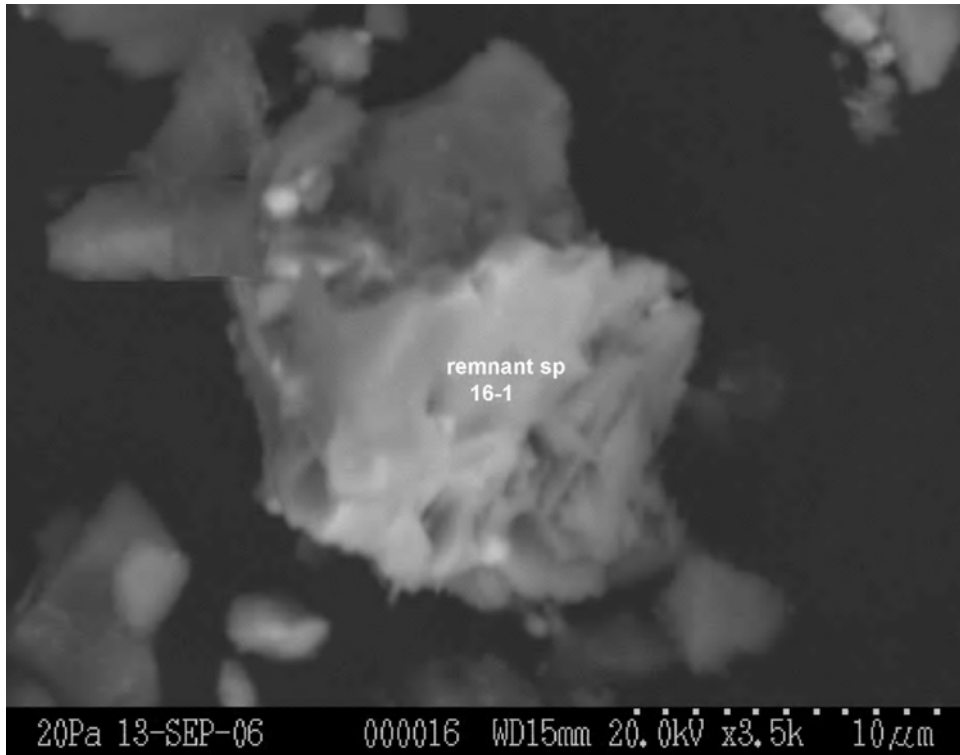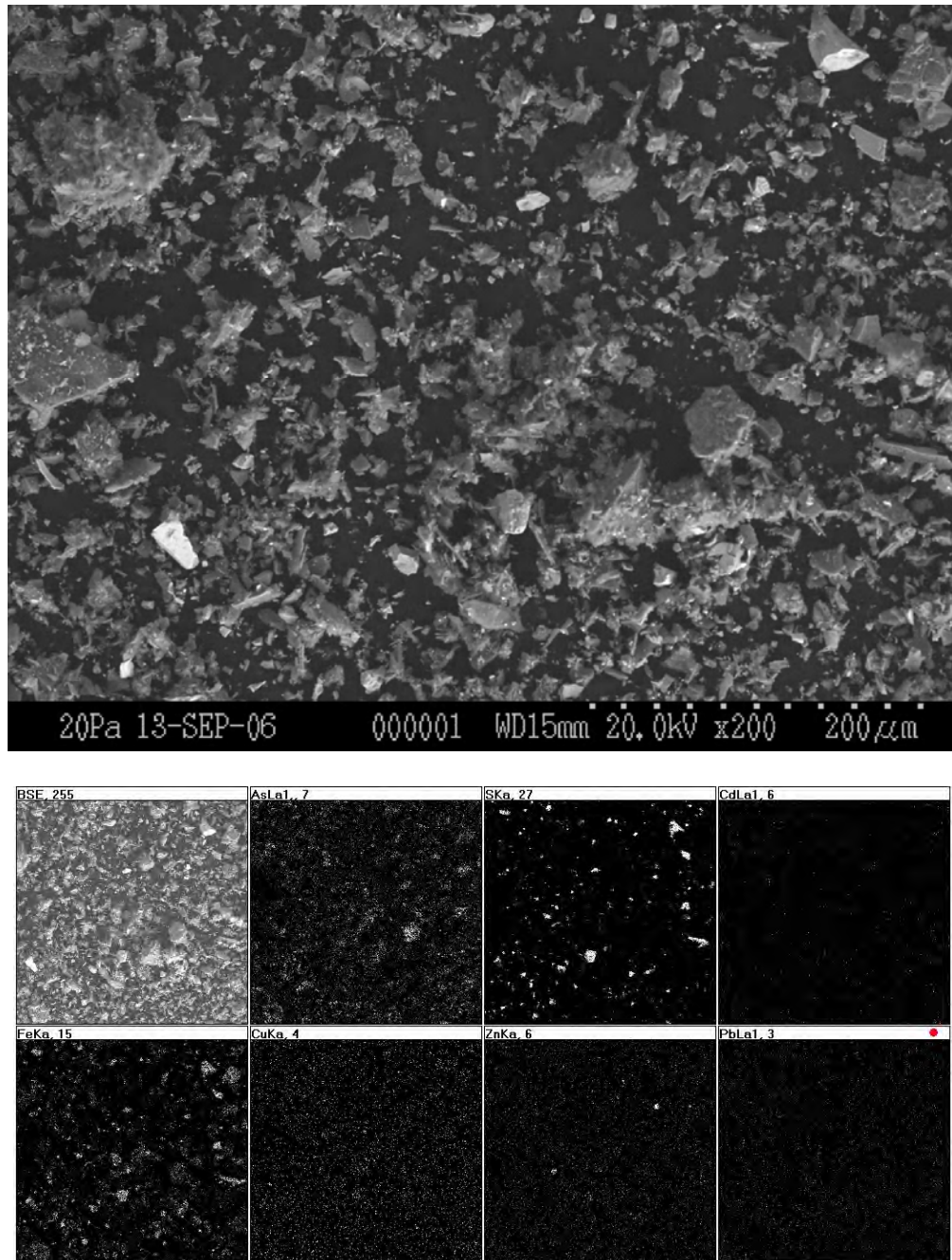
Figure C-16. Backscattered electron image (top) of a remnant pyrite grain found in Core 3 at 0.0-0.5 cm depth along with the EDX spectra acquired at various areas of the grain. The varying Fe/S ratios suggest that the pyrite grain was oxidized to various extents along different exposed surfaces.
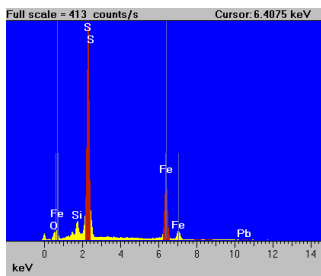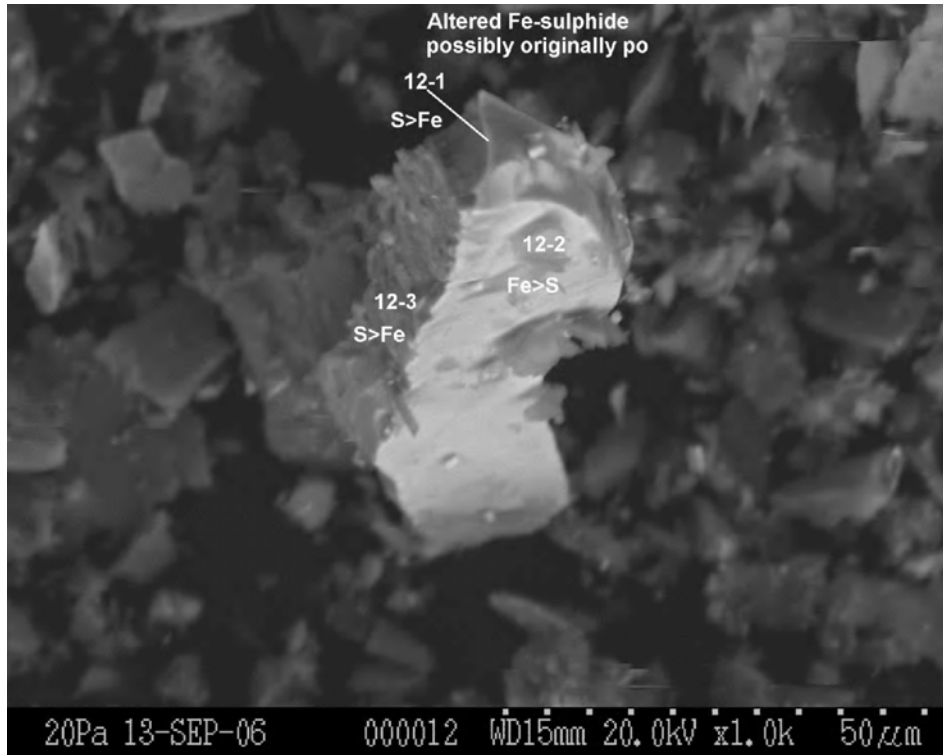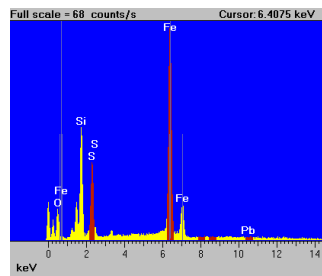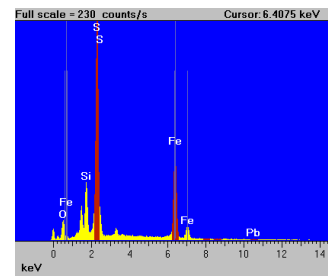
Figure C-17. Backscattered electron image (top) of an iron sulphide grain, possibly originally pyrrhotite, along with spot EDX spectra (bottom) taken at various surfaces of the grain. The varying Fe/S ratios suggest that the mineral was altered to various extents along different exposed surfaces.
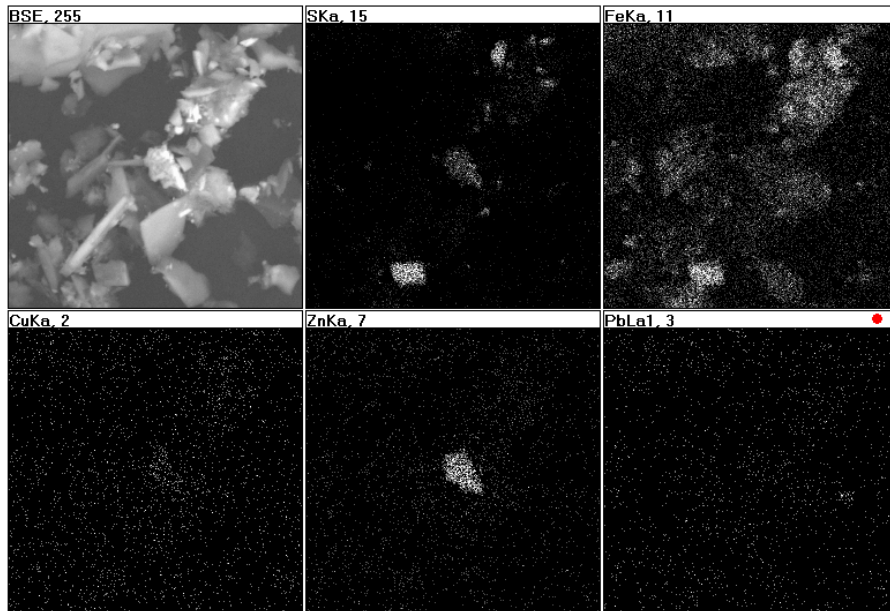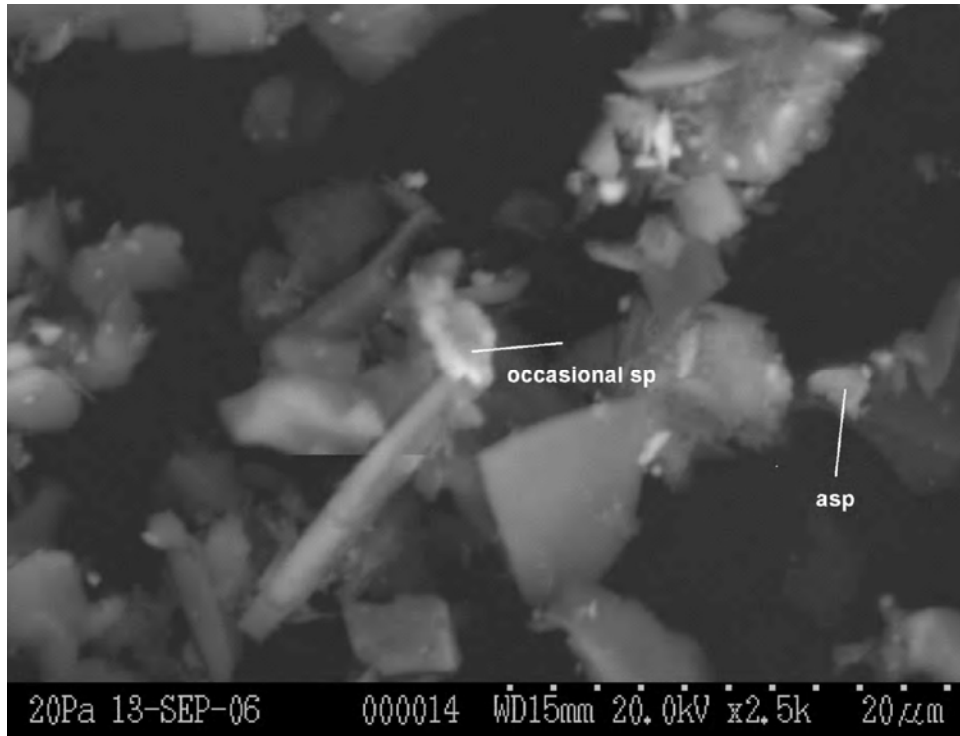
Figure C-18. Backscattered electron image (top) of rare sphalerite (sp) and arsenopyrite (asp) found among pyrite in Core 3 at 0.0-0.5 cm depth. The corresponding X-ray maps for S, Fe, Cu, Zn and Pb (bottom) show that the pyrite grains were replaced to various extents by Fe-oxyhydroxide while Cu appears to be preferentially associated with sphalerite.
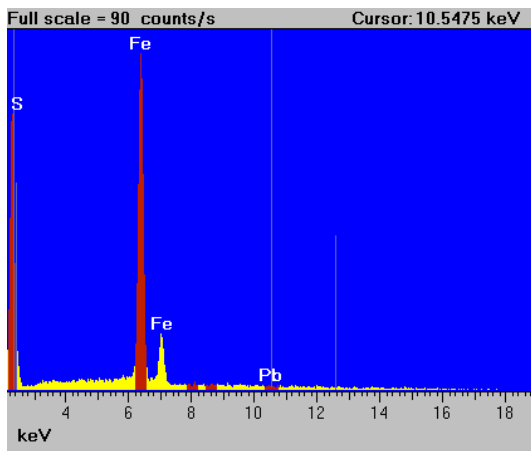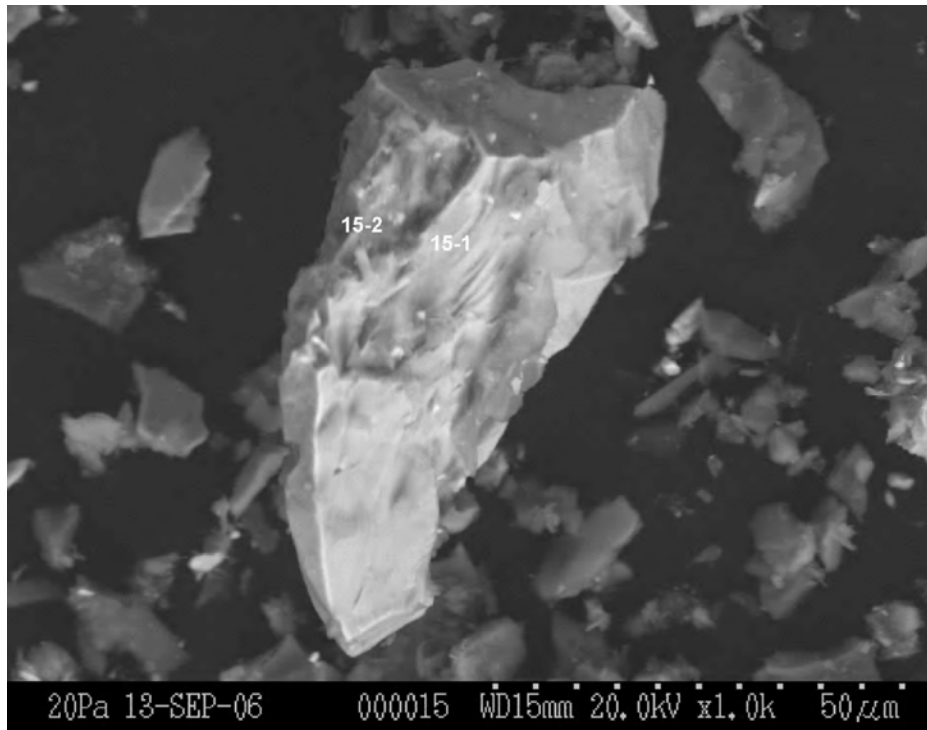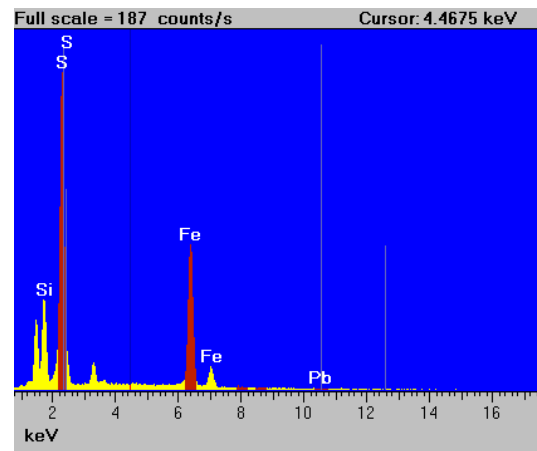
Figure C-19. Backscattered electron image (top) of a relatively fresh pyrite grain found in Core 3 at 0.0-0.5 cm depth. The varying Fe/S ratios in the EDX spectra (bottom) support the occurrence of minor oxidation.

Figure C-20. Backscattered electron image (top) of a remnant sphalerite (sp) found in Core 3 at 0.0-0.5 cm depth along its EDX spectrum (bottom).

Core 3, 4.5-5.5 cm: Abundant, relatively unaltered pyrite and some eroded grains of sphalerite were observed. Rare chalcopyrite and pyrrhotite were also found.

Figure C-21. Backscattered electron image of a selected area in the grain mount of Core 3 at 4.5-5.5 cm depth (top), showing the general morphology of the tailings particles. The corresponding X-ray maps (bottom) for Mg (mislabeled as As), S, Ca, Fe, Cu, Zn and Pb demonstrate pyrite as the dominant sulphide, while some sphalerite also occurs.
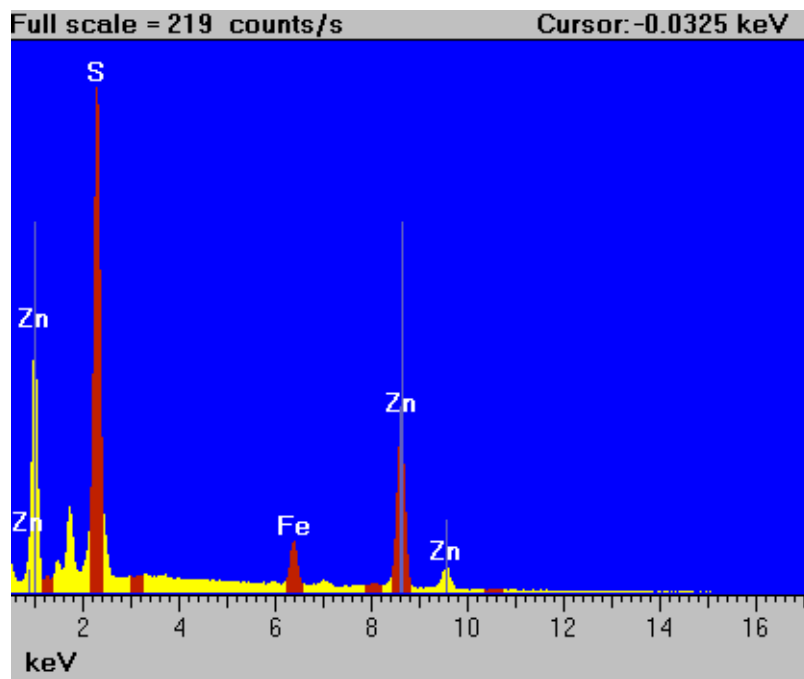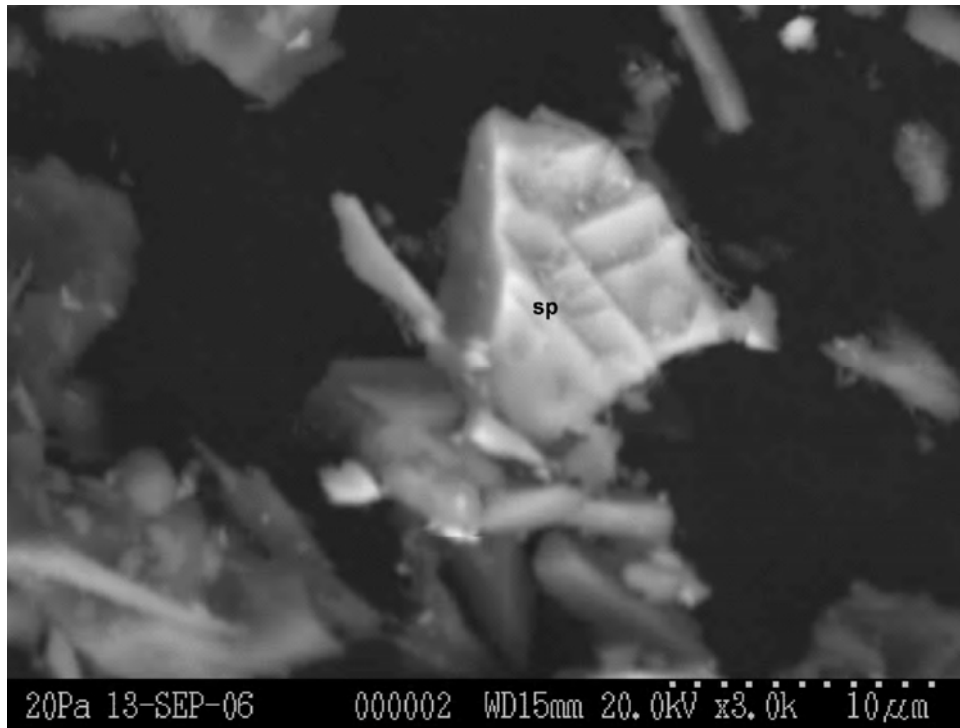
Figure C-22. Backscattered electron image (top) of a partially dissolved sphalerite (sp) found in Core 3 at 4.5-5.5 cm depth. The spot EDX spectrum (bottom) indicates that some associated pyrite is likely present.
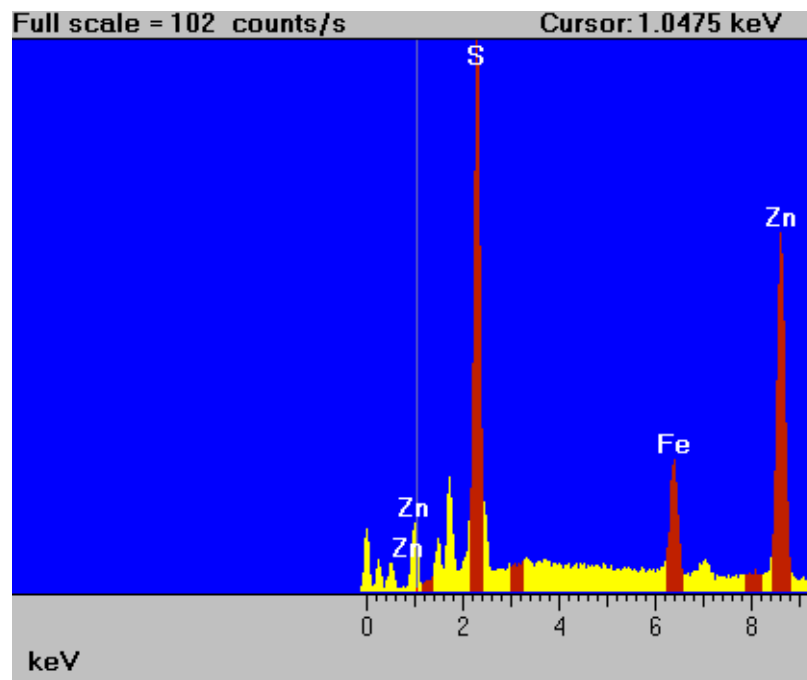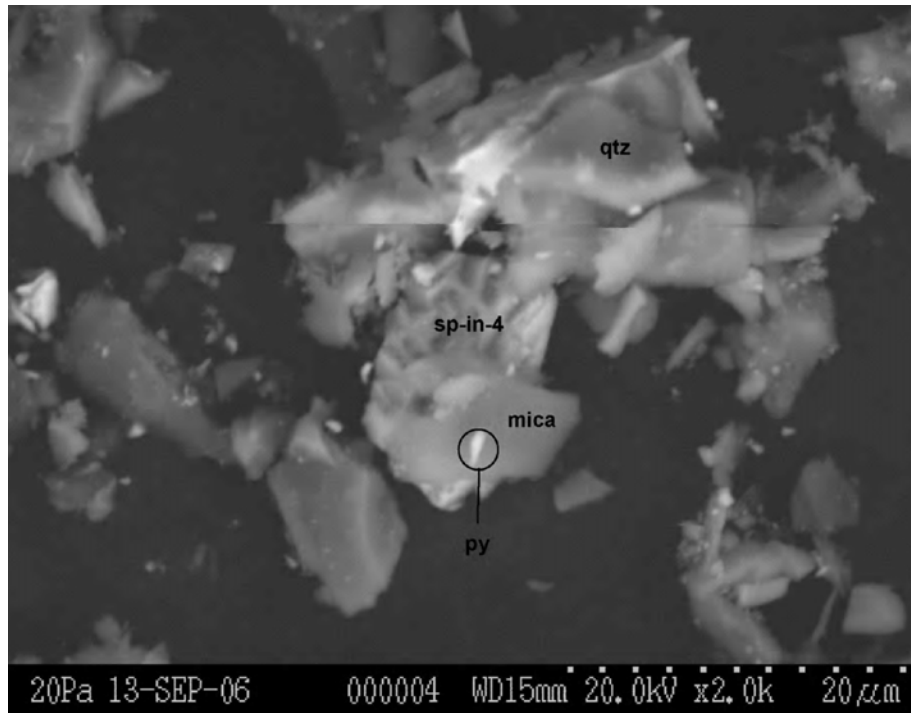
Sp-in-4

Figure C-23. Backscattered electron image of pyrite (py) and sphalerite (sp) observed among mica and quartz (qtz) in Core 3 at 4.5-5.5 cm depth (top). The EDX spectrum (bottom) taken at the spot sp-in-4 indicates the presence of pyrite associated with the partially dissolved sphalerite.
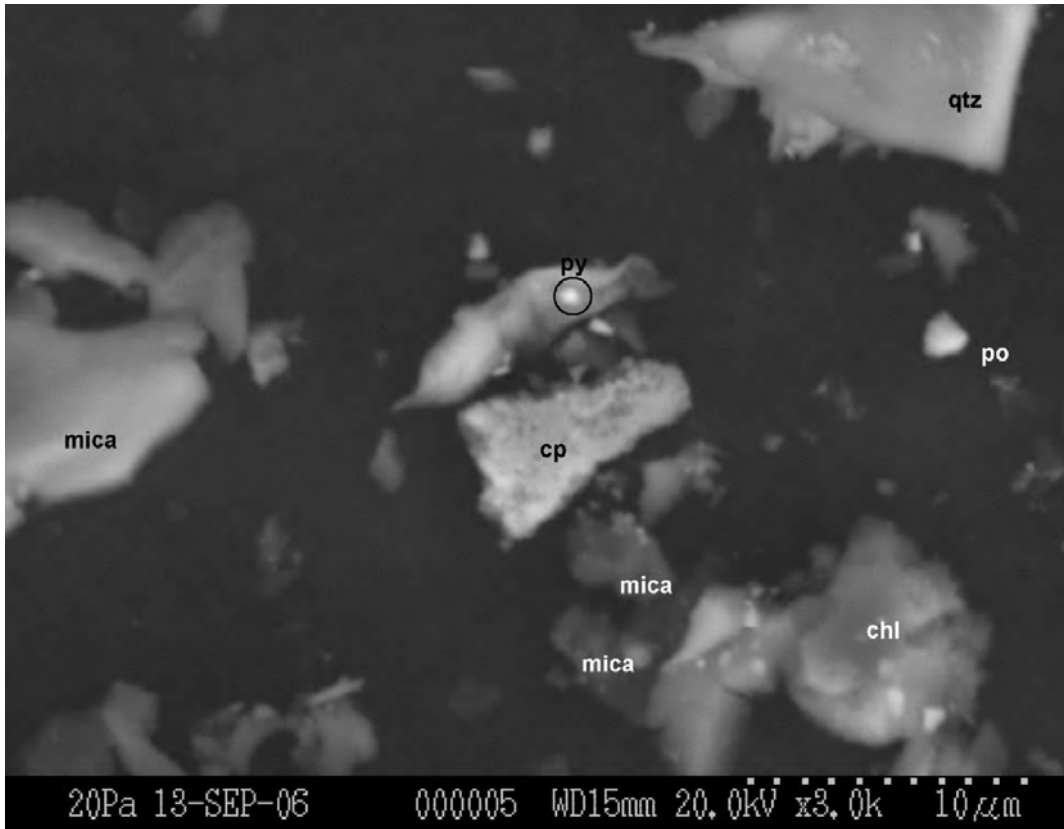
Figure C-24. Backscattered electron image of small grains of pyrite (py), chalcopyrite (cpy) and pyrrhotite (po) observed among the silicates, quartz (qtz), chlorite (chl) and mica in Core 3 at 4.5-5.5 cm depth.
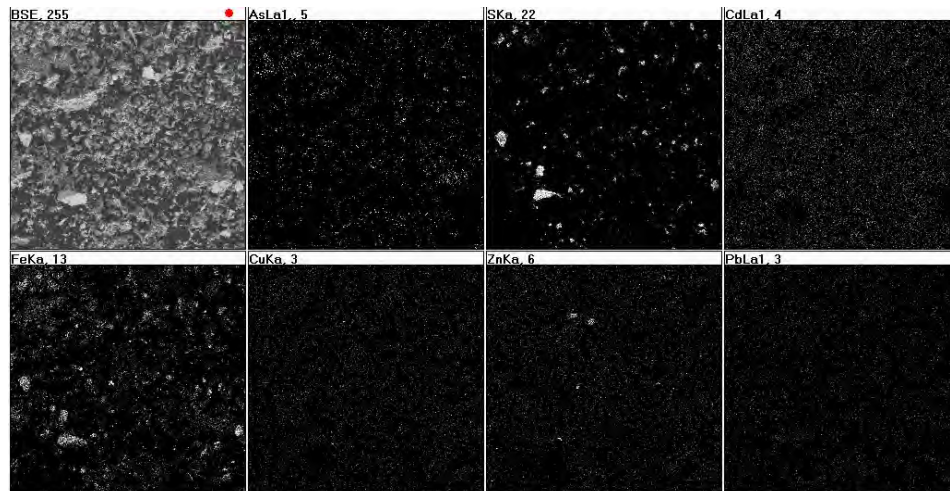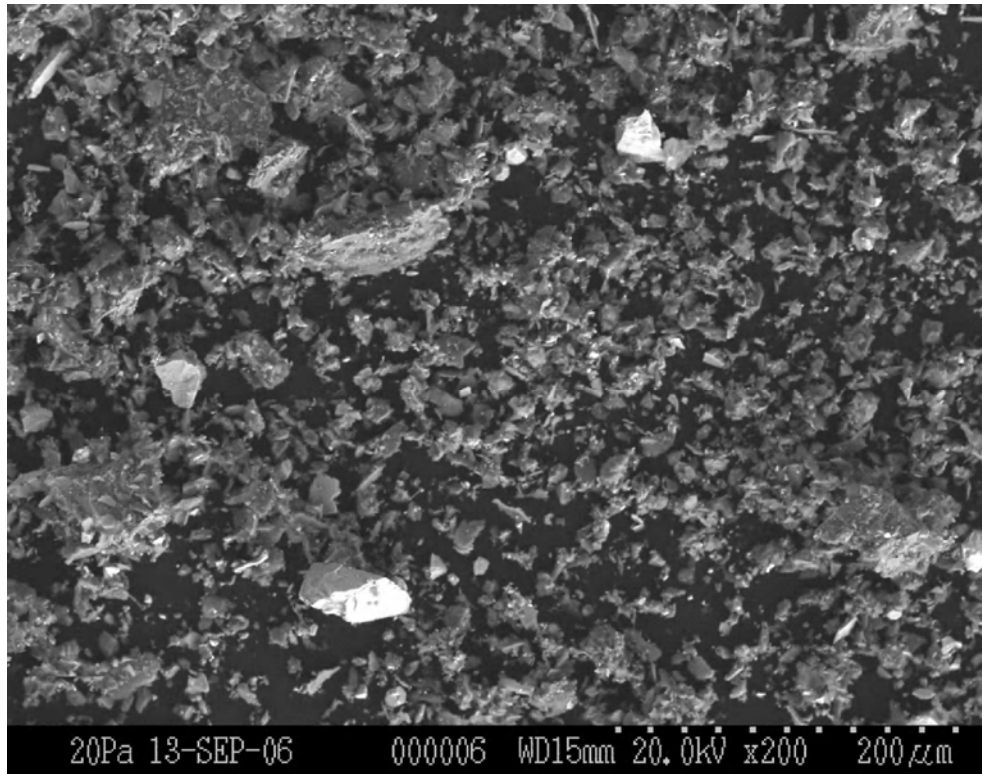
Figure C-25. Backscattered electron image (top) of another selected area of the grain mount of Core 3 at 4.5-5.5 cm depth, showing the general morphology of the tailings solids. The corresponding X-ray maps (bottom) for As (which should read Mg), S, Ca, Fe, Cu, Zn and Pb support the occurrence of abundant pyrite and rare sphalerite in the sample.
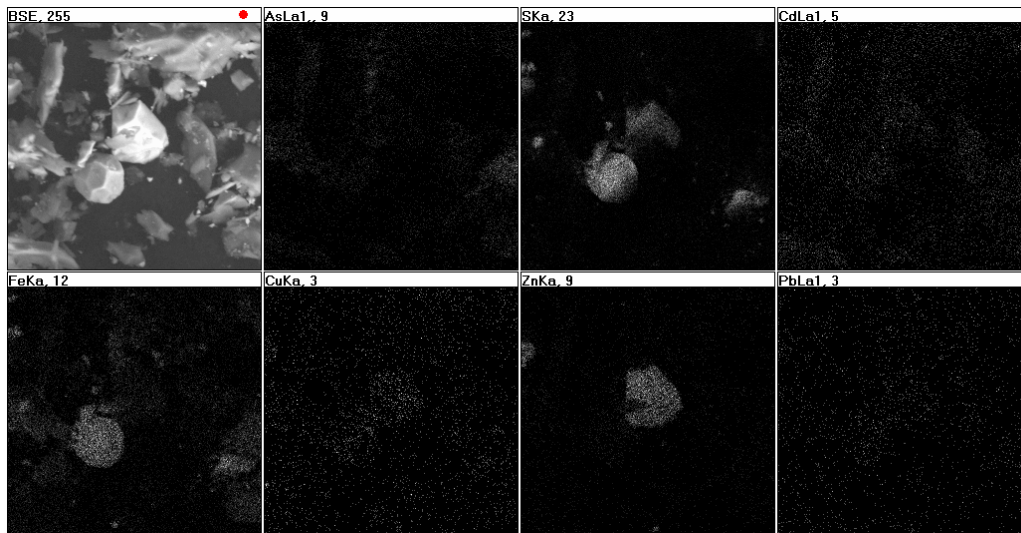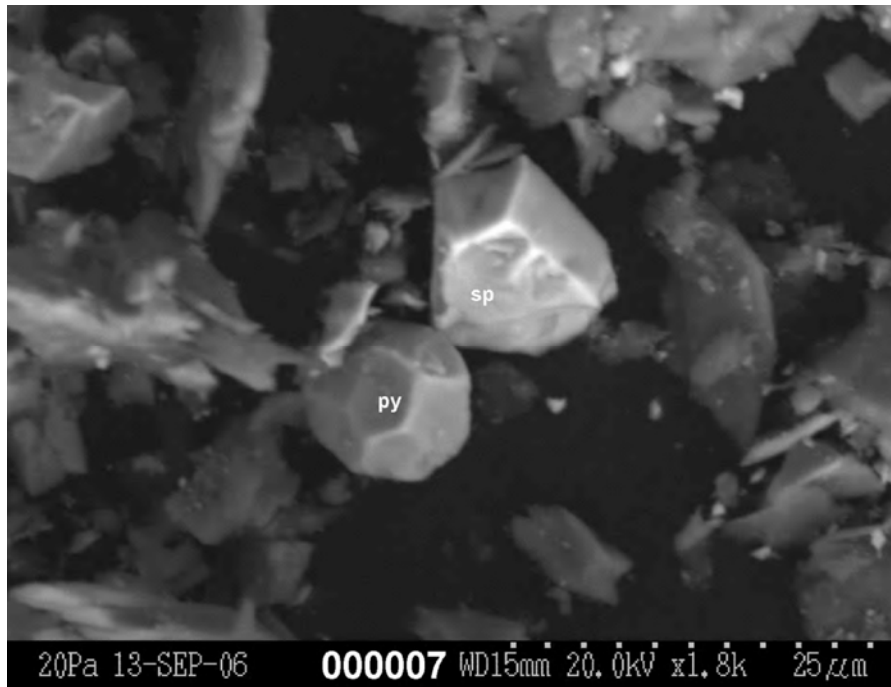
Figure C-26. Backscattered electron image (top) of pyrite (py) and sphalerite (sp) found in Core 3 at 4.5-5.5 cm depth. The X-ray maps (bottom) clearly shows that Cu is preferentially associated with Zn in sphalerite. (Note that the first X-ray map should read Mg instead of As.)
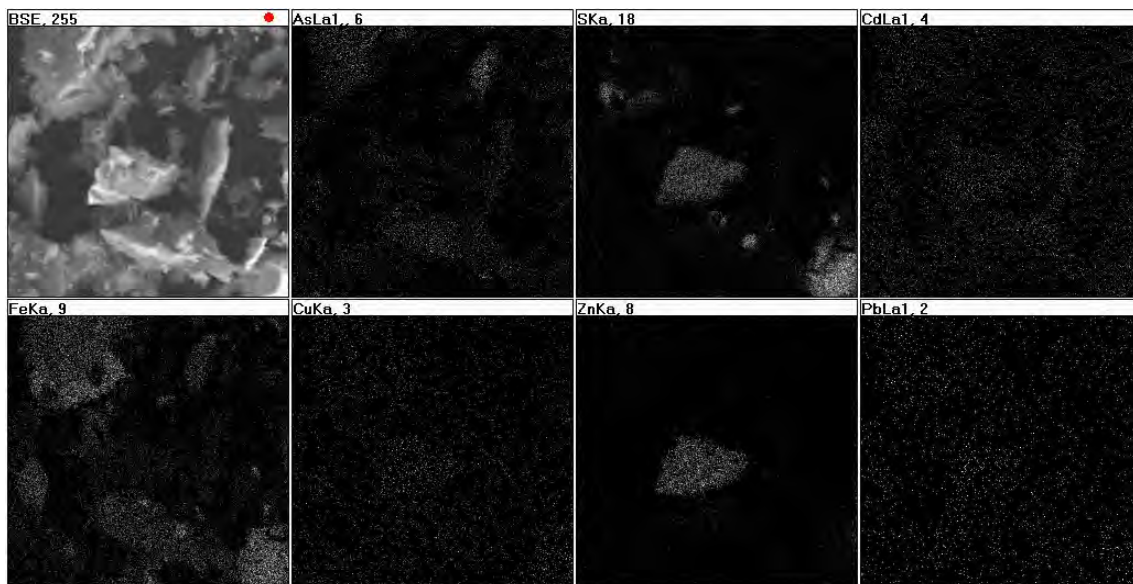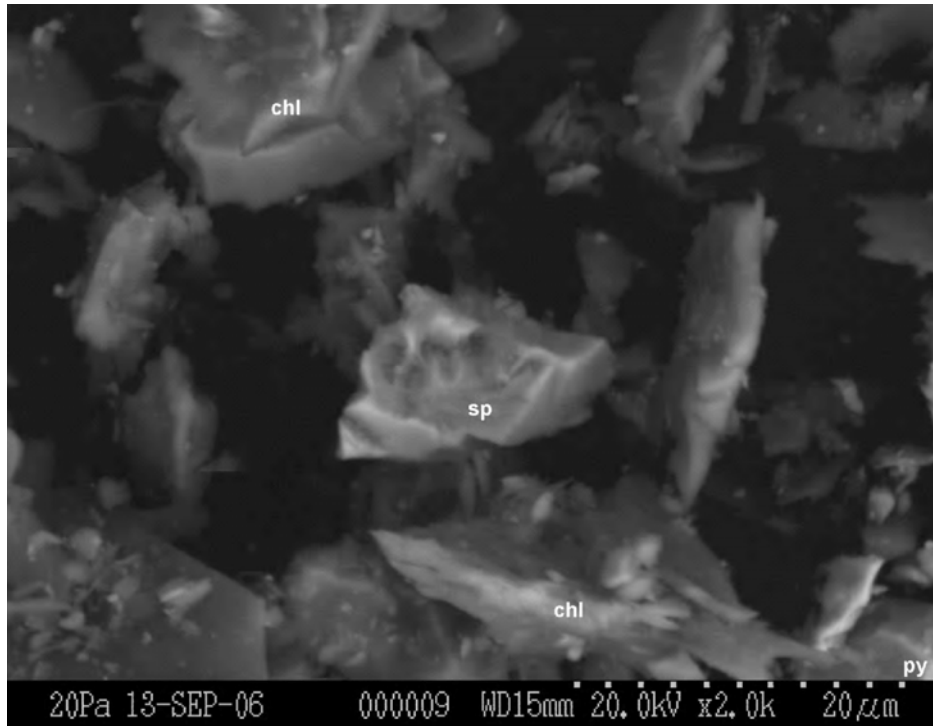
Figure C-27. Backscattered electron image of a partially weathered sphalerite (sp) observed amidst chlorite (chl) in Core 3 at 4.5-5.5 cm depth. The presence of pyrite (py) in the lower right hand corner is supported by the X-ray maps for Fe and S. Note that the first X-ray map for the series should read Mg instead of As such that the bright spots reflect the presence of chlorite.

APPENDIX D – Louvicourt Summary MEND Project 2.12.1

Background

The primary objectives of the Louvicourt project were to assess and demonstrate the effectiveness of shallow water covers in a man-made basin and determine the benefits of the placement of organic or inorganic barriers at the tailings/water cover interface. This demonstration was to enhance the current state of knowledge with both site-specific design information for the closure of the full scale Louvicourt basin as well as generic design and predictive modelling information for application to other reactive tailings sites.

The Louvicourt project included the construction of two test cells adjacent to the tailings basin in August 1996. These cells were nearly rectangular, measuring about 20 m x 20 m, with 2 to 3 m of tailings and 0.3 m of water cover. The cells were filled with tailings from the Louvicourt mill.

The Louvicourt Project Reports, MEND 2.12.1

Five reports were prepared for the "Evaluation of Man-made Subaqueous Disposal Option as a Method of Controlling Oxidation of Sulphide Minerals" project. They are:

MEND 2.12.1.b-Background and General Description. This report by Golder Associés Ltée (Golder, July 2001) provides background information on the Louvicourt project, an overview of the component studies and a description of the field cell construction and instrumentation.

MEND 2.12.1d-Reactivity Assessment and Subaqueous Oxidation Rate Modelling for Louvicourt Tailings. This report by the Noranda Technology Centre (Noranda, December 2000) presents the results of the tailings characterization program, static and dynamic ARD assessment, an interpretation of the data, and the presentation of predictive modelling results on the effectiveness of the shallow water cover in a full-scale application.

MEND 2.12.1e-Column Studies. This report by the Canada Centre for Mineral and Energy Technology (CANMET, December 2000) presents the results of flooded column studies with variable water depths and surface barriers.

MEND 2.12.1c-Subaqueous Disposal of Reactive Mine Tailings, Louvicourt Mine Test Cells, Geochemical Sampling and Analysis. This report by the Institut National de la Recherche Scientifique (INRS-EAU, March 2001) describes the geochemical sampling methods used to monitor the field cells and provides a technical evaluation of cell performance. From 1996 to 1998, the chemistry of the interstitial water near the tailings/water interface was monitored using *in-situ* dialysis. The pH and dissolved oxygen (DO) profiles across the tailing-water interface were monitored using microelectrodes. Penetration of DO into the tailings was limited to < 7 mm, even in the presence of DO produced by benthic periphyton. In contrast to Cu, mobilization

of Cd and Zn from the surface layer was indicated by the presence of sub-surface peaks in the concentrations of these two metals in the tailings interstitial water and by an increased proportion of labile fractions in the solid phase relative to the underlying tailings. The observed Cd and Zn releases from the submerged tailings were however very small and would thus have only minor impacts on the overlying water quality.

MEND 2.12.1.a-Synthesis Report. This report by SENES Consultants Limited (SENES, July 2002) provides highlights of the Louvicourt project studies and an evaluation of the findings and lessons learned. The following conclusions are drawn.

1) Shallow water covers in man-made basins are an effective means of controlling sulphide oxidation. Oxidation rates are reduced by at least 3 orders of magnitude as compared with unsaturated surface tailings deposits.

2) The low rates of oxidation observed in the column and field cell studies result in metals release (notably Cd and Zn) to the overlying water cover. Measured metal fluxes would not likely result in metals levels in the effluent exceeding discharge standards.

3) The measured depth of oxygen penetration into the tailings is typically less than 1 cm. Sampling and measurement of porewaters within such a very small zone is difficult and complicates the interpretation of the geochemistry within this layer.

4) It is apparent that periphyton growth affects oxidation and the transport of oxygen into the tailings. Although the exact role and impact of vegetation is uncertain, other studies to date have shown no significant degradation of water cover quality as a result of plant growth.

5) Barriers between the tailings and the water cover generally serve to limit the access of oxygen to the submerged tailings and act to reduce the diffusive flux of contaminants from the tailings porewater. From this study it is clear that barrier materials may be a significant source of dissolved contaminants and full characterization of these barrier materials must be included in the cover design process. Careful consideration must be given to the short-term impacts that these materials may have on water quality, and whether these impacts outweigh the longer-term benefits. From the Louvicourt column studies, there was no short-term benefit to barriers the tailings/water interface. Given the similar performance of the water cover option without barriers, there would be no basis at this time to suggest additional barriers would be warranted for the Louvicourt site.

Finally, the synthesis report contains two recommendations for future work.

1) Further research into the role of aquatic vegetation on the performance of water covers is warranted.

2) Further monitoring of the test cells would assist in assessing the longer term performance of shallow water covers.